

**A HYBRID EXACT STRIP AND FINITE ELEMENT METHOD
FOR MODELLING DAMAGE IN COMPOSITE PLATES**



Thesis submitted in fulfilment of the requirement for the degree of

Doctor of Philosophy

By

Basem Saoud Suliman

February 2018

School of Engineering, Cardiff University

PAPERS PRODUCED FROM THIS THESIS

Suliman, B., Featherston, C. A. and Kennedy, D. Vibration analysis of damaged plates by hybrid exact stiffness and finite element method. *Proceedings of the 24th UK Conference of the Association for Computational Mechanics in Engineering*. 31 March – 01 April 2016, Cardiff University, Cardiff.

David Kennedy, Carol A. Featherston, Basem Suliman, Yulin Luo. Exact Strip Modelling and Vibration Based Identification of Damage in Plate Assemblies. *11th International Symposium on Vibrations of Continuous Systems*. Llanberis, UK, July 16-22, 2017.

Suliman, B., Featherston, C. A. and Kennedy, D. Reduced order techniques for modelling the effects of damage in composite plates. *21st International Conference on Composite Materials*, Xi'an, 20-25th August 2017.

Suliman, B., Featherston, C. A. and Kennedy, D. A hybrid method for modelling damage in composites. 'Submitted to Computers and Structures, 2018.'

DECLARATION

This work has not been submitted in substance for any other degree or award at this or any other university or place of learning, nor is being submitted concurrently in candidature for any degree or other award.

Signed (candidate) Date

STATEMENT 1

This thesis is being submitted in partial fulfillment of the requirements for the degree of(insert MCh, MD, MPhil, PhD etc, as appropriate)

Signed (candidate) Date

STATEMENT 2

This thesis is the result of my own independent work/investigation, except where otherwise stated, and the thesis has not been edited by a third party beyond what is permitted by Cardiff University's Policy on the Use of Third Party Editors by Research Degree Students. Other sources are acknowledged by explicit references. The views expressed are my own.

Signed (candidate) Date

STATEMENT 3

I hereby give consent for my thesis, if accepted, to be available online in the University's Open Access repository and for inter-library loan, and for the title and summary to be made available to outside organisations.

Signed (candidate) Date

ABSTRACT

Delamination is a frequent cause of failure in laminated structures, particularly under compressive loads. The presence of delaminations in composite laminates reduces their overall stiffness. In addition, delaminations tend to grow rapidly under postbuckling loads, causing further reductions in the structural strength and leading ultimately to a sudden structural failure. Recently, many studies have been carried out to investigate the effects of delaminations on the buckling and vibration behaviour of composite structures. Finite element analysis is often used to perform these due to its ability to model complex geometries, loading and boundary conditions, but this comes at a high computational cost. The exact strip method provides an efficient alternative approach using an exact dynamic stiffness matrix based on a continuous distribution of stiffness and mass over the structure, so avoiding the discretization to nodal points that is implicit in finite element analysis. However due to its prismatic requirements, the exact strip method can model damaged plates directly only if the damaged region extends along the whole length of the plate. This thesis introduces a novel combination of exact strip and finite element analysis which can be used to model more complex cases of damaged plates. Comparisons with pure finite element analysis and a previous technique based on the exact strip method demonstrate the capability and efficiency of this hybrid method for a range of isotropic and composite plates.

ACKNOWLEDGEMENTS

Foremost, I would like to express my deepest gratitude to ‘’Allah’’ the creator of mankind, the creator of life and death.

I express my gratitude to my supervisors Prof. David Kennedy and Prof. Carol Featherston for their excellent supervision, continuous encouragement and support. You are brilliant supervisors. Thanks also must go to Prof. Alan Kwan for his invaluable advice and insightful discussions.

Last but not the least, many thanks go to my family and I dedicated my work to you.

TABLE OF CONTENTS

PAPERS PRODUCED FROM THIS THESIS	i
DECLARATION.....	ii
ABSTRACT	iii
ACKNOWLEDGEMENTS.....	iv
1 Introduction.....	1
1.1 Composites	1
1.2 Defects in composites.....	6
1.2.1 Defects occurring during the manufacturing process	7
1.2.2 In-service defects	8
1.3 Delamination	9
1.3.1 Types of delamination.....	10
1.4 The effect of damage on composite structures	14
1.5 Conclusions	15
1.6 Thesis outline	15
2 Literature review	19
2.1 The effect of delaminations and damage on the behaviour of composites..	19
2.2 The exact strip method	24
3 VICONOPT and Exact Strip Method	28
3.1 VICONOPT	28
3.2 Exact Strip Method.....	30

3.2.1	VIPASA analysis	32
3.2.2	VICON analysis	34
4	Modelling the effect of damage on the critical buckling of composite plates using VICONOPT.....	36
4.1	The effect of ply orientation on the critical buckling load and buckling mode shape	37
4.1.1	Perfect composite plate	38
4.1.2	Composite plates with through-the-length and through-the-width delaminations	41
4.1.3	The effect of the ply orientations on the critical buckling mode shape	46
4.2	Modelling delaminated composite plates	51
4.2.1	Example 4.1: Single and multiple delaminations at the same depth....	52
4.2.2	Example 4.2: Single and multiple-delaminations at varying depths....	54
4.3	The effect of delaminations on the global buckling load	55
4.4	Summary	58
5	The VICONOPT and Finite element (VFM) hybrid model	59
5.1	Theory and formulation used in FE analysis.....	60
5.1.1	Stiffness properties of rectangular plates in bending	60
5.1.2	Equivalent mass matrix for rectangular plate element.....	61
5.2	Theory and formulation for VFM	66
5.2.1	Example of plate assembly using VFM	72

5.2.2	Solution time	76
6	Modelling the effect of damage in natural frequencies using the VFM method.....	78
6.1	VICON model	81
6.2	ABAQUS models	81
6.3	Smearred method (SM).....	82
6.4	Numerical study	85
6.4.1	Reduced stiffness isotropic plates	85
6.4.1.1	Through the length damage (TTLSR)	86
6.4.1.2	Embedded rectangular damage (ERSR)	86
6.4.2	Delaminated composite plates.....	89
6.4.2.1	Through-the-length delaminations (TTLD).....	89
6.4.2.2	Embedded rectangular delamination (ERD).....	90
6.4.2.3	Effect of delamination location.....	99
6.4.2.4	Effect of aspect ratio	104
6.5	Solution time application to VFM.....	106
7	Overall conclusions and future works	108
7.1	Conclusions	108
7.2	Future works.....	111
8	References.....	113
9	Appendices.....	117

9.1	Appendix 1	117
9.2	Appendix 2	122
9.3	Appendix 3	123
9.4	Appendix 4	129

List of Figures

Figure 1-1 Composite materials (a) short random fiber reinforced composites (b) continuous fiber reinforced composites (c) particulate composites (d) laminated composites [5].	2
Figure 1-2 Composite laminate structure	3
Figure 1-3 Composite use in Boeing 787, figure reproduced from AERO Magazine [9].	6
Figure 1-4 Basic delamination modes [20].	11
Figure 1-5: A composite plate containing an embedded rectangular delamination at depth hd .	12
Figure 1-6: Typical surface delaminations: (a) open in tension, (b) closed in compression, (c) open quasi-elliptic, (d) closed elliptic, (e) pocket-like, (f) pocket-like with a transverse crack [14].	13
Figure 2-1: Modelling a plate with differing properties in the y direction using VICONOPT.	26
Figure 2-2: Sketch of VICONOPT model for a laminate of length l , width B and thickness h , having an embedded rectangular delamination of length $d (= \mu l)$ and width b , (Figure reproduced from Damghani et al. (2014)).	26
Figure 3-1 Some typical structures, which VICONOPT can analyse [42]	29

Figure 3-2 Component plate with a combination of in-plane loading [43].....	29
Figure 3-3 Perturbation edge displacements, and nodal lines of a plate.....	32
Figure 3-4: Illustration of the infinitely long structure [58].....	35
Figure 4-1 Ply composite plate (a) the boundary conditions of the plate and the external load applied (N_L) (b) the plate with a single full width through-the-length delamination at a depth of $2h/16$	43
Figure 4-2 First natural frequency mode shape of a plate with through-the-length and through-the-width delamination located at the mid thickness.	43
Figure 4-3: Critical buckling force intensities for plates with ply orientation for plate cases 1 and 3 and different delamination depths.....	44
Figure 4-4 Critical buckling force intensities for plates with ply orientations for plate cases 4, 5, 6 and 7 and different delamination depths.....	46
Figure 4-5: The relationship between critical buckling force intensities and delamination depth for different buckling half-wavelengths λ (and hence mode shapes) for plate case 1.	47
Figure 4-6: The relationship between critical buckling force intensities and delamination depth for different buckling half-wavelengths λ (and hence mode shapes) for plate case 3.	48

Figure 4-7: The relationship between critical buckling force intensities and delamination depth for different buckling half-wavelengths λ (and hence mode shapes) for plate case 4.	49
Figure 4-8: The relationship between critical buckling force intensities and delamination depth for different buckling half-wavelengths λ (and hence mode shapes) for plate case 5.	49
Figure 4-9: The relationship between critical buckling force intensities and delamination depth for different buckling half-wavelengths λ (and hence mode shapes) for plate case 6.	50
Figure 4-10: The relationship between critical buckling force intensities and delamination depth for different buckling half-wavelengths λ (and hence mode shapes) for plate case 7.	50
Figure 4-11: (a) Composite plate with single mid-delamination. (b) composite plate with multiple delaminations.	53
Figure 4-12: Critical buckling stress versus the delamination ratio β/b	53
Figure 4-13 Composite plate with delaminations at depths $h/4$, $h/2$ and $3h/4$	54
Figure 4-14: Critical buckling force intensities for plates with different delamination ratios and single and multiple delaminations.	55
Figure 4-15: (a) Mid-width delaminated plate. (b) cut-out model for a delaminated composite plate.....	57

Figure 4-16: Critical buckling force intensity for a plate with a mid-width delamination based on the cut out plate model and the predicted global buckling stress.....	57
Figure 5-1: VICON and FE method (VFM) modelling a damaged plate.	59
Figure 5-2 Rectangular plate element showing displacements and sign conventions [66].....	61
Figure 5-3: Damaged plate modelled by VFM.	66
Figure 5-4 Assembling two plates using VFM. (a) exact strip and FE components. (b) the assembled structure.	73
Figure 5-5: An example of a banded, symmetric VIPASA matrix	77
Figure 6-1 Types of damage studied.	79
Figure 6-2 Methods used to model different types of damage.....	79
Figure 6-3: Plate containing centrally located (a) through-the-length damage (b) embedded rectangular damage.....	80
Figure 6-4: Isotropic plate with through the length damage modelled by VICON. ..	81
Figure 6-5 Identical plates containing embedded delaminations modelled by (a) VFM (b) ABAQUS.....	83
Figure 6-6 Smearing method for modelling embedded reduced stiffness damage....	84

Figure 6-7 Sketch of VICONOPT model for a laminate of length l , width B and thickness h , having an embedded rectangular delamination of length $d (= \mu l)$ and width b , (Figure reproduced from Damghani et al. (2014))...... 85

Figure 6-8: Lowest natural frequency for isotropic plates (ω_1) against width β/b for centrally located damage using the three techniques, Smearing Method (SM), ABAQUS and VFM. (a) through-the-length damage and $f = 0.75$. (b) through-the-length damage and $f = 0.25$ 87

Figure 6-9: Lowest natural frequency of isotropic plates (ω_1) against width β/b for centrally located damage using the three techniques, Smearing Method (SM), ABAQUS and VFM. (a) embedded rectangular damage, $d = 50\text{mm}$ and $f = 0.67$. (b) embedded rectangular damage, $d = 50\text{mm}$ and $f = 0.3$ 88

Figure 6-10: Lowest natural frequency of composite plates (ω_1) against width β/b for centrally located through the length delamination using ABAQUS and VFM. (a) Delamination depth is at $h/4$ from the plate top surface (b) Delamination depth is at $h/2$ from the plate top surface..... 91

Figure 6-11: Lowest natural frequencies of composite plates (ω_1) against width β/b for centrally located embedded rectangular delaminations, using the Smearing Method (SM), ABAQUS and VFM. (a) delamination depth = $h/4$, $d = 25\text{mm}$. (b) delamination depth = $h/2$, $d = 25\text{mm}$. (c) delamination depth = $h/4$, $d = 50\text{mm}$. (d) delamination depth = $h/2$, $d = 50\text{mm}$ 93

Figure 6-12: Mode shape corresponding to the lowest natural frequency of a composite plate having a centrally located embedded rectangular delamination with depth = $h/4$, $d = 50\text{mm}$ and $\beta/b=0.3$ obtained using the Smearing Method (SM).	94
Figure 6-13: ABAQUS, VFM and SM plots of the out-of-plane deflection in the normalised mode shape of the lowest natural frequency for a composite plate containing an embedded rectangular delamination. (a) Delamination length $d=0.5l$, depth $0.5h$, width $\beta=0.5b$, see Figure 6-11(d). (b) Delamination length $d = 0.5l$, depth $0.25h$, width $\beta = 0.6b$, Figure 6-11 (c).....	98
Figure 6-14 Plate containing embedded delaminations.	99
Figure 6-15: Lowest natural frequency of composite plates (ω_1) against widthwise position and depth of embedded rectangular delaminations.	101
Figure 6-16: Lowest natural frequency of composite plates (ω_1) against lengthwise position and depth of embedded rectangular delaminations.	103
Figure 6-17: The effect of aspect ratio (b/l) on the lowest natural frequency for different delamination sizes, $d = 50\text{mm}$	105
Figure 6-18 Plots of normalized first natural frequency against aspect ratios for different delamination width with $d=50\text{mm}$	106
Figure 6-19 (a) Damaged plate modelled in VFM. (b) form of the global dynamic stiffness matrix.	107

Figure 9-1 Plots of lowest natural frequency against different delamination sizes, $d =$
25mm and 50mm, of composite plate with various aspect ratios (b/l). 132

List of Tables

Table 1-1 Applications of composite laminates in industry [7].....	4
Table 1-2 Advantages and disadvantages of composite laminates [7].	5
Table 4-1: Different cases of stacking sequences	39
Table 4-2: Critical buckling stresses and buckling wavelengths for plate cases 1, 2 and 3.....	41
Table 4-3: Critical buckling stresses and buckling wavelengths for plate cases 4, 5, 6 and 7.....	41
Table 5-1 Stiffness matrix for rectangular plate in bending: submatrix $\mathbf{k}_{I,I}$ based on compatible deflections [all coefficients to be multiplied by $[E t^3 / (12 (1-\nu^2) ab)]$] [55].	62
Table 5-2: Stiffness matrix for rectangular plate in bending: submatrix $\mathbf{k}_{I,I}$ based on compatible deflections [all coefficients to be multiplied by $[E t^3 / (12 (1-\nu^2) ab)]$] [55].	63
Table 5-3: Stiffness matrix for rectangular plate in bending: submatrix $\mathbf{k}_{II,II}$ based on compatible deflections [all coefficients to be multiplied by $[E t^3 / (12 (1-\nu^2) ab)]$] [55].	64

1 Introduction

The advantages of using lightweight structures in a number of industries have directed engineers to the use of new materials. Composite materials have been introduced as an example of new man-made lightweight materials, which can be tailored for specific applications [1]. The mechanical properties of these composite materials can be influenced by creating different combinations and geometries, for example high strength/stiffness fibres (such as glass, carbon etc) and matrices (including thermoset or thermoplastic resins) during the manufacturing stage [2]. Nowadays engineers are able to tailor-make advanced laminated composite materials, which are stiffer and lighter than any other structural materials [3]. However, composite materials require adequate testing in order to understand their complex behaviour.

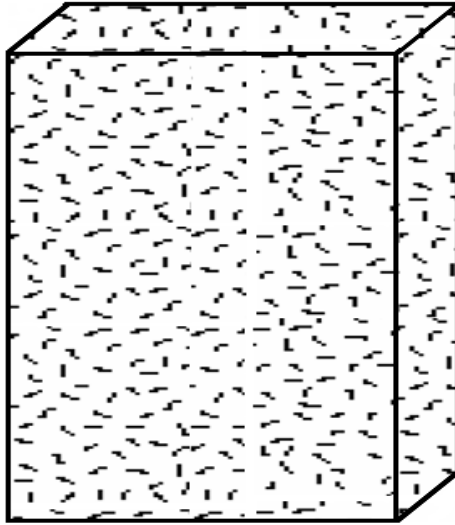
Composite material applications, damage types and mechanisms and the effect of this damage on the behaviour of a composite structure are briefly discussed in this chapter to introduce the thesis.

1.1 Composites

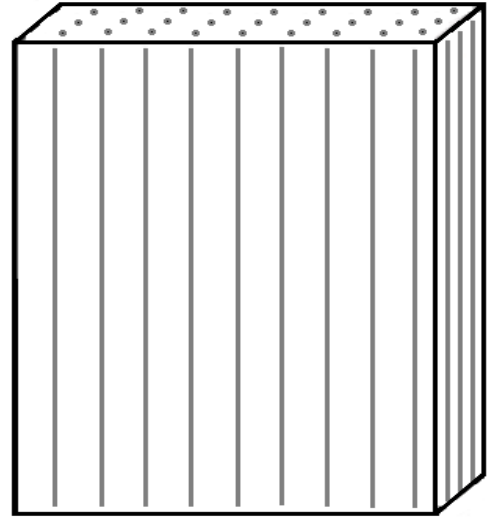
Structural materials can be divided to isotropic or anisotropic materials [4]. Composite materials, anisotropic materials, are formed by uniting two or more separate materials such that they have better engineering properties. Composite materials can be categorised into [5, 6]:

- Fibrous composites, fibers in a matrix, that can be short or continuous
- Particulate composites, particles in a matrix
- Laminated composites, layers of various materials

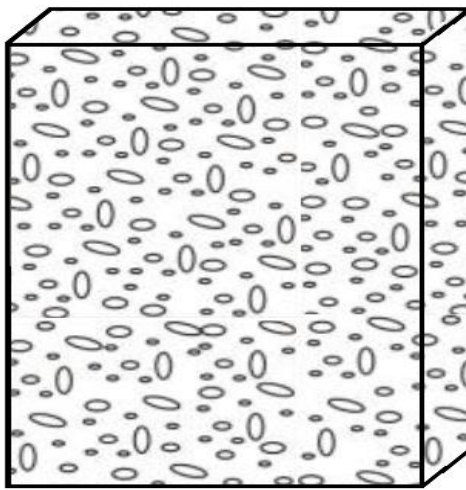
(a)



(b)



(c)



(d)

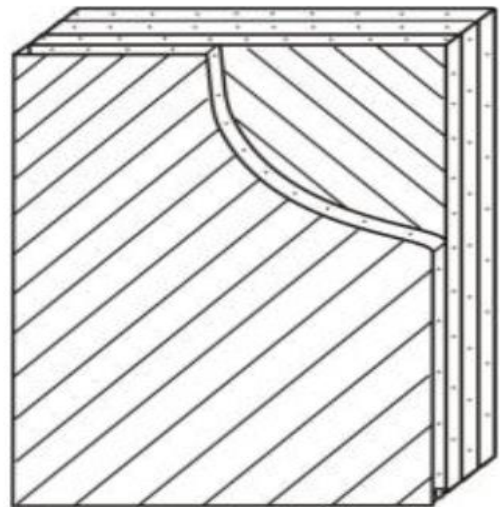


Figure 1-1 Composite materials (a) short random fiber reinforced composites (b) continuous fiber reinforced composites (c) particulate composites (d) laminated composites [5].

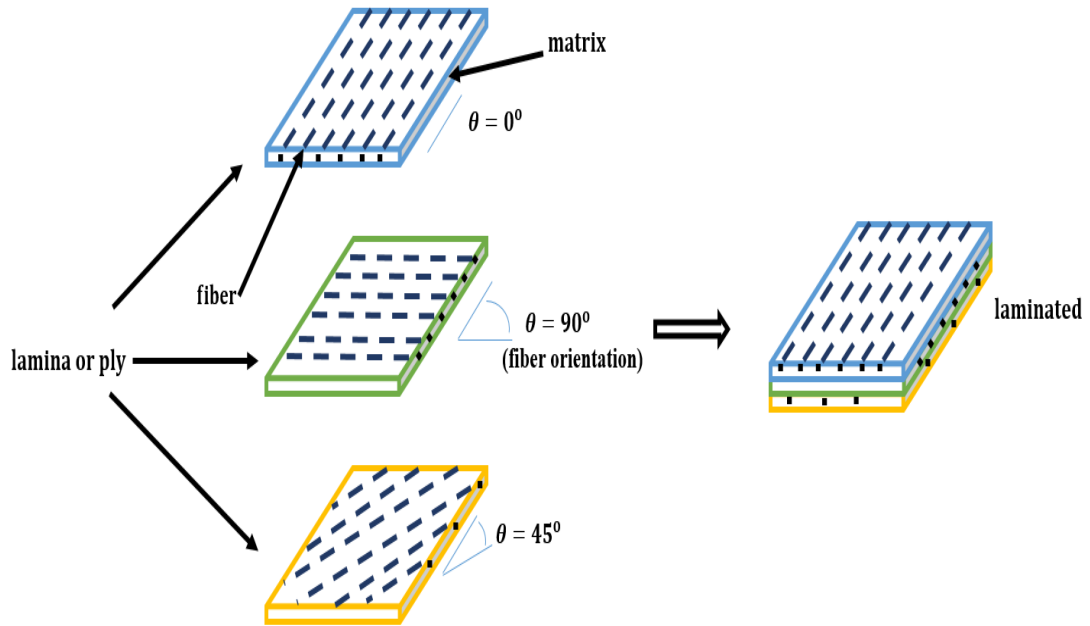


Figure 1-2 Composite laminate structure

Fibrous composites can be short fiber (usually randomly orientated fibers) or long fiber (continuous fiber) reinforced composites as shown in Figure 1-1 (a & b). Figure 1-1 (c) shows the use of particles as the reinforcement to create particulate composites. Figure 1-1 (d) illustrates the structure of a laminated composite material. In this type of composite the material, thickness, and the fiber orientations in each lamina play a key role in the mechanical properties of the composite. The sequence of various orientations of the plies in a laminated composite is called the *stacking sequence*, see Figure 1-2. Typical applications in a range of different industries and the advantages and disadvantages of a composite laminate and are summarized in Table 1-1 and Table 1-2 respectively.

Table 1-1 Applications of composite laminates in industry [7-9]

Branch of industry	Application
Rocket construction	Load-carrying structural elements, fuel tanks, aerial elements, rocket boosters
Aircraft construction	Tail assembly, stabilizers, inner lining of cabins, wing, fuselage, radomes, leading edges, ailerons, wings, etc (see Figure 1-3)
Machine building	Transmission cases, gear wheels, machine elements, fly wheels, pipes, robot arms, bearings, ...
Automotive industry	Wheel rims, trunk covers, hoods, steering columns, inner lining of cabins, suspension arms, trailers, telecabins
Medical equipment	Implants, artificial joints
Sports industry	Surfing, skis, clubs, canoes, bicycles, bows and arrows, surf boards
Telecommunication	Parabolic aerials, insulation for electrical construction, antennas, radomes
Oil production	Elements of frames for offshore drilling rigs
Civil engineering	Facing materials, strengthening of building structures, concrete molds, swimming pools, doors, furniture, bathrooms, partitions
Energetics	Rotor blades of wind power stations
Industrial engineering	Reservoirs, pipelines

Table 1-2 Advantages and disadvantages of composite laminates [7, 10].

Advantages	Disadvantages
High specific strength	Loss of strength due to aging of adhesive joints
Thermoinsulation	High technological requirements for the accuracy of production
Sound-proofing	Necessity of modifying the methods of non-destructive testing of structures
High fatigue characteristics	High sensitivity to impact loads
High corrosive resistance	Brittleness and damage tolerance is resin-dominated properties
Low tendency to loss stability	Temperature has an effect on composite mechanical properties
Decrease in the number of assembling operations due to the development of more complex components	Susceptibility to impact damage and delamination

Recently, composite laminates have been increasingly used in many fields such as civil, mechanical and aerospace applications because of their high strength and stiffness combined with low density when compared to some other materials such as isotropic materials. Using composite materials in an aircraft fuselage for example

therefore can provide much better specific strength' than could be achieved using isotropic materials. Minimizing the mass of an aircraft's structure through the use of composites reduces the cost of materials and manufacturing, as well as fuel consumption and atmospheric emissions. Examples of the use of composite laminates in aircraft include the Airbus A-380.800 which is 25% composite, the Airbus 350-900 which is 52% composite and the Boeing 787.800, see Figure 1-3, which is 50% composite [2].

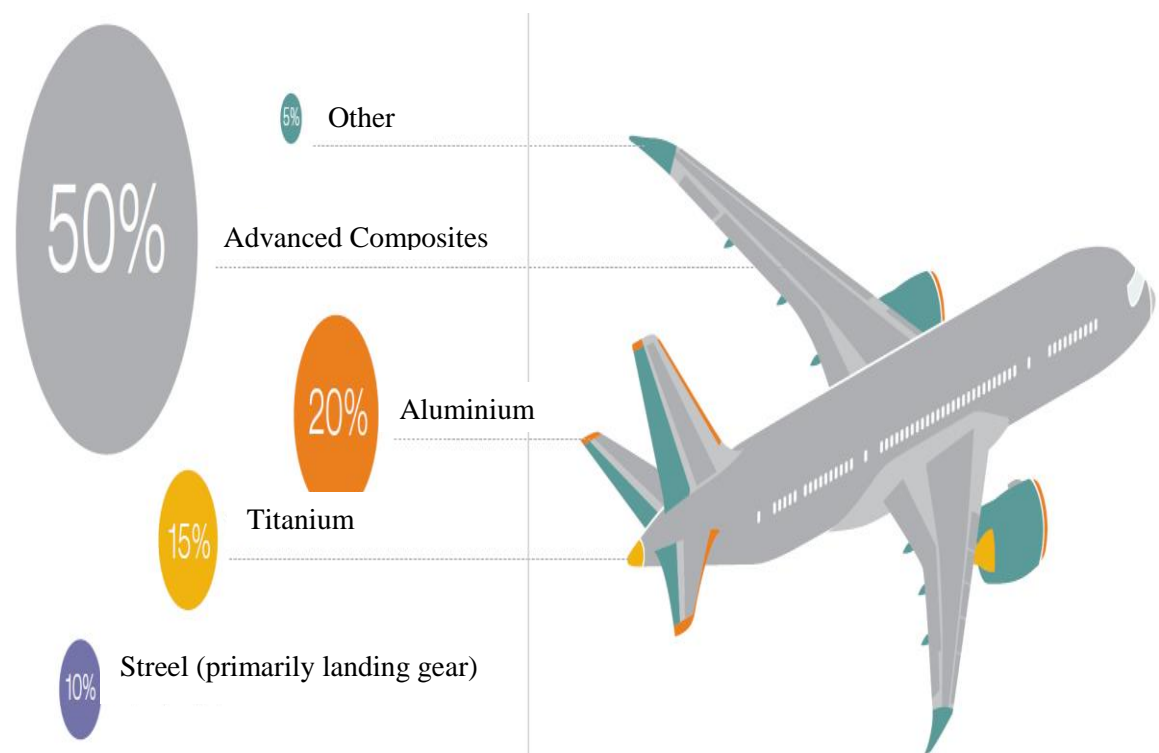


Figure 1-3 Composite use in Boeing 787, figure reproduced from AERO Magazine [9].

1.2 Defects in composites

Composite materials are prone to many different imperfections many of which can be introduced during the manufacturing process [11]. Composites can also be degraded due to a number of scenarios during their service life. All of these defects are known

to negatively affect the performance of a composite structure although to differing degrees.

The following sections describe the types of defect which can be introduced: during the manufacturing process; during operation and during the service life of the component.

1.2.1 Defects occurring during the manufacturing process

Nowadays engineers use complicated techniques for manufacturing well-consolidated fiber and resin products such as hot pressing or autoclaving. In these kinds of manufacturing process, the quality of the finished material depends on proper compaction pressure being applied correctly at particular moments during the heating cycle and using proper techniques for efficiently bleeding off the excess resin without affecting the quality of the surface finish. During the manufacturing process, defects can be introduced with different sizes and frequencies of occurrence depending on the nature of the process cycle [12]. However, defects which are typically generated during these manufacturing processes, include:

- Voids, which can be due to air not properly controlled during cure.
- Foreign inclusions.
- Fiber debonding due to incorrect cure conditions.
- Fiber misalignment, which can cause local change in fibre volume fraction.
- Ply misalignment because of mistakes made in lay-up of the component plies.
- Wavy fibers, which can seriously affect laminate strength.
- Cracks and holes in the matrix material.
- Fibre breakage.

Chapter 1: Introduction

- During the manufacturing process, delaminations can be produced due to contamination during lay-up process or by machining, particularly when bonding stiffeners to panels.

The presence of voids or the porosity are often cited as the most important manufacturing defect likely to arise. Porosity can occur in practice due to insufficient resin applied or the resin being incorrectly cured [11-13].

1.2.2 In-service defects

Degradation in composites during service can be due to a number of mechanisms depending on the environment and the sensitivity or the nature of the materials used. Examples of these mechanisms include static overload, overheating, lightning strike, impact and fatigue load. However, despite the varied mechanisms only a small number of different types of defect result. Smith [12] listed these defects in order of importance as the following:

- Delaminations.
- Bond failures.
- Cracks
- Ingress of moisture.
- Fracture or buckling of fibers.
- Failure of the interface between the fibers and matrix.

Due to its importance as a failure mechanism the work carried out in this thesis is mainly focused on studying the effects of damage due to delamination on the

behaviour of laminated plates under vibration using a developed novel hybrid technique.

1.3 Delamination

Delamination is one of the most frequently encountered problems in composite materials, sometimes also known as an interface cracking which occurs between the laminae of a laminate. This cracking can be as a result of manufacturing defects such as air entrapment, incomplete wetting or trapped air bubbles between plies, or a debonding of two layers because of high stress concentrations (free edge effects). It can also be caused as a result of shrinkage cracks and adhesion failure. The transportation and installation stage can be another case where delaminations can originate, particularly since loads and actions during this stage differ in level and character from the ones used in design, for example, impacts upon the surfaces of a composite structure caused due to tool drop or low velocity impact of foreign objects. Finally during the operation stage, delaminations can occur because of inadequate design or off-design situations [14]. Other causes of delamination for example fatigue load or low-velocity impact [15, 16]

It is known that delamination is one of the most frequent causes of failure in composite laminate structures, particularly those subjected to compressive loads [17, 18]. The presence of delaminations in composite structures can reduce their overall stiffness and strength and cause degradation. Delaminations can grow rapidly under postbuckling loads potentially leading to sudden structural failure [19]. They can also cause significant reductions in the associated natural frequencies or load-carrying

capacity of the structure. Delaminations are particularly important because they can be difficult to detect visually as they often do not cause any effect to the external surface.

1.3.1 Types of delamination

Delamination in composite laminates can be categorised based on which interlaminar fracture mode is developed. Figure 1-4 illustrates the three main delamination modes. Mode 1 is the peeling or opening mode, mode 2 is the sliding or in-plane shear mode and mode 3 is the twisting or out of plane shear mode [20].

Bolotin [21] distinguished delaminations in composites based on their location through the thickness of the plate, the value of h_d in Figure 1-5, into internal delaminations and near-surface delaminations. Internal delaminations were defined as those with delamination depths comparable to half the thickness of the composite laminate. With this kind of delamination the delaminated section usually deforms following the overall structure (i.e. it demonstrates global behaviour) as long as the delamination is small. The behaviour of near-surface delaminations can be more complicated due to the fact that deformation of the delaminated area does not always follow that of the overall structure, with localised effects often seen, see Figure 1-6.

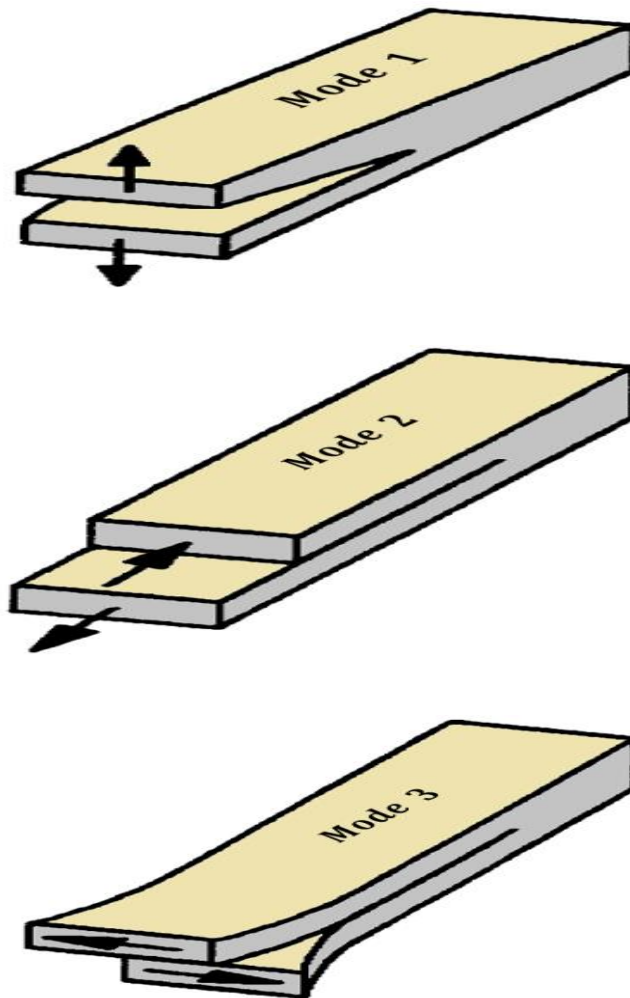


Figure 1-4 Basic delamination modes [20].

Near-surface delaminations can be further categorised based on their geometric shape. Figure 1-6 illustrates different types of surface delamination categorised based on the geometry of the delaminated region. A continuous delamination, in which the delamination originates and grows when the plate is under a tensile load, is shown in Figure 1-6 (a). A continuous or closed compression-caused delamination is illustrated in Figure 1-6 (b). Figure 1-6 (c) or elliptic and continuous as Figure 1-6 (d) illustrates. At the edges of components pocket-like or pocket-like accompanied by transverse cracking surface delaminations can also occur as shown in Figure 1-6 (e) and (f)

respectively [14]. Circular, triangular and rectangular delamination shapes can also be added as types of near-surface delamination.

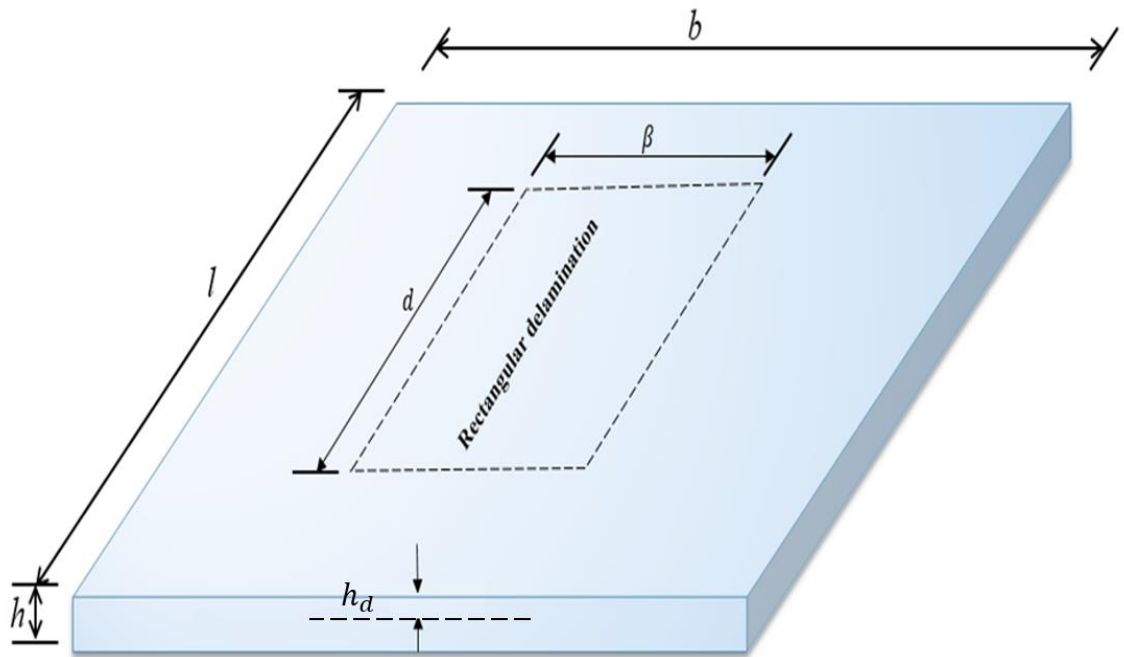


Figure 1-5: A composite plate containing an embedded rectangular delamination at depth h_d .

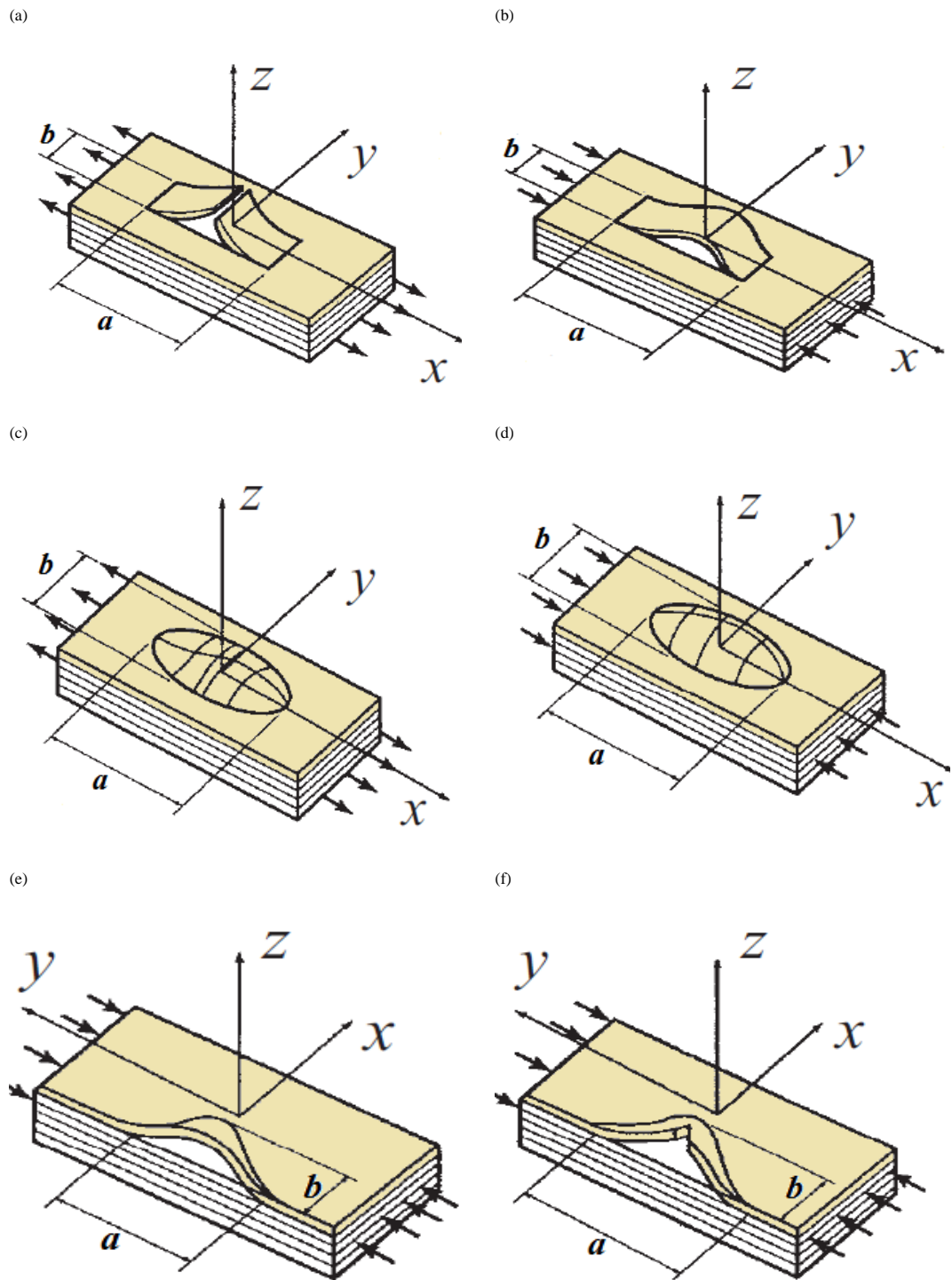


Figure 1-6: Typical surface delaminations: (a) open in tension, (b) closed in compression, (c) open quasi-elliptic, (d) closed elliptic, (e) pocket-like, (f) pocket-like with a transverse crack [14].

1.4 The effect of damage on composite structures

As composite structures are increasingly replacing many currently used materials, mainly because of the weight reduction [22], intensive research, both numerical and experimental, has to be carried out to study the effect of different types of potential damage on the performance of laminated structures under various load cases. In section 1.2 different defects commonly found in composite structures were identified and this section briefly discusses the effect of each of these types of damage on the behaviour of the composite laminate.

It is identified that the presence of damage in composite structure may affect its stiffness and strength negatively. Sreehari and Maiti [23] presented a numerical study on the buckling and post buckling of composite plates containing internal flaws. The damage was assumed to consist of a centrally located rectangular patch. It was found that the decrease of the critical buckling load resulting from an increase in the size of this damage was sensitive to the kind of load applied, either uniaxial or biaxial, and the stacking sequence of the laminated plate. Santos et al. [24] detailed the effect of vertical and inclined holes on the impact strength of carbon-fibre reinforced composites. Plates incorporating damage were submitted to low impact tests and the results were compared with perfect plates. For the perfect plates (control samples), this impact load caused complex damage as a result of the interaction between delamination and matrix cracking. Higher levels of damage were detected in the area around the vertical hole with significant effect on the delamination shape, which was more noticeable in case of inclined hole. Li [25] studied delamination and transverse crack growth in laminated composite plates and shells under line distributed load. It

was found that aspects such as the material's properties, the distance between the delamination and the transverse cracks, their sizes and locations and the nature of the load applied were all elements that affected the direction and rate of the growth of the damage.

1.5 Conclusions

It can be concluded that predicting the way in which damage affects the global performance of a composite structure or the level of reduction in its overall stiffness and strength depends on the following aspects:

- The type of damage, whether the damage is a hole, delamination, crack, etc.
- The size of the damage.
- The location of the damage.
- The material properties.
- The nature of the load applied.
- The boundary conditions of the damage.
- Any combination of the above.

1.6 Thesis outline

The work contained in this PhD is based on using the exact strip method working in combination with finite element theory to improve its ability to model a wider variety of damaged plates, using the exact strip method to model the undamaged parts of the structure and finite element analysis to model the area surrounding the damage. The aims of this novel hybrid method, denoted VFM, are

Chapter 1: Introduction

- To add a capability to the exact strip method for handling a wider range of more complicated damaged plate structures.
- To achieve the simplicity and computational efficiency, possible with the exact strip method and the capability of finite element method to model complicated cases of damage.

The VFM method will be used to understand the vibration behaviour, in particular the natural frequencies, of isotropic plates containing regions of reduced stiffness and delaminated composite plates. This is important not only at the design stage because it allows the effects of various types of damage to be determined, but also as the first step in the development of damage detection techniques, since an accurate prediction of these effects is the first stage in solving the inverse problem i.e. to determine the location and size of a defect based on changes in its natural frequencies.

The aims will be achieved by completion of the following objectives:

- 1) Understanding the theories and formulations used in VICONOPT and the Exact Strip Method and using them to study the effect of damage in composite plate structures.
- 2) Introducing a novel hybrid method by combining Finite Element Analysis and the Exact Strip Method.
- 3) Using this new method to model the effect of damage on the natural frequencies a series of plates and verifying the results by comparing them with pure finite element method results.

The work is structured into seven chapters. Following the introduction, Chapter 2 includes a literature review on analysing the behaviour of damaged composite plate

Chapter 1: Introduction

structures. Studies of different types of damage with various configurations, and the techniques used to model the damage, are summarized. The research gap is defined in this chapter to improve the ability of the exact strip method to model a wider variety of damaged plates. The aim of this thesis was to develop a novel hybrid method (VFM), combining the exact strip method and the finite element theory, which can be used to address damage problems in composite laminates which cannot be handled directly using the exact strip method. VFM combines the simplicity and efficiency of the exact strip method and the versatility of the finite element method.

Chapter 3 reviews the theory and the formulations used in the exact strip method and introduces the computer program VICONOPT through which it is implemented and the theoretical basis of the two strands of the programme VIPASA (Vibration and Instability of Plate Assemblies including Shear and Anisotropy) and VICON (VIPASA with Constraints) analysis, highlighting the features that are essential in understanding the remainder of the work.

Chapter 4 studies the effect of damage on the critical buckling of composite plates using VICONOPT. Work is outlined which investigates the effect of the ply orientation by considering different stacking sequences of the plies, on the critical buckling load and its mode shape including an analysis of both through-the-length and through-the-width single and multiple delaminations and the effect of delamination on the global buckling load.

Chapter 5 introduces a novel technique combining the exact strip method with finite element theory (VFM) and details the theory and formulation used in this method. VFM is developed to enable the modelling of more complex geometries of damage

Chapter 1: Introduction

than the pure exact strip method whilst retaining much of the computational efficiency offered using exact strip.

Chapter 6 VFM is used to study the effect of damage, including embedded and through-the-length delamination and regions of stiffness reduction, on the behaviour of vibrating composite laminates in undamped free vibration. Configurations such as the size of the damage, the plan location and through the thickness location of the damage, and the plate aspect ratios are considered. The results obtained are compared with VICON analysis, ABAQUS finite element analysis and a previous smeared method to prove the effectiveness of this method.

Finally, Chapter 7 provides the overall conclusion of the results of the analyses undertaken and the methods used and discusses potential future work.

2 Literature review

This chapter describes research carried out in previous studies to investigate the effect of delaminations on the buckling and vibration behaviour of composite structures and the techniques which have been used.

2.1 The effect of delaminations and damage on the behaviour of composites

Delaminations can reduce the overall stiffness of a structure and grow rapidly under postbuckling loads potentially leading to sudden structural failure. They can also cause significant reductions in the associated natural frequencies of the structure. Many researchers have investigated the effects of damage on the buckling or vibration behaviour of composite structures.

Lee and Park [19] investigated the buckling behaviour of delaminated composite structures using enhanced assumed strain (EAS), three-dimensional finite element formulations. Laminated composite plates containing through-the-width or embedded delaminations were studied with the effect of varying parameters including delamination locations, sizes, stacking sequences and aspect ratios investigated. Multiple delaminations in the embedded rectangular delamination region were also explored. The numerical results presented focused on the effects of these parameters on the local buckling. They found that the EAS formulations provide faster analysis and better accuracy when compared with conventional approaches based on finite element theory.

Pekbey and Sayman [26] investigated numerically and experimentally the behaviour of rectangular laminated composite plates with centrally located through-the-thickness

Chapter 2: Literature review

strip delaminations. Variations in structural configuration were considered, including stacking sequence, delamination sizes and specimen geometry. Experimentally, compression tests were carried out, and numerically, finite element modelling, using ANSYS [27], was used for analysing the critical buckling load of composite plates with various configurations. Good agreement was found between the experimental measurements and the finite element predictions.

Cappello and Tumino [28] presented a numerical analysis of the behaviour of composite plates with multiple delaminations subjected to uniaxial load. Both buckling and post-buckling behaviour of composite plates with multiple delaminations was studied using finite elements analyses (ANSYS). Interaction between local and global buckling and the location and size of delaminations was studied and the influence of delamination length and position as well as the stacking sequence of the plies on the critical buckling load of the plate was determined.

The pre- and post-buckling behaviour of a composite laminate containing a strip delamination was examined numerically and experimentally by Karihaloo and Stang [29] who introduced guidelines for assessing the threat posed by interlaminar matrix delamination. The analytical solution of the problem was significantly simplified in order that the assessment procedure developed could be used by designers.

Liu et al. [30] explored the effect of multiple through-the-width delaminations on the postbuckling properties of flat composite laminates under compressive load. They used a virtual crack closure technique (VCCT), combined with a finite element approach, to deal with delamination growth. It was found that the results from the VCCT were in relatively good agreement with the results obtained from existing

models and experiments. The work was extended by Liu and Zheng [31] in order to use the technique to study the buckling and postbuckling behaviours of symmetric and unsymmetric composite laminates containing through-the-width multiple delaminations.

Nikrad et al. [32] introduced a layerwise theory to investigate the postbuckling behaviour of and delamination growth in geometrically imperfect composite plates. The theory adopted the Ritz method and assumed displacement fields, x , y and z , in order to reduce the computational cost. Different boundary conditions, delamination types and locations were considered. The technique was shown to be capable of predicting the local and global buckling of a delaminated composite plate following validation against finite element simulations.

Yazdani et al. [33] presented a first-order shear deformation theory, based on the finite element method, for modelling multi-layered composite laminates. This method was used to investigate delamination in composite laminates with curvilinear fibres. It was concluded that the theory was effective when analysing laminates in which variations in stiffness within the surface of plies, is of concern.

Szekrényes [34] studied the displacement and stress fields in symmetrically delaminated, layered composite plates subjected to bending by using a modified version of the third-order shear deformation theory by Reddy [5]. Results for simply-supported delaminated plates were compared with a 3D finite element model. Whilst overall agreement was established, some differences were found in the case of normal and transverse shear stresses.

Chapter 2: Literature review

Wang et al [35] studied the effect of single and multiple embedded delaminations on the buckling behaviour and compressive failure load of glass fibre reinforced plastic specimens. Finite element analysis was used to develop a deep understanding of the mechanisms of compressive failure. Reasonable agreement was obtained between the finite element analysis results and experimental measurements for the range of specimens with different delamination geometries that were tested.

Aslan and Şahin [36] conducted an investigation into the effect of the delaminations induced by low velocity impact on the critical buckling and compressive failure loads of E-glass/epoxy composite laminates. In their study, experimental measurements were compared with a numerical study using the finite element analysis, ANSYS 11.0 package. A good agreement between the numerical and experimental results was obtained.

Park et al [37] carried out a free vibration analysis of composite skew laminates containing delaminations around quadrilateral cutouts. A finite element formulation based on high-order shear deformation theory (HSDT) was used to model the delamination around the cutouts. The effect of skew angle on a rectangular plate's natural frequencies and mode shapes was explored. Various parameters such as delamination size, stacking sequence, length-to-thickness ratio and cutout size were considered.

Jayatilake et al [38] studied the effect of delaminations on the free vibration behaviour of multilayer sandwich panels with interlayer delaminations. A series of parametric studies using a developed three dimensional finite element model were conducted

where each sandwich layer was modelled using first order shear deformation theory based plate elements.

Devendiran et al [39] performed an experimental and theoretical free vibration analysis study of damaged and undamaged CFRP/GFRP laminate beams with rectangular notches. Damage was created in the laminates at varying distances along the transverse axis of the beam to help understand its influence on material and geometrical properties. The experimental measurements were compared and validated with the results obtained from the finite element model.

Wang et al [40] used the perturbation method to study the behaviour of laminated composite plates containing local reductions in stiffness under vibration. This degradation in structural stiffness was considered to be representative of the effect of damage. Damage was characterised based on three parameters, namely damage severity, damage anisotropy, and damage location/area. The results from the proposed method were compared with numerical finite element analyses and it was found that the proposed solution could be applied to the vibration analysis of orthotropic laminated plates containing small amounts of damage.

In recent years, the majority of the research carried out in this field has used finite element analysis to model laminates incorporating one or more damaged regions. The FE method provides a versatile approach, capable of handling many combinations of load and boundary conditions for a range of damage shapes. However, even with today's computer hardware, this type of analysis still often comes at a high computational cost. During an aircraft's preliminary design stage when many alternative configurations and load cases need to be considered, fast and reliable

analysis tools are required. The exact strip method [41] provides an efficient alternative approach using an exact dynamic stiffness matrix based on a continuous distribution of stiffness and mass over the structure, so avoiding the discretization to nodal points that is implicit in FE analysis. In this method, the deflection is assumed to take the form of a number of half wavelengths in the axial direction.

2.2 The exact strip method

In 1974 W. H. Wittrick and F. W. Williams developed the computer program VIPASA [42] at the University of Birmingham . This program is based on exact flat plate theory in which the continuous distribution of stiffness over a structure is assumed [43]. After enhancement by the NASA-Langley research centre VIPASA was released in 1976 [44]. In 1982 VICON (VIpasa with CONstraints) was developed at Cardiff University in collaboration with British Aerospace and NASA [45]. The key difference between the methods implemented in each of these programs is that VICON introduces Lagrangian multipliers to couple responses at different values of half-wavelength λ in order to satisfy constraints such as simply supported end conditions. This same collaboration later led to the release of VICONOPT, VICON with Optimisation, in 1990 [43].

VICONOPT (VIpasa with CONstraints and OPTimization) is able to model plates which have different properties and even different thickness in the transverse direction (y) by modelling them as different plates as shown in

Figure 2-1. However, all the plates need to be the same length in the axial direction (x). In this way VICONOPT is able to model damaged plates as long as the damaged region stretches along the whole length of the plate in the x direction.

In 1967 The finite strip method, the root of the exact strip method, was first presented by Cheung. This hybrid Ritz approach is an efficient analysis tool for structures with regular geometry and simple boundary conditions[46]. This limitation is solved by Cheung and Kong [47] where a new finite strip method is presented and it is applied to the vibration of rectangular plates with complicated boundary and internal support conditions to show its efficiency. Guo et al. [48] investigated various approaches for analyzing the vibration of plates with stepped thicknesses. Improving the classical finite strip method by replacing the static shape function of the strip element model by a dynamic function is presented in this paper. This work led to developing a dynamic finite strip method which improves solution accuracy.

Damghani et al. [49] studied the critical buckling of composite plates with delaminations using exact stiffness analysis. They modelled the delamination as through the length in order to satisfy the prismatic requirements of VICONOPT. They highlighted the simplicity of modelling the damage and the competitive analysis time of this approach against the finite element method. This work was later extended (Damghani et al. [50]) to study the global buckling behaviour of a composite plate with a single rectangular delamination. This method was based on replacing the longitudinal portion of the plate containing the delamination, the delaminated strip, with an equivalent prismatic structure as shown in Figure 2-2. The delaminated strip is replaced with three strips each having the same length. Two of them, strips 1 and 2 in Figure 2-2, represent the top and bottom parts of the embedded rectangular delamination and the third strip represents the undamaged parts of the delaminated strip.

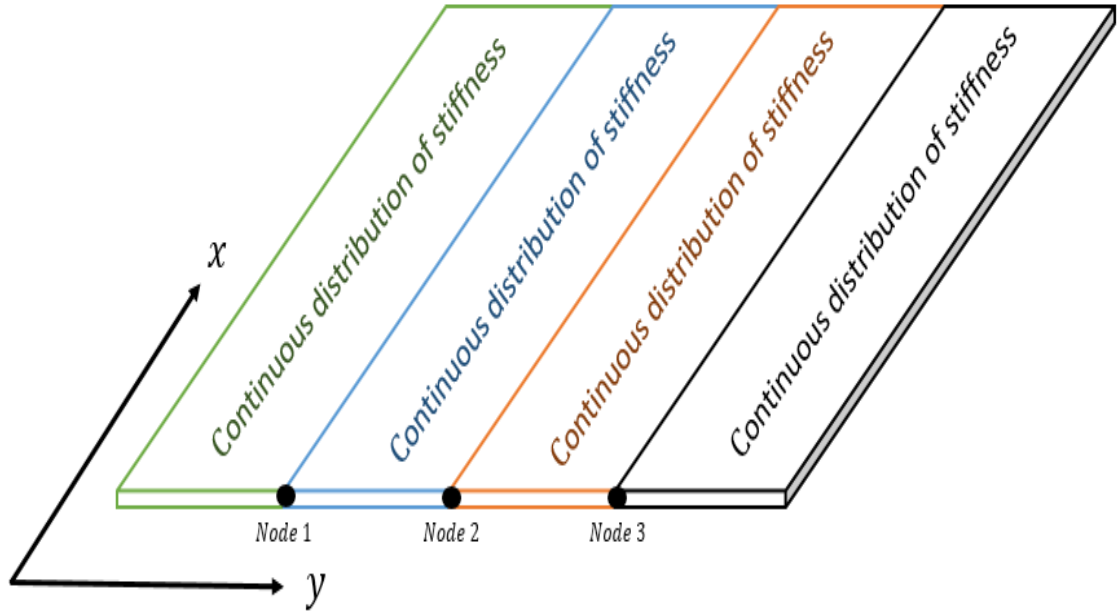


Figure 2-1: Modelling a plate with differing properties in the y direction using VICONOPT.

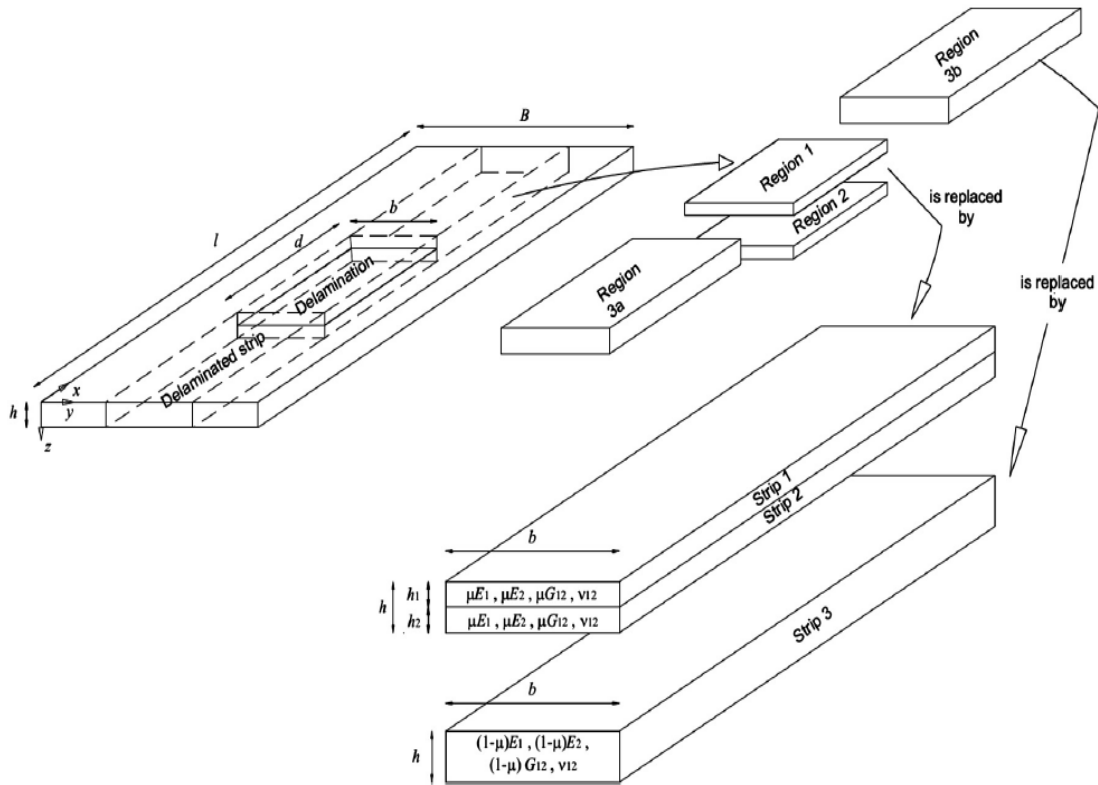


Figure 2-2: Sketch of VICONOPT model for a laminate of length l , width B and thickness h , having an embedded rectangular delamination of length $d (= \mu l)$ and width b , (Figure reproduced from Damghani et al. (2014)).

Chapter 2: Literature review

This approach, called the Smeared Method (SM), is capable of representing the global buckling behaviour. However, it predicts conservative local behaviour in some cases and cannot capture local effects in others due to the way in which the damage is modelled.

3 VICONOPT and Exact Strip Method

VICONOPT (VIpasa with CONstraints and OPTimization) as outlined previously, is a computer program that incorporates the earlier programs VIPASA[42] and VICON [45]. Williams et al. [43] summarized the key features of VICONOPT for both buckling and vibration analysis. It is designed for efficient, accurate buckling and vibration analysis and optimum design of prismatic plate assemblies. Typical applications are the metal and composite stiffened panels used in aircraft wing and fuselage panels. The program is based on the exact strip method, which assumes a continuous distribution of stiffness and mass over the structure.

More details in relation to both the exact strip method and the program VICONOPT are given in the following sections.

3.1 VICONOPT

VICONOPT covers the buckling and vibration behaviour of any prismatic assembly of anisotropic plates with Figure 3-1 showing some typical cross sections. Each plate can be subjected to a uniform longitudinal compressive force N_L , a transverse compressive force N_T and an in-plane shear flow N_S (all defined as stress resultants, or force per unit width) as shown in Figure 3-2. For any combination of N_L , N_T and N_S , critical buckling loads, undamped natural frequencies and the corresponding mode shapes can be found, more details are included in sections 3.2 and 5.2 . Due to using procedures based on the Wittrick–Williams algorithm these outputs come with certainty [51].

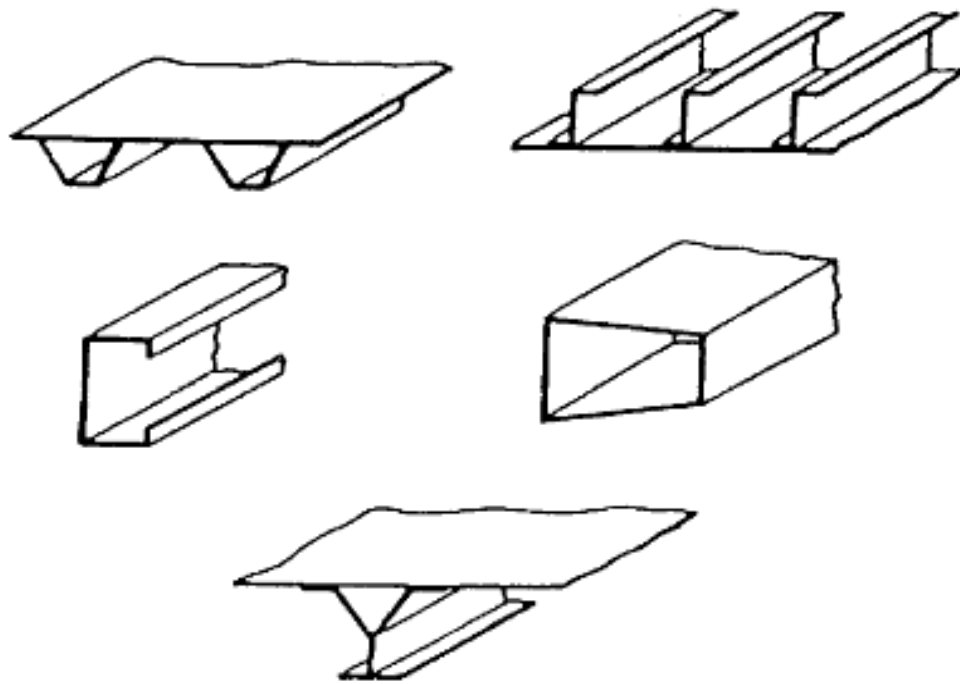


Figure 3-1 Some typical structures, which VICONOPT can analyse [42]

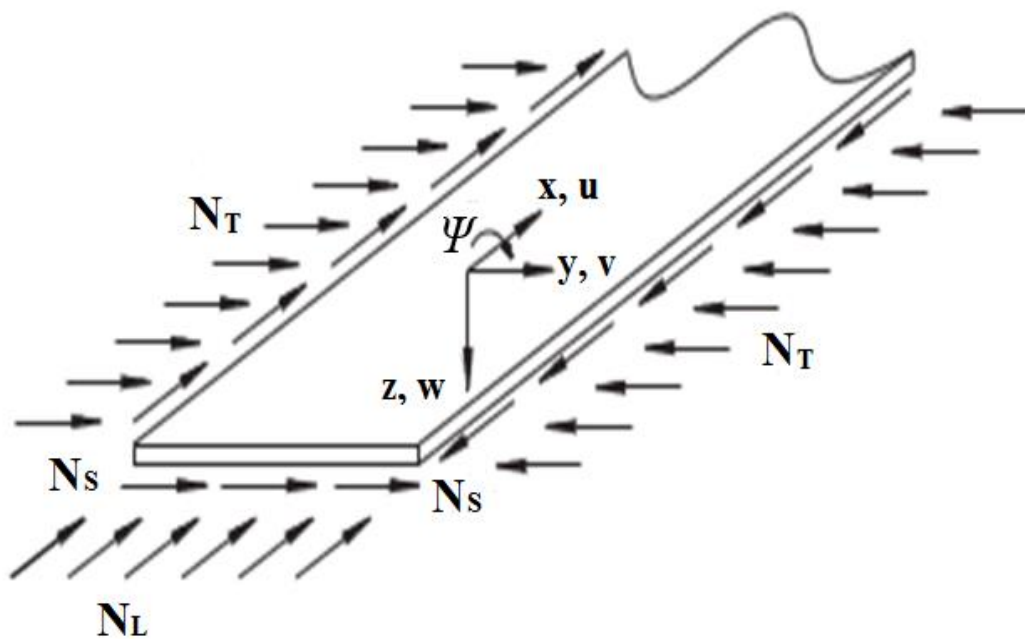


Figure 3-2 Component plate with a combination of in-plane loading [43]

The analysis option of VICONOPT allows the assembly of laminated composite plates from any sequence of arbitrarily oriented orthotropic plies. Normally, the composite laminates are made of on-axis and off-axis plies. The data needed for the program to model such composite laminates are the material properties, orientations, thicknesses and properties of the plies.

3.2 Exact Strip Method

VIPASA is a powerful program for the accurate analysis of vibration and buckling of prismatic plate assemblies. VIPASA analysis uses the stiffness matrix method based on exact flat plate theory [42]. However, if the plate carries in-plane shear loading, the mode shapes will be skewed and the desired support conditions will not be satisfied. In fact, this imposes a limitation on the general applicability of VIPASA. Anderson, et al. [45] presented a solution to this problem, denoted VICON, by coupling the VIPASA stiffness matrices for different wavelength responses using the Lagrangian Multipliers Method. Supports at arbitrary locations, including simply supported ends and supports provided by an elastic supporting structure are included in this solution. The complete generality and capability of VIPASA were retained in the VICON program [45]. Like VIPASA, VICON uses exact strip analysis in which the continuous distribution of stiffness and mass over the structure is assumed. The way that the Lagrangian Multipliers are incorporated for finding exact natural frequencies or critical buckling loads is detailed by Williams and Anderson [52] and relevant parts are summarised in Section 5.2 below. However, Table 3-1 summarizes of the advantage and limitation of the exact strip method against the finite element method.

The use of exact strip theory in free vibration or critical buckling analysis yields transcendental eigenproblems which cannot be solved by the linear eigensolvers employed in finite element analysis. Instead, the Wittrick-Williams (W-W) algorithm [53-55] is used in VIPASA and VICON for finding all the required natural frequencies or critical load factors. In its simplest form, the W-W algorithm may be stated as [42]

$$J = J_0 + s\{\mathbf{K}\} \quad (3.1)$$

where J is the number of eigenvalues which lie between 0 and a specified trial frequency or load factor. $s\{\mathbf{K}\}$ is known as the sign count of the transcendental stiffness matrix \mathbf{K} and is found by counting the number of negative elements on the leading diagonal of \mathbf{K}^Δ , the matrix formed from \mathbf{K} by performing Gauss elimination without scaling or row interchanges. J_0 is the value J would have if the components of the displacement vector were all clamped and can often be determined analytically.

Table 3-1 Capability comparison of exact strip method against finite element method

Exact strip method	Finite element method
No discretization of plates	Each plate is discretized into many elements
Internal displacements found exactly	Internal displacements depend on shape functions
Small, transcendental eigenproblem	Large, linear eigenproblem
Wittrick-Williams algorithm	Standard methods of solution
Restricted to prismatic geometry and loading	Applicable to irregular geometries and loading
Fast solution times	Slower solution times

3.2.1 VIPASA analysis

VIPASA is based on the assumption that all the components of displacement (i.e. u , v , w and ψ in Figure 3-2 vary sinusoidally along any longitudinal line with a half-wavelength λ . Simply supported end conditions are modelled by choosing values of λ which divide exactly into the panel length l . Figure 3-3 shows the perturbation edge forces and displacements, and the nodal lines, of a plate during buckling or vibration.

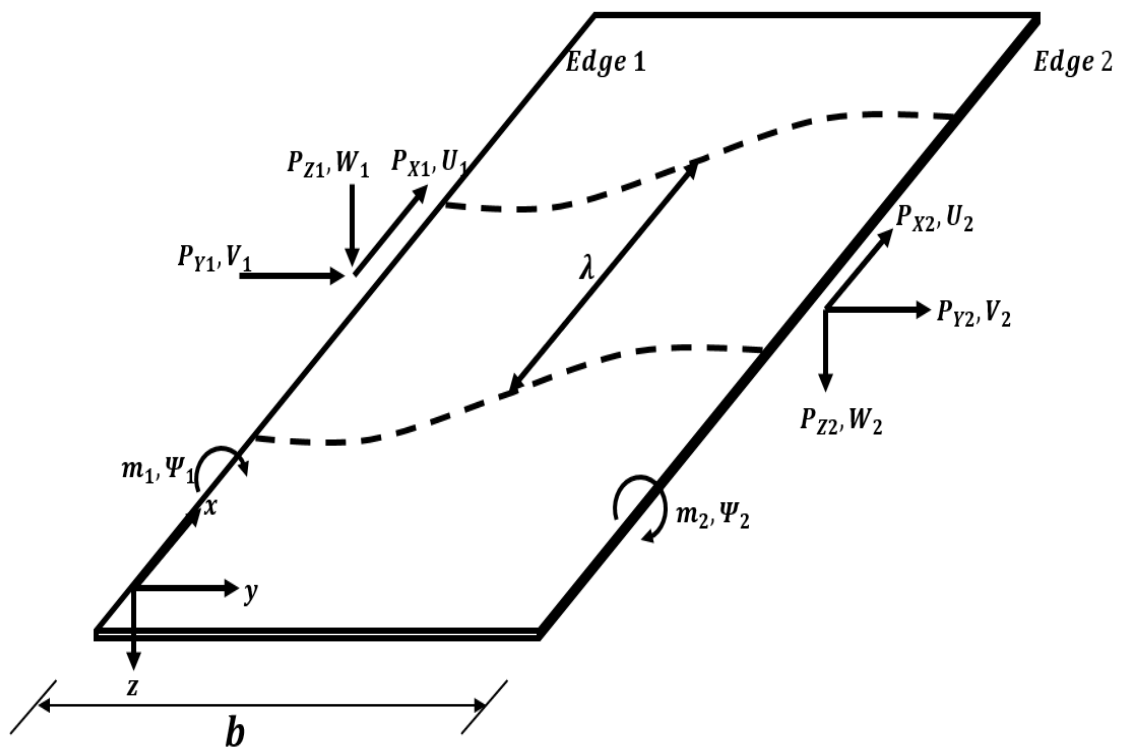


Figure 3-3 Perturbation edge displacements, and nodal lines of a plate.

All edge forces and displacements are to be multiplied by $\exp(i\pi x / \lambda) * \cos(2\pi n t)$, where n is the frequency and t is time. Wittrick and Williams [42] split the sinusoidal forces and displacements acting at the edge of a

component plate structure into uncoupled out of plane and in plane deformations where the elastic properties of each one are defined by the following equations:

$$\begin{bmatrix} m_x \\ m_y \\ m_{xy} \end{bmatrix} = - \begin{bmatrix} D_{11} & D_{12} & D_{13} \\ D_{12} & D_{22} & D_{23} \\ D_{13} & D_{23} & D_{33} \end{bmatrix} \begin{bmatrix} \kappa_x \\ \kappa_y \\ 2\kappa_{xy} \end{bmatrix} \quad (3.2)$$

$$\begin{bmatrix} n_x \\ n_y \\ n_{xy} \end{bmatrix} = - \begin{bmatrix} A_{11} & A_{12} & 0 \\ A_{12} & A_{22} & 0 \\ 0 & 0 & A_{33} \end{bmatrix} \begin{bmatrix} \varepsilon_x \\ \varepsilon_y \\ \gamma_{xy} \end{bmatrix} \quad (3.3)$$

where m_x and m_y are the bending moments and m_{xy} is the twisting moments. κ_x and κ_y are the curvatures and κ_{xy} is the twist. n_x, n_y, n_{xy} and $\varepsilon_x, \varepsilon_y, \gamma_{xy}$ are the membrane force and the membrane strains respectively. **A** and **D** are elements of membrane and out-of-plane bending stiffness matrices. Figure 3-3 details the sign conventions for both bending moments and membrane forces.

A total of four degrees of freedom for each nodal line are illustrated in Figure 3-3, where u and v are the in-plane displacements in the x and y directions respectively, while w and Ψ are the out-of-plane displacement in the z direction and rotation about the x direction respectively. Vectors of perturbation displacements \mathbf{d}_j , perturbation forces \mathbf{p}_j and stiffness matrices \mathbf{k} are defined by the equations [42]

$$\mathbf{p}_j = \{m_j \ p_{zj} \ p_{yj} \ p_{xj}\} \quad (j = 1,2) \quad (3.4)$$

$$\mathbf{d}_j = \{\Psi_j \ w_j \ v_j \ u_j\} \quad (j = 1,2) \quad (3.5)$$

$$\mathbf{p} = \mathbf{k} \mathbf{d} \quad (3.6)$$

where

$$\mathbf{p} = \{\mathbf{p}_1 \quad \mathbf{p}_2\}^T, \quad \mathbf{d} = \{\mathbf{d}_1 \quad \mathbf{d}_2\}^T, \quad (3.7)$$

$$\mathbf{k} = \begin{bmatrix} \mathbf{k}_{11} & \mathbf{k}_{12} \\ \mathbf{k}_{21} & \mathbf{k}_{22} \end{bmatrix} \quad (3.8)$$

Although this analysis does not cover coupling between the in-plane and out-of-plane displacements, subsequent developments in VICONOPT can automatically handle coupled cases using a numerical procedure [56, 57], allowing completely general composites with fully populated **A**, **B** and **D** stiffness matrices to be considered.

3.2.2 VICON analysis

As mentioned the key difference between VICON and VIPASA is that VICON introduces Lagrangian multipliers to couple the responses at different values of half-wavelength λ . This approach expresses the deflection of the plate assembly as a Fourier series involving an appropriate set of λ [45]. The results given by VICON are for an infinitely long plate assembly, with supports which repeat at longitudinal intervals of the length l .

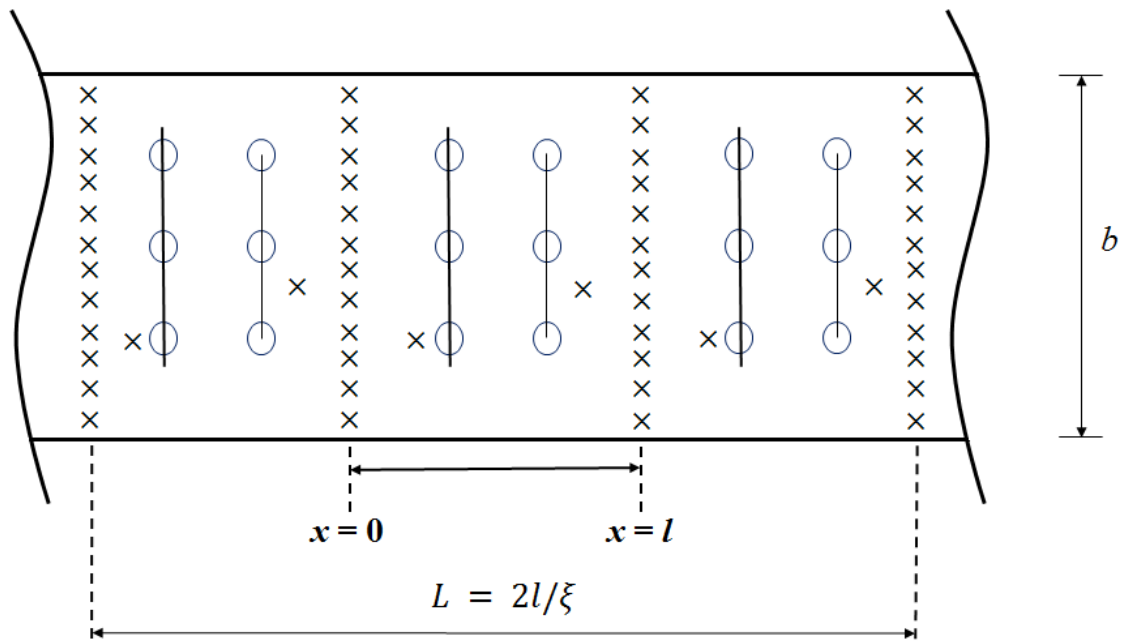


Figure 3-4: Illustration of the infinitely long structure [58].

Figure 3-4 is an illustration of a plan view of a plate assembly for an infinitely long structure repeating at intervals of l . Crosses denote point supports and circles denote points of attachment to a transverse supporting structures. Mode shapes are assumed to repeat over a length $L = 2l/\xi$, for some value of the parameter ξ lying in the range $0 \leq \xi \leq 1$. More details of the equations used in VICON are given in section 5.2.

4 Modelling the effect of damage on the critical buckling of composite plates using VICONOPT

VICONOPT, based on the exact strip method, is a powerful tool that performs buckling and vibration analysis and optimum design for any assembly of composite plates with prismatic properties [56]. Damghani [49] demonstrated the reliability of the exact strip method in studying the buckling behaviour of perfect composite plates and laminates with through-the-length delamination and the results are verified against results obtained from finite element method (ABAQUS).

This chapter outlines work carried out to investigate the effect of the size, depth and ply orientation of through-the-length and through-the-width delamination and single and multiple through-the-length delaminations on the critical buckling load and mode shape of a plate structure. An investigation is made on the effect of in-depth delamination with respect to the ply orientations of the top and bottom parts of the delamination and the in-plane force system on the buckling behaviour of composite plates. No previous study has been found which investigates the effect of in-depth damage on buckling capability. VICONOPT is used to perform a series of parametric studies in which delaminated composite plates are modelled for the cases of single and multiple delaminations at the same and varying depth. A study examining the effect of through-the-width delaminations on the global buckling load is then presented.

4.1 The effect of ply orientation on the critical buckling load and buckling mode shape

Many factors can affect the critical buckling load and mode shape of laminated composite plates. For example, both the orientation and the layup sequence (symmetric or antisymmetric) of the plies can significantly influence the buckling load. Featherston and Watson [59] studied the effect of varying ply orientation on the buckling load of a series of flat plates, in order to determine the optimum design for a symmetrical, balanced lay-up, under shear and in-plane bending. Lee and Park [19] studied the effect of the stacking sequence on the buckling load of a laminated plates having different through-the-width delamination sizes using enhanced assumed strain (EAS) three-dimensional finite element (FE) formulation. Many other researchers have studied ply orientation and its effect on the critical buckling loads of both damaged and perfect composite plates using different techniques and tools [60-65].

In this section, perfect and delaminated composite plates are analysed using VICONOPT. These plates are simply supported on all four sides (*SSSS*). Boundary conditions are satisfied exactly along the plate edges $y = 0$ and $y = b$. By coupling the sinusoidal buckling response using Lagrangian multipliers, the VICON analysis option of VICONOPT satisfies the boundary conditions at specified points along the ends $x = 0$ and $x = l$, see Figure 3.4. The plates considered are subjected to a longitudinal compressive force N_L . By subjecting the plate to a longitudinal compressive force it is possible to determine how and in what way the ply orientation affects the buckling load and the buckling mode shape. This section starts by analysing the effect of the plate's ply orientation in relation to the direction of the load applied on the critical

buckling load and the buckling mode shape of a perfect plate. The work is then extended to study the local buckling loads and mode shapes of plates containing through-the-length and through-the-width delaminations at various depths. The aim of analysing this kind of delamination is to investigate the relationship between the critical buckling load and mode shape and the ply orientations of the top and bottom parts of the delaminated plate.

The more general case of embedded delaminations will be considered in chapter 5 where the study will be extended to looking at the highly interrelated problem of predicting the natural frequencies of the plate and the effect of delamination damage on these frequencies.

4.1.1 Perfect composite plate

In this section, a symmetric 16 ply composite plate of length $l = 100$ mm, width $b = 100$ mm, and thickness of $h = 2$ mm having a number of different stacking sequences is studied. The material properties of each ply are: Young's modulus $E_1 = 130$ kN mm⁻² and $E_2 = 10$ kN mm⁻², shear modulus $G_{12} = 10$ kN mm⁻² and Poisson's ratio $\nu_{12} = 0.3$. The plies have a thickness of 0.125 mm and symmetric stacking sequences. Table 4-1 details seven cases of plates with different ply orientations (with 0° corresponding to the longitudinal direction (x in Figure 4-1)). The plates are examined to study the effect of these stacking sequences on the critical buckling load and mode shape.

Table 4-1: Different cases of stacking sequences

<i>Case number</i>	Ply orientations
1	$[0^0 / 0^0 / 0^0 / 0^0 / 0^0 / 0^0 / 0^0 / 0^0]_s$
2	$[45^0 / 45^0 / 45^0 / 45^0 / 45^0 / 45^0 / 45^0 / 45^0]_s$
3	$[90^0 / 90^0 / 90^0 / 90^0 / 90^0 / 90^0 / 90^0 / 90^0]_s$
4	$[-45^0 / 45^0 / -45^0 / 45^0 / -45^0 / 45^0 / -45^0 / 45^0]_{-s}$
5	$[0^0 / 45^0 / -45^0 / 90^0 / 0^0 / 45^0 / -45^0 / 90^0]_s$
6	$[90^0 / 45^0 / -45^0 / 0^0 / 90^0 / 45^0 / -45^0 / 0^0]_s$
7	$[90^0 / 45^0 / -45^0 / 0^0 / 90^0 / 45^0 / -45^0 / 90^0]_s$

In order to calculate the critical buckling load, the load factors for ten half-wavelengths, i.e. values of λ , are checked. In the VIPASA option of VICONOPT the ten half-wavelengths would be $\lambda = l/1, l/2, l/3 \dots l/10$. In the VICON option they would be for ten different ξ values, the first being $\xi = 1$, the second $\xi = 0$ and the remainder being equally spaced between 0 and 1. If the load factor is F_C , the trial axial load is P_A and the plate width is b , equation (4.1) can be used to calculate the critical buckling force intensity resultant.

$$N_{xc} = \frac{F_C \times P_A}{b} \text{ (Nmm}^{-1}\text{)} \quad (4.1)$$

The lowest load factor from the wavelengths checked is the one that is needed to calculate the critical buckling force intensity N_{xc} . The corresponding buckling half-wavelength λ relates to the buckling mode shape.

Table 4-2 presents the critical buckling force intensities and the contour plots of the associated critical buckling modes for unidirectional laminates with lay-ups as defined in cases 1, 2 and 3 in Table 4-1. The table shows that the ply orientations in case 2 result in the largest critical buckling force intensity of 133.40 N/mm. The critical buckling force intensities for cases 1 and 3 in relation to those for case 2 are about 18% and 51% lower respectively. The buckling half-wavelength λ refers to the buckling mode shape obtained from VIPASA analysis and ξ refers to the buckling mode shape obtained from using VICON analysis. The plate comprising all 0° plies (case 1) buckles at $\lambda = l$ while, the plate of 90° plies (case 3) buckles at $\lambda = l/2$. Case 2, where the plies are orientated at 45° , buckles at $\xi = 1$. However, moving the orientation angle of the plies in case 3 toward 90° changes the buckling half-wavelength λ from $\lambda = l$ to $\lambda = l/2$.

Table 4-3 illustrates the critical buckling force intensities and the buckling wavelengths of the ply orientations defined in cases 4, 5, 6 and 7. Due to the symmetrical, balanced nature of the ply orientations in these plates the table shows that all four cases buckle with $\lambda = l$. The plate with plies orientated according to case 4 has the highest critical buckling stress (182.46 Nmm^{-1}) of all seven cases. cases 5, 6 and 7 have almost the same critical buckling stress due to the minor differences in their ply orientations.

Table 4-2: Critical buckling stresses and buckling wavelengths for plate cases 1, 2 and 3.

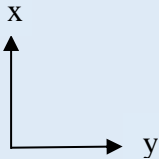
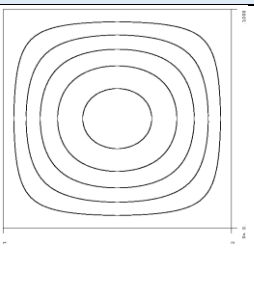
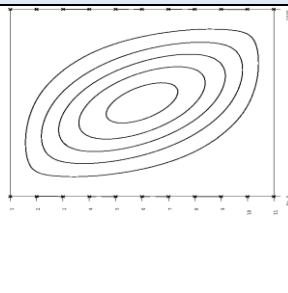
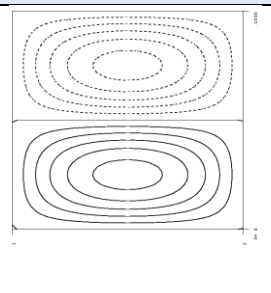
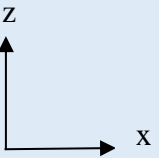
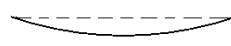
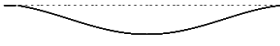

VICONOPT	Case 1	Case 2	Case 3
N_{xc} (Nmm ⁻¹)	109.88	133.40	65.16
			
	 $\lambda = l$	 $\xi = 1$	 $\lambda = l/2$

Table 4-3: Critical buckling stresses and buckling wavelengths for plate cases 4, 5, 6 and 7.

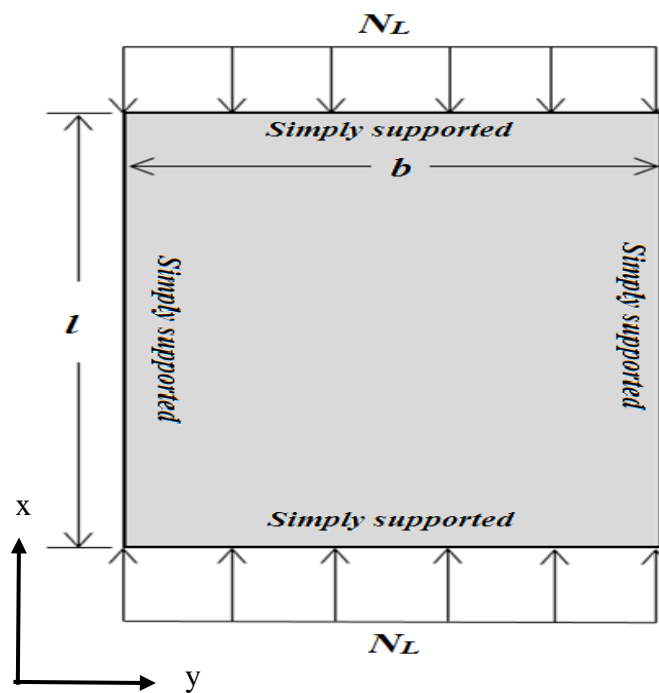
VICONOPT	Case 4	Case 5	Case 6	Case 7
N_{xc} (Nmm ⁻¹)	182.46	145.00	145.32	145.36
$\lambda =$	1	1	1	1

4.1.2 Composite plates with through-the-length and through-the-width delaminations

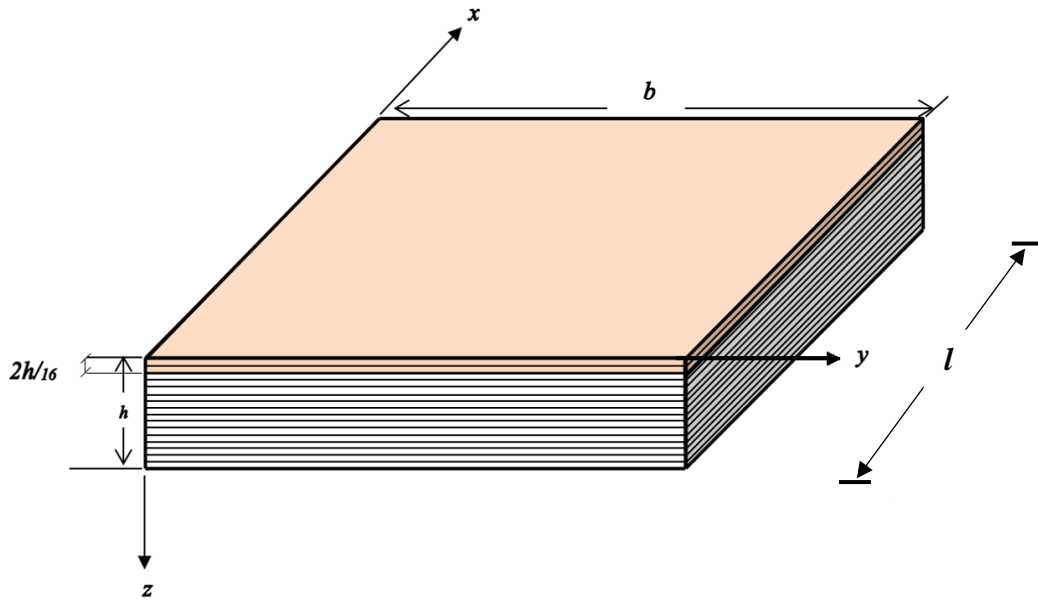
Plates with the same ply properties and plate dimensions as those used in the previous section were then used to explore the effect of through-the-length and through-the-width delaminations. Again, the plates were assumed to be simply supported on all four edges and subjected to a longitudinal compressive force as shown in Figure 4-1

(a). They were assumed to have a single through-the-length and through-the-width delamination. The effect of introducing this delamination at different depths was studied, at locations of $h/16$, $h/8$, $h/4$, $3h/8$ and $h/2$ below the top surface, i.e. between the 1st and 2nd, 2nd and 3rd8th and 9th plies of the laminate. Figure 4-1 (b) illustrates the case where the delamination is at a depth of $h/8$.

In each case it was found that the upper plate only buckles, at all depths except when the delamination is located half way through the thickness of the plate ($h/2$). At this depth, both plates buckle at the same time but in opposite directions due to the symmetry of the layup about the mid-plane as shown in Figure 4-2.



(a)



(b)

Figure 4-1 Ply composite plate (a) the boundary conditions of the plate and the external load applied (N_L) (b) the plate with a single full width through-the-length delamination at a depth of $2h/16$.

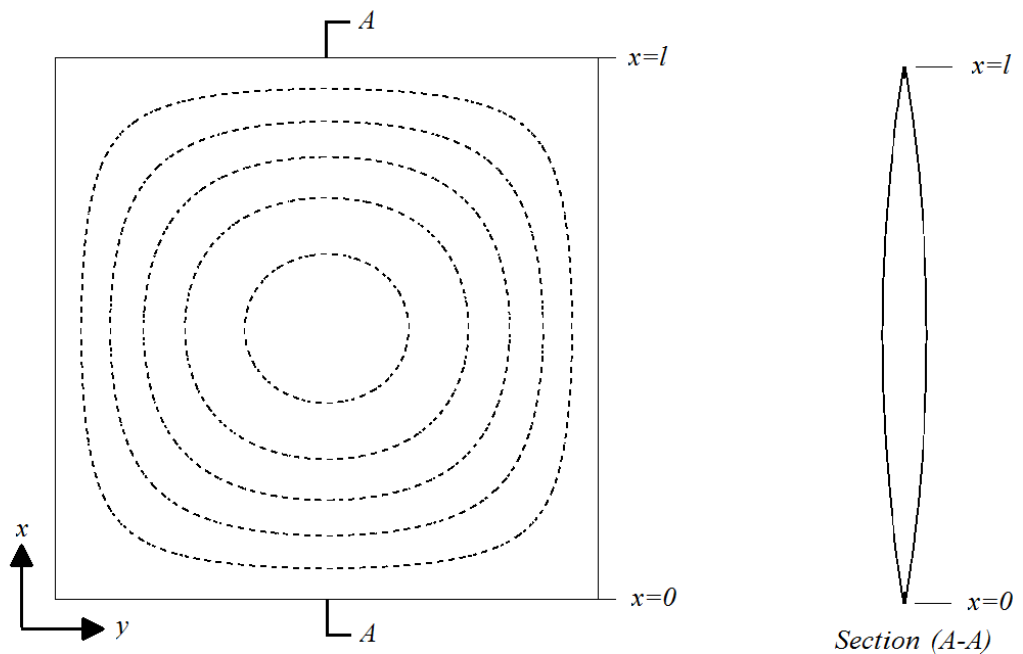


Figure 4-2 First natural frequency mode shape of a plate with through-the-length and through-the-width delamination located at the mid thickness.

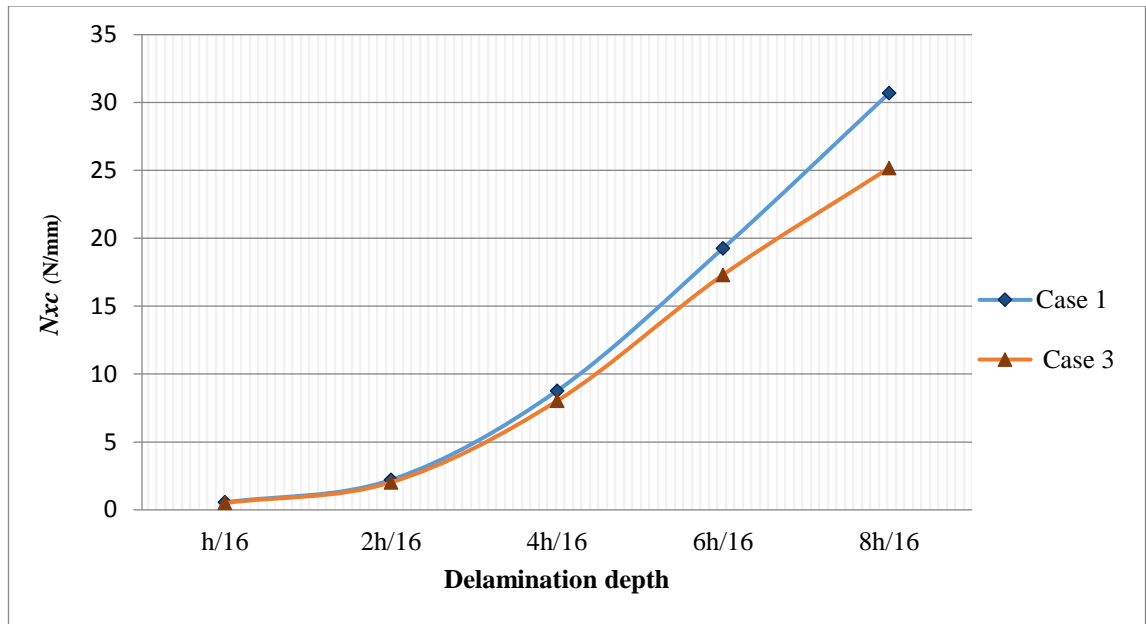


Figure 4-3: Critical buckling force intensities for plates with ply orientation for plate cases 1 and 3 and different delamination depths.

Figure 4-3 shows that the relationship between the depth of the delamination and the buckling load for plates with lay-ups according to cases 1 and 3. As well as the increase in buckling load which occurs with increased depth due to the increased stiffness of the locally buckling upper section, it can be seen that the difference in critical buckling force intensities between cases 1 and 3 increases as the delamination moves towards the mid-thickness of the plate. It can be concluded that, when the delamination is close to the surface the buckling force intensity is actually the buckling load of the thinner laminate portion of the laminate, which is the lowest. However, the rest of the plate is much thicker and capable of carrying much higher load. When the delamination is located at the mid thickness ($8h/16$), the thickness of the two parts of laminate is equal and larger, and so the buckling force intensity is higher than the other cases of delamination depths. In this work, no contact was modelled between the two parts of the laminate.

Figure 4-4 presents the same relationships for plates with the ply orientations defined for cases 4, 5, 6 and 7. Again it can be seen that the critical buckling load of the delaminated plates increases as the delamination is moved toward the mid-thickness of the plate. The increasing rate at which the critical buckling force intensity changes as the delamination moves deeper is also demonstrated. This is as expected since the flexural stiffness of the locally buckling upper plate is proportional to the cube of its thickness which effectively increases as the delamination moves towards the centre, directly affecting its critical buckling force intensity. Figure 4-4 also demonstrates the significant effect that the ply orientations of the delaminated part have on the value of the critical buckling load. For instance, the plate case 5 $[0^0/45^0// -45^0/90^0/0^0/45^0/-45^0/90^0]_S$ has a critical buckling force intensity of 1.35 N/mm when the full width delamination is located at a depth of $2h/16$. In this case, the delaminated part consists of the two plies 0^0 and 45^0 . However, the plate case 6 $[90^0/45^0// -45^0/0^0/90^0/45^0/-45^0/0^0]_S$ has a critical buckling force intensity of 6.80 N/mm when the full width delamination is located at the same depth resulting in the delaminated part consisting of the two plies 90^0 and 45^0 . The critical buckling force intensity of the delaminated plate case 6 is therefore five times the critical bulking force intensity of the delaminated plate case 5 under the same conditions. This is due to the fact that the proportion of the load carried by the outer two plies is significantly reduced since the 0^0 ply which attracts a much higher load than the 90^0 ply is now moved to the lower plate. Noting that the two cases, 5 and 6, are similar in their ply orientations and the stacking sequences of the plies at 45^0 and -45^0 , they differ only in the stacking sequence of the plies, 0^0 and 90^0 , being swapped. This can have a significant effect

when the delaminated region contains only a small number of plies for instance the case here.

In summary, in terms of the critical buckling load of a composite plate, it can be concluded that combining on-axis and off-axis plies enhances the stiffness of the whole plate. The optimum layup sequence depends on which of the in-plane force systems is applied.

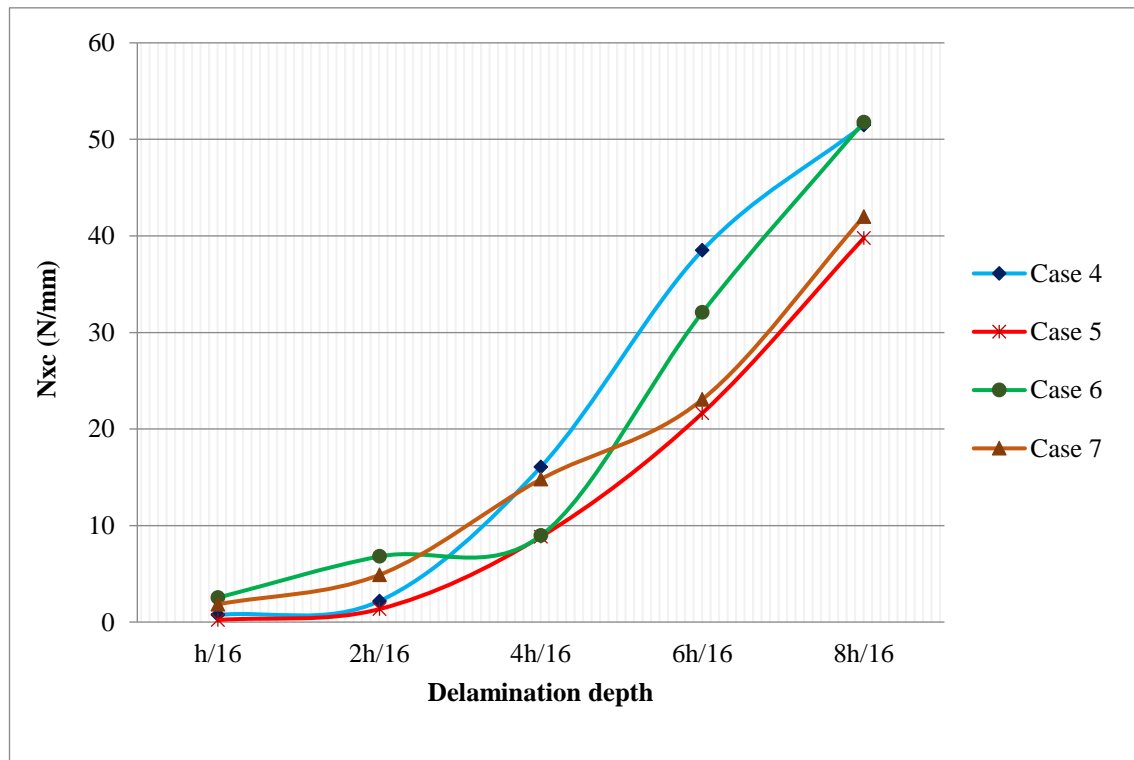


Figure 4-4 Critical buckling force intensities for plates with ply orientations for plate cases 4, 5, 6 and 7 and different delamination depths.

4.1.3 The effect of the ply orientations on the critical buckling mode shape

The effect of the ply orientation on the buckling mode shape is investigated for all seven plate cases. As mentioned previously, the buckling half-wavelength λ corresponding to the lowest load factor F_C refers to the critical buckling mode shape.

The relationship between the critical buckling force intensity, the delamination depth and the buckling half-wavelength λ can be plotted using equation 4.1. For all cases the buckling half-wavelengths (λ) $1/5, 1/6, 1/7, 1/8, 1/9, 1/10$ have been excluded from Figure 4-5 to Figure 4-10 because they are far from being critical.

From Figure 4-5 the plate $[0^\circ/0^\circ/0^\circ/0^\circ/0^\circ/0^\circ/0^\circ/0^\circ]_s$ can be seen to buckle at $\lambda = l$ for all delamination depths. The laminate $[90^\circ/90^\circ/90^\circ/90^\circ/90^\circ/90^\circ/90^\circ/90^\circ]_s$ on the other hand, buckles at $\lambda = l/3$ for the majority of delamination depths with the exception of the case when the delamination occurs at the middle of the plate thickness at $h/8$ when the plate buckles at $\lambda = l/2$, see Figure 4-6.

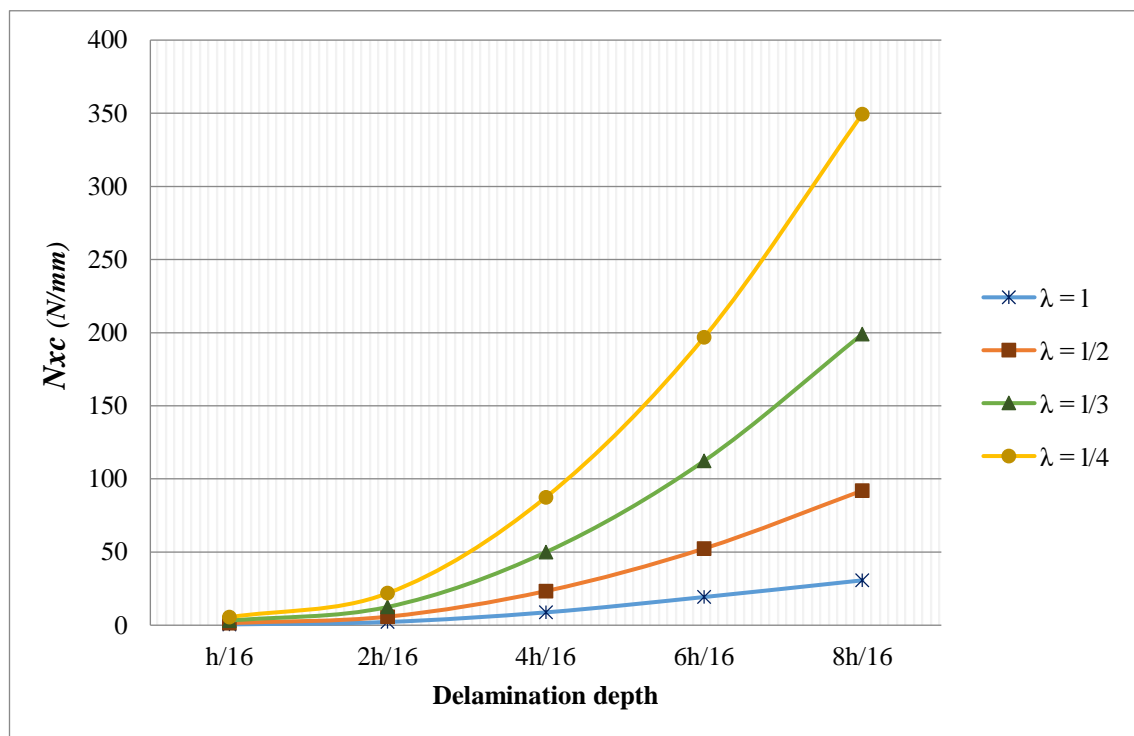


Figure 4-5: The relationship between critical buckling force intensities and delamination depth for different buckling half-wavelengths λ (and hence mode shapes) for plate case 1.

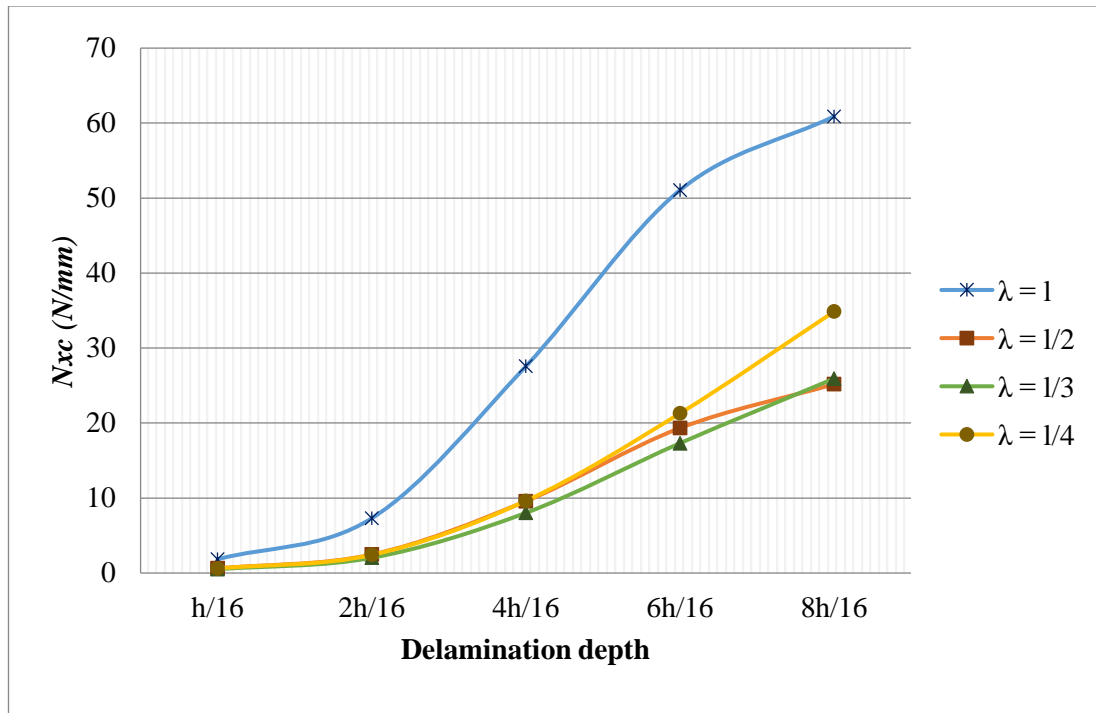


Figure 4-6: The relationship between critical buckling force intensities and delamination depth for different buckling half-wavelengths λ (and hence mode shapes) for plate case 3.

Figure 4-7 shows that the plate case 4 $[-45^\circ / 45^\circ / -45^\circ / 45^\circ / -45^\circ / 45^\circ / -45^\circ / 45^\circ]_s$ buckles with $\lambda = 1$ when the delamination is at $h/8$ and at $\lambda = 1/2$ when the delamination occurs anywhere else through the thickness. In Figure 4-8, the laminate for plate case 5 $[0^\circ / 45^\circ / -45^\circ / 90^\circ / 0^\circ / 45^\circ / -45^\circ / 90^\circ]_s$ buckles with $\lambda = 1$ when the delamination is located at $h/16$, $h/8$, $3h/8$ or $h/2$, while it buckles with $\lambda = 1/2$ when the delamination is at a depth of $4h/16$. From Figure 4-9 the $[90^\circ / 45^\circ / -45^\circ / 0^\circ / 90^\circ / 45^\circ / -45^\circ / 0^\circ]_s$ laminate (case 6) with a delamination depth of $h/16$ buckles at $\lambda = 1/3$, but with delamination depths of $h/8$, $h/4$ or $6h/16$ buckles at $\lambda = 1/2$ and with a delamination depth of $h/2$ buckles at $\lambda = 1$. In Figure 4-10 the plate $[90^\circ / 45^\circ / -45^\circ / 90^\circ / 0^\circ / 45^\circ / -45^\circ / 90^\circ]_s$ buckles at a wavelength of $1/3$ when the delamination is located at a depth of $h/16$ or $h/4$, while it buckles at a wavelength of $1/2$ if the delamination depth is $h/8$, $3h/8$ or $h/2$.

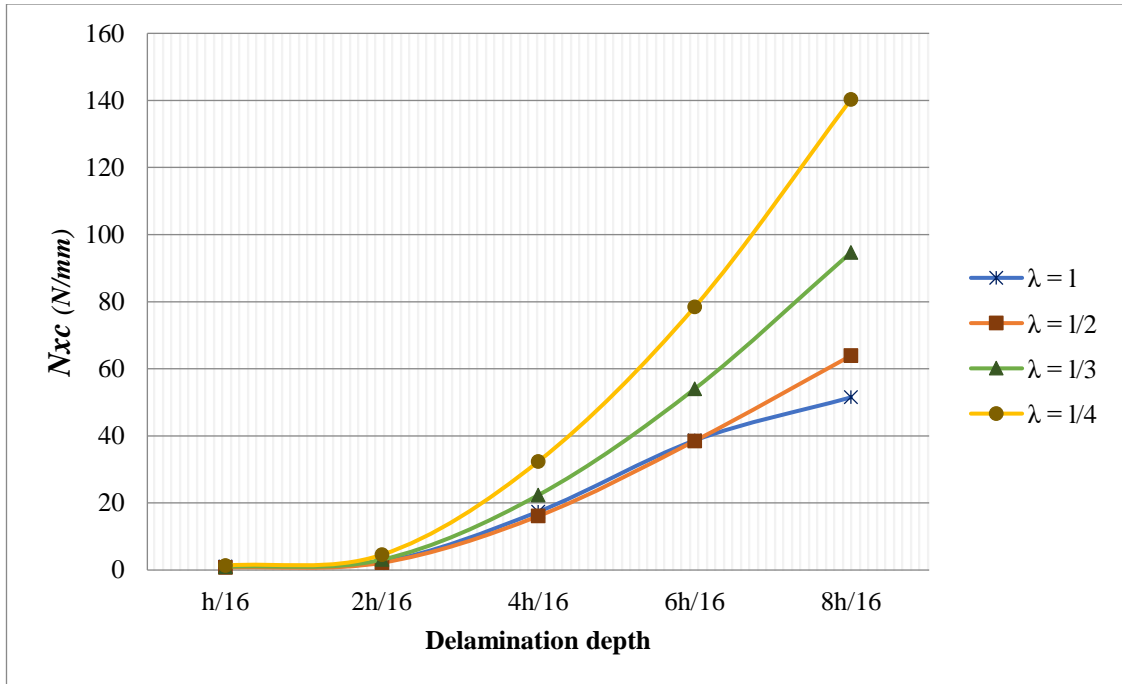


Figure 4-7: The relationship between critical buckling force intensities and delamination depth for different buckling half-wavelengths λ (and hence mode shapes) for plate case 4.

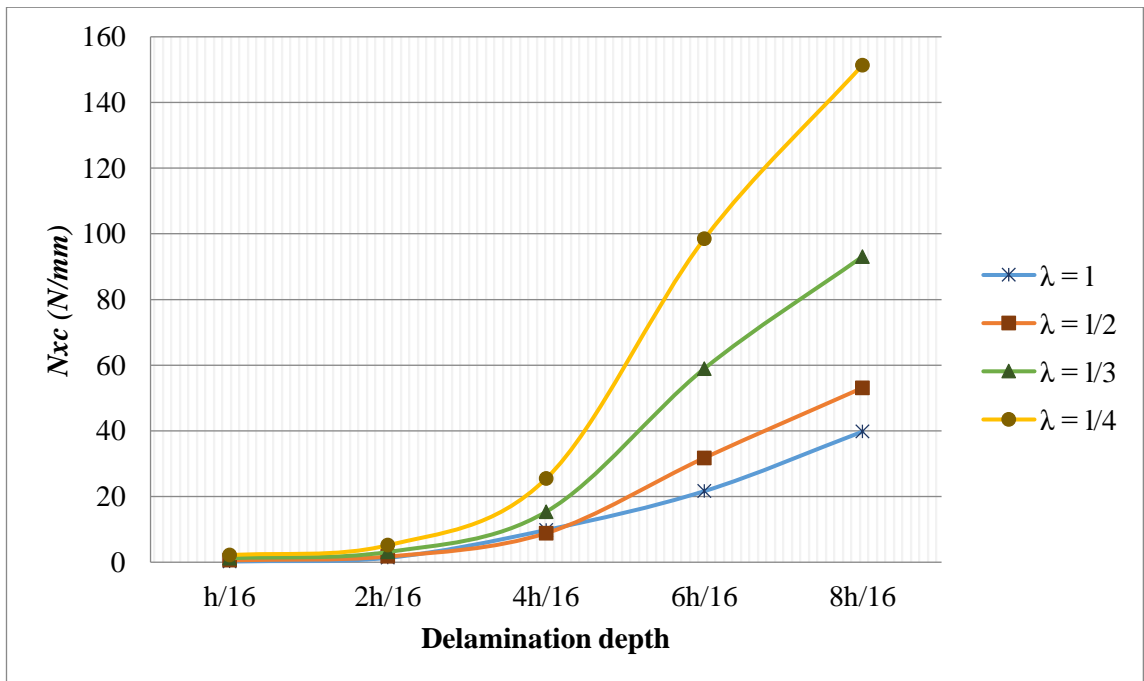


Figure 4-8: The relationship between critical buckling force intensities and delamination depth for different buckling half-wavelengths λ (and hence mode shapes) for plate case 5.

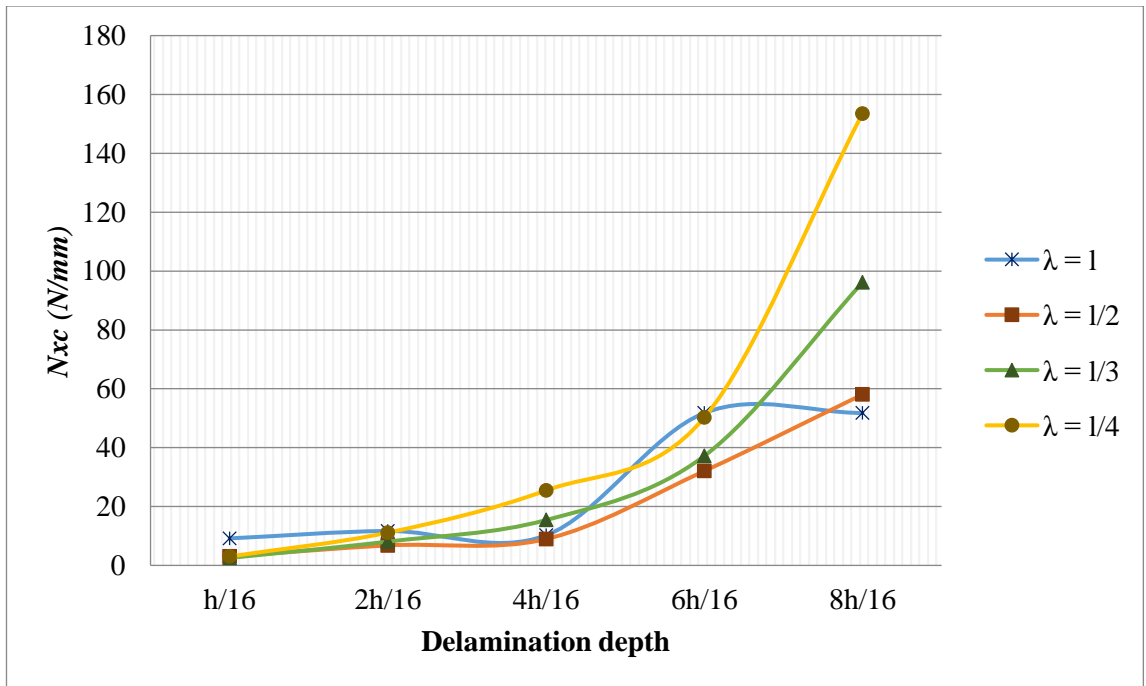


Figure 4-9: The relationship between critical buckling force intensities and delamination depth for different buckling half-wavelengths λ (and hence mode shapes) for plate case 6.

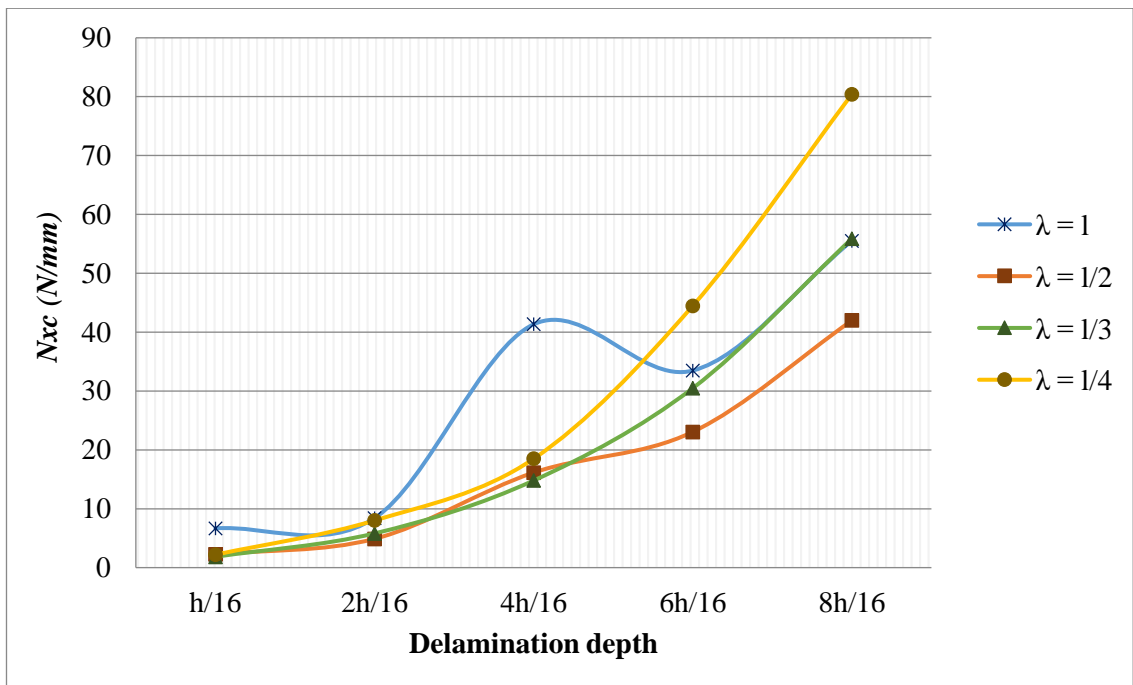


Figure 4-10: The relationship between critical buckling force intensities and delamination depth for different buckling half-wavelengths λ (and hence mode shapes) for plate case 7.

It can be seen from these results that there are two factors which affect the way that a laminated plate buckles. The first of these is the ply orientation with respect to the in-plane loads. The other is the boundary conditions of the delaminated layer. It can be seen that the boundary conditions at the edges of the delaminated layer change from being clamped to simply supported depending on the depth of the delamination and hence the thickness of the delaminated layer relative to the remaining plate. When the delaminated layer has a thickness less than the thickness of the remaining structure, the edges are effectively clamped. However, when the delamination occurs at the mid-thickness of the plate the boundaries of the two identical plates are simply supported, see Figure 4-2.

4.2 Modelling delaminated composite plates

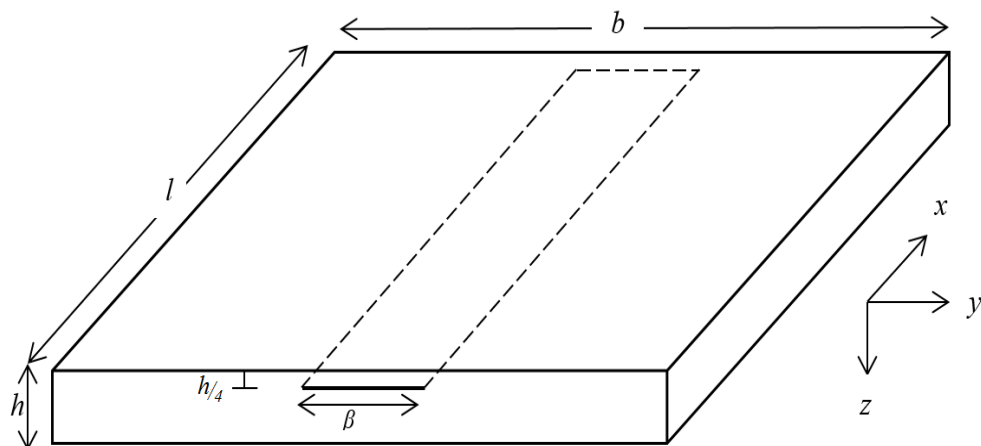
In this section several configurations of delaminated laminates have been considered, all consisting of 16 plies oriented at $[0^\circ/45^\circ/-45^\circ/90^\circ/0^\circ/45^\circ/-45^\circ/90^\circ]_s$ and having material properties as presented in section 4.1.1. The effect of through-the-length multi-delamination zones on the critical buckling load is studied. The first case considered is that of multiple delamination zones all located at the same depth, having equal delamination widths β and spaced equally. This case will be compared with a single mid-width delamination at the same depth and with the same delamination width for every delamination width studied. The second case looks at the effect of mid-width delamination zones which occur simultaneously at varying depths. The results will be compared with plates having single mid-width delaminations with the same delamination width for every delamination width studied.

4.2.1 Example 4.1: Single and multiple delaminations at the same depth

The geometry of the plate analysed in this work had a thickness $h = 2$ mm, length $l = 100$ mm and width $b = 100$ mm. Figure 4-11 (a) shows the plate with a single mid-width delamination of width β at a depth of $h/4$. In Figure 4-11 (b) the same plate is modelled with multiple delaminations at the same depth $h/4$ each having the same width β .

The relationship between the delamination ratio β/b and the critical buckling force intensity is presented in Figure 4-12. The plots show that the critical buckling force intensities are almost equal for both delamination cases (a) and (b) for $\beta/b \leq 0.3$. In this interval of delamination sizes, plates with delamination case (a) buckle locally and plates with delamination case (b) show local buckling of all delaminated regions at the same load. For $\beta/b > 0.33$, case (b) changes from a plate having 3 delamination zones at depth $h/4$ to a plate having a single full-width delamination at depth $h/4$. This explains the sharp decrease in the critical buckling force intensity of case (b) when $\beta/b > 0.33$.

(a)



(b)

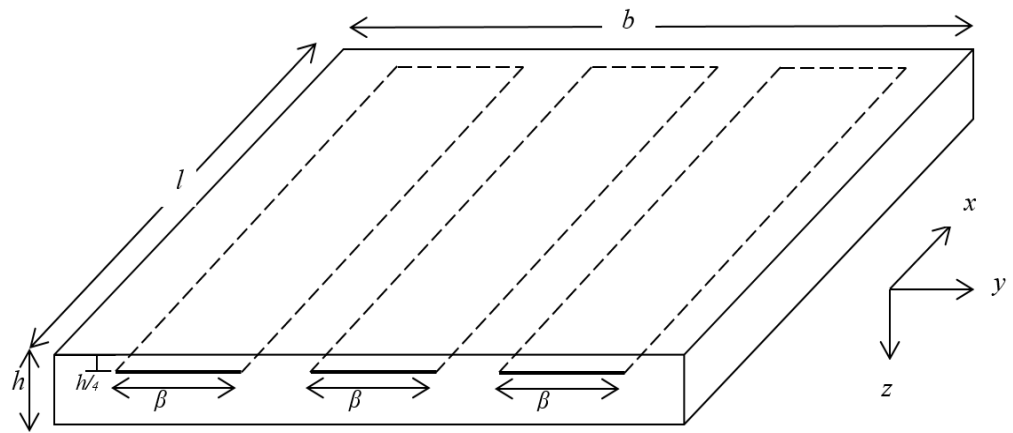


Figure 4-11: (a) Composite plate with single mid-delamination. (b) composite plate with multiple delaminations.

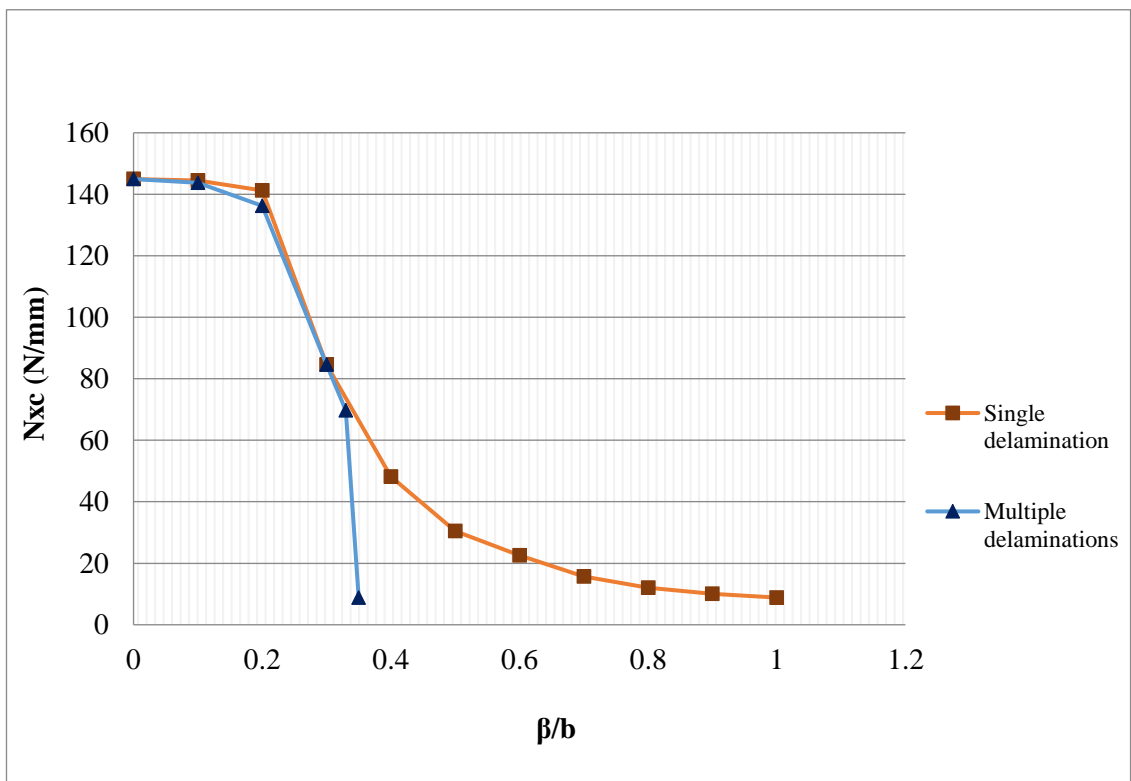


Figure 4-12: Critical buckling stress versus the delamination ratio β/b

4.2.2 Example 4.2: Single and multiple-delaminations at varying depths

The plate used in this example is identical to the one used in example 4.1. In this case however the plate is modelled with multiple delaminations at $h/4$, $h/2$ and $3h/4$ as shown in Figure 4-13. The relationship between the critical buckling force intensity and the delamination ratio β/b is studied and compared with the case presented in Figure 4-11 (a). Figure 4-14 shows that there are slight differences, between 0-10%, in the critical buckling loads between plates with single and multiple delaminations distributed vertically through the thickness of the plate. From this example, it can be concluded that the presence of multiple delaminations located identically at varying depths reduces the critical buckling force intensity between 0-10% more than the reduction caused by a single delamination.

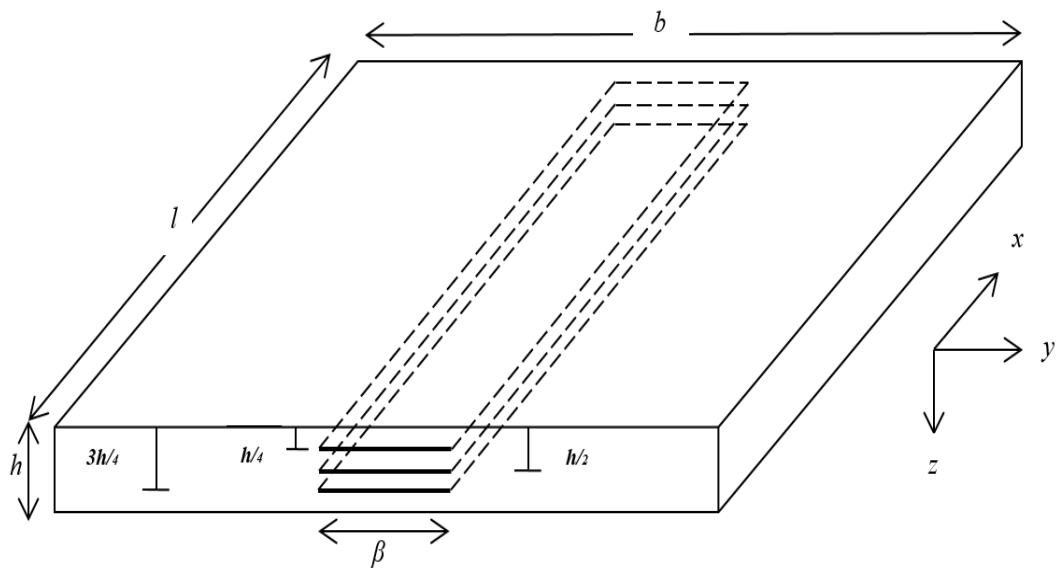


Figure 4-13 Composite plate with delaminations at depths $h/4$, $h/2$ and $3h/4$

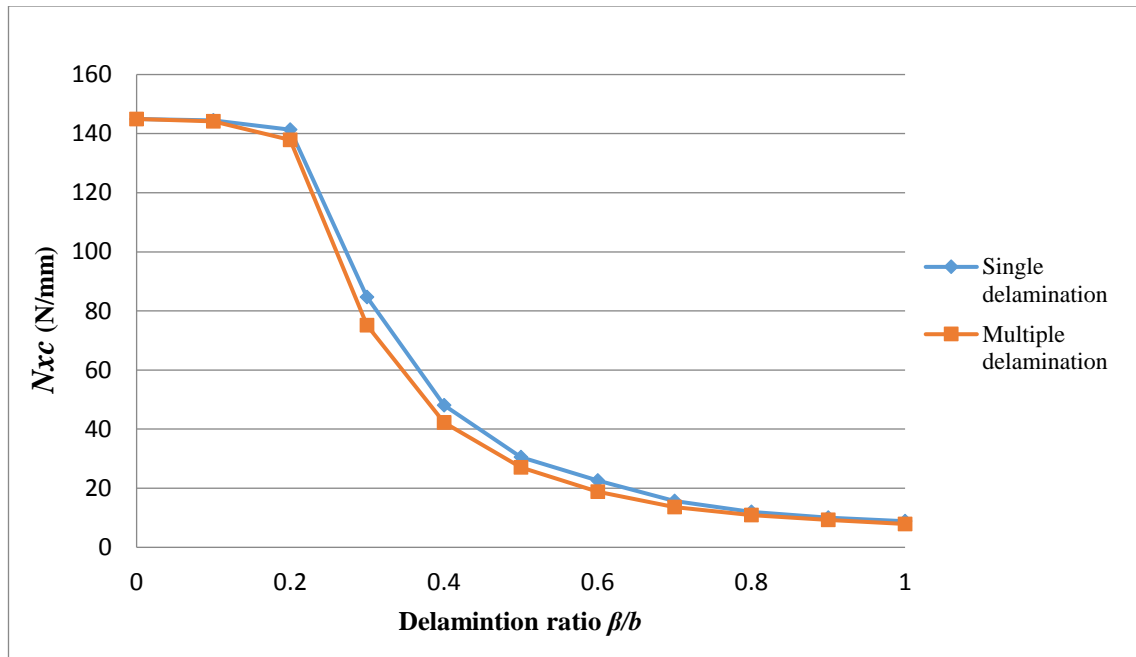


Figure 4-14: Critical buckling force intensities for plates with different delamination ratios and single and multiple delaminations.

4.3 The effect of delaminations on the global buckling load

In order to study the effect of delamination ratio β/b on the global buckling load of a plate, two different models were used and the results compared. The first one was consistent with the approach taken so far i.e. the delaminated region was modelled by two plates on top of each other as shown in Figure 4-15 (a). The second removed the delaminated part of the plate completely as shown in Figure 4-15 (b).

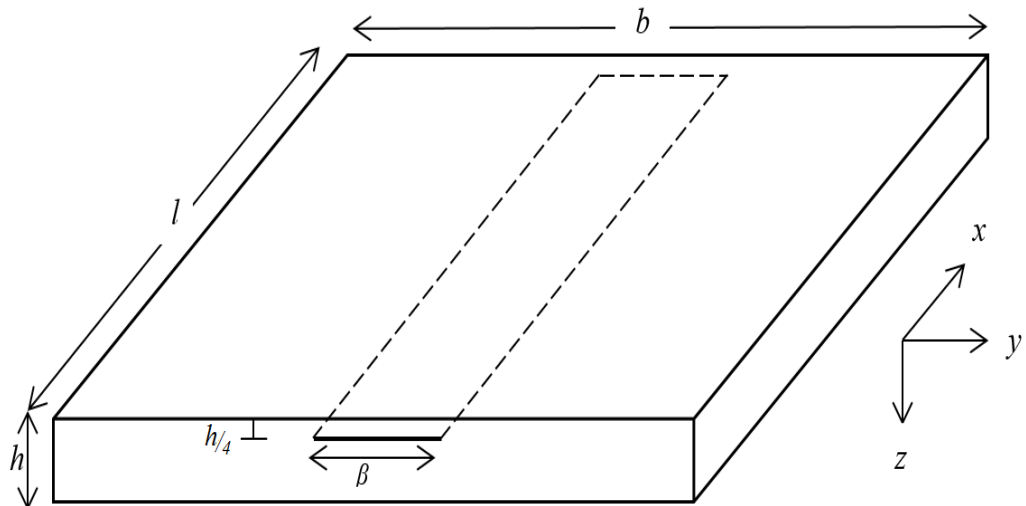
The critical buckling force intensities for both plates were determined and the results are presented in Figure 4-16. The figure shows that a plate with a delamination at $h/4$ buckles globally until the delamination ratio reaches 0.2 after which the delaminated region starts to buckle locally first. However, when the delaminated region is removed the plate buckles globally at all values of β/b . It can be seen that the plate is able to carry much more load before it buckles globally. For instance, for a delamination ratio

of $\beta/b=0.4$ using the first model the plate buckles locally at 48.1 N/mm but the same plate with the same β/b value needs a stress of over 110 N/mm to buckle globally. Referring to Figure 4-15, the global buckling force intensity of a delaminated plate can deduced as

$$P_g = P_{d2} + \left[\frac{\beta}{b} \times \frac{d}{h} \times P_{d1} \right] \quad (4.2)$$

where P_g is the global buckling force intensity of the delaminated plate shown in Figure 4-15 (a), P_{d1} is the critical buckling force intensity of the delaminated plate shown in Figure 4-15 (a). P_{d2} is the critical buckling force intensity of the same plate but with the delaminated part removed as shown in Figure 4-15 (b) and d is the delamination depth. Using the equation 4.2, Figure 4-16 includes a curve for the predicted global buckling force intensity of a plate with a delamination at depth $h/4$.

(a)



(b)

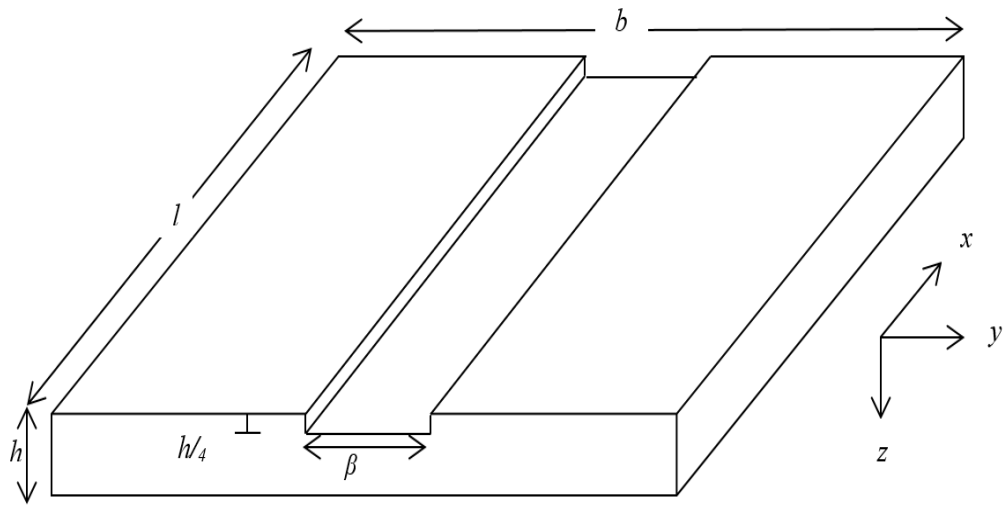


Figure 4-15: (a) Mid-width delaminated plate. (b) cut-out model for a delaminated composite plate.

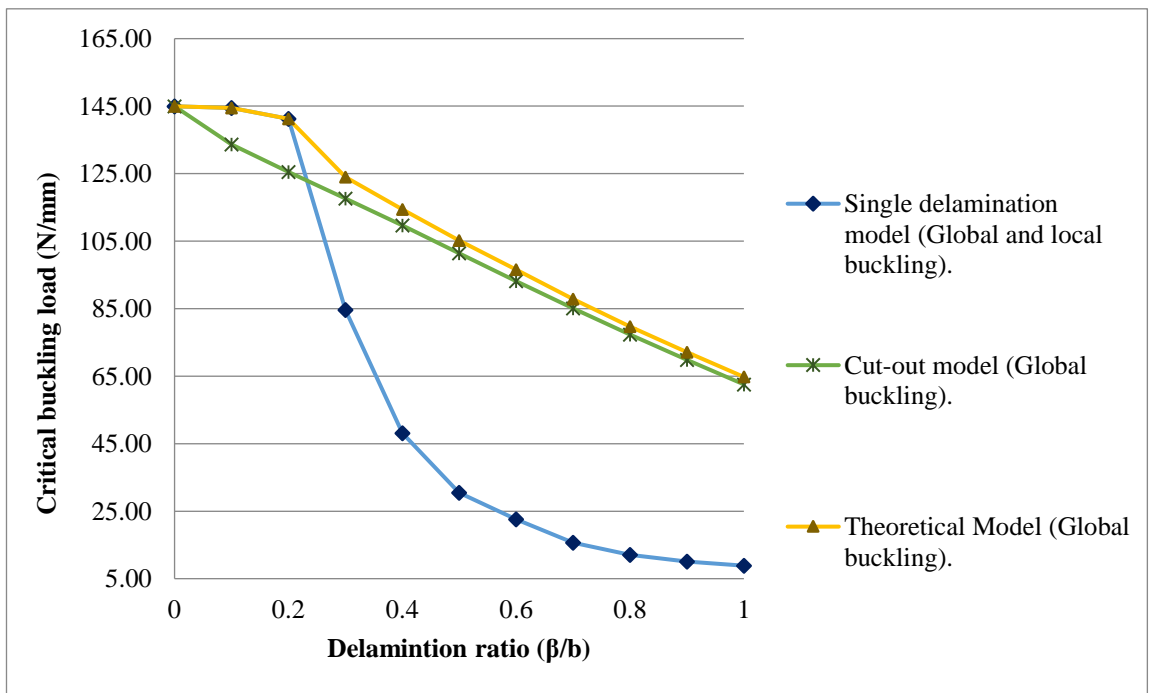


Figure 4-16: Critical buckling force intensity for a plate with a mid-width delamination based on the cut out plate model and the predicted global buckling stress.

4.4 Summary

This chapter has demonstrated the ability of VICONOPT to model the effect of different configurations where the delamination extends through the length and hence the problem is prismatic. It can be concluded that the critical buckling load and the critical mode shape of a delaminated composite plate are very sensitive to the ply orientations with respect to the nature and the direction of the load applied. It is also found that a delaminated composite plate buckling locally can carry much more load before a global buckling behaviour occurs.

The remainder of the thesis will look at developing a solution which allows non prismatic problems to be solved whilst retaining the advantages (i.e. computational efficiency) of the exact strip method.

5 The VICONOPT and Finite element (VFM) hybrid model

VFM is a novel combination of exact strip method and FE. Its purpose is to improve the ability of the exact strip method to model more complex cases of damaged plates. VFM uses FE analysis to model the longitudinal portion of the plate which contains the damage, as shown in Figure 5-1, and the exact strip method, i.e. VICON analysis, to more efficiently model the remainder of the plate.

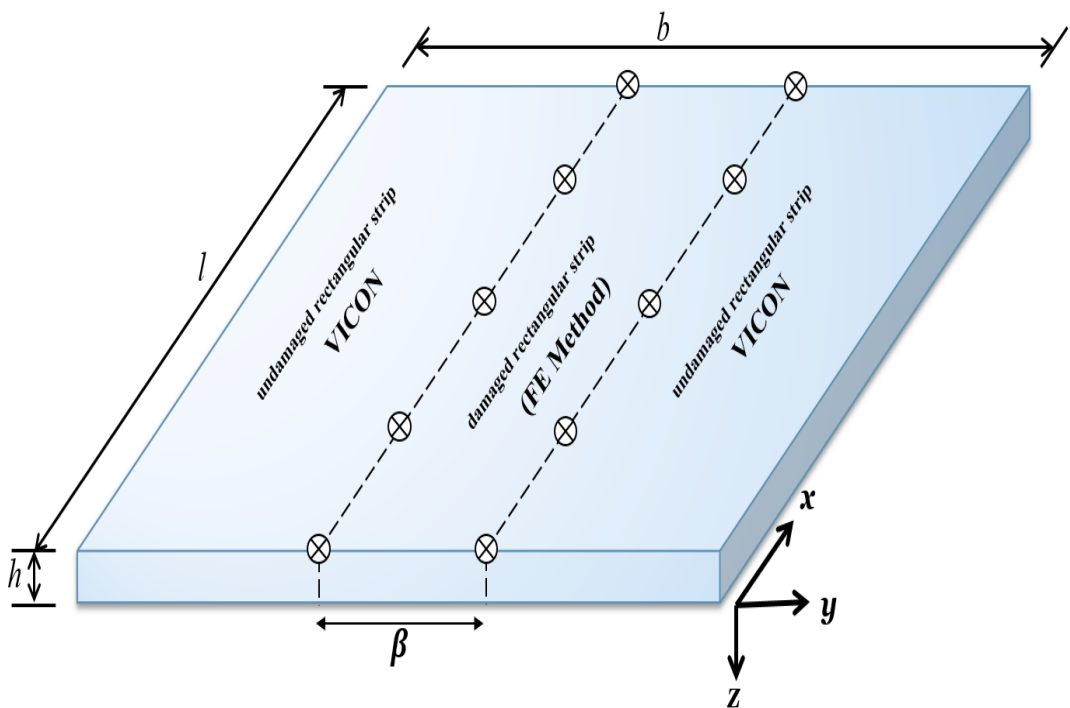


Figure 5-1: VICON and FE method (VFM) modelling a damaged plate.

The theory and equations used in the exact strip method have already been detailed in chapter 3, The following sections will describe the theory and formulation used in the FE method and how VFM incorporates the two methods to model damaged structures.

5.1 Theory and formulation used in FE analysis

FE is a stiffness matrix method based on discrete-element idealization, where the actual continuous plate structure is replaced by a mathematical model made up from elements of finite size having known properties that can be expressed in matrix form. For the purposes of the present free vibration analysis, the static stiffness matrix and equivalent mass matrix of a rectangular plate in bending are required. Przemieniecki [66] used matrix methods to derive and solve the basic equations in order to find the stiffness and equivalent mass properties of individual unassembled rectangular elements. These element properties are then assembled to create the global stiffness matrix and equivalent mass matrix for plate structures.

5.1.1 Stiffness properties of rectangular plates in bending

Bogner, et al. [67] introduced deflection functions which ensure the compatibility of both the deflection and slope between adjacent elements in order to create a stiffness matrix [66]. The sign conventions established in Figure 5-2 are considered in deriving the stiffness matrix of Eq. (5.1), where for convenience the submatrices $\mathbf{k}_{I,I}$, $\mathbf{k}_{II,I}$ and $\mathbf{k}_{II,II}$ are presented separately in Tables 5-1, 5-2 and 5-3. The derivation is given in Appendix 1.

$$\mathbf{k} = \begin{bmatrix} \mathbf{k}_{I,I} & \mathbf{k}_{II,I} \\ \mathbf{k}_{I,II} & \mathbf{k}_{II,II} \end{bmatrix} \quad \begin{matrix} \text{Symmetric} \\ \end{matrix} \quad (5.1)$$

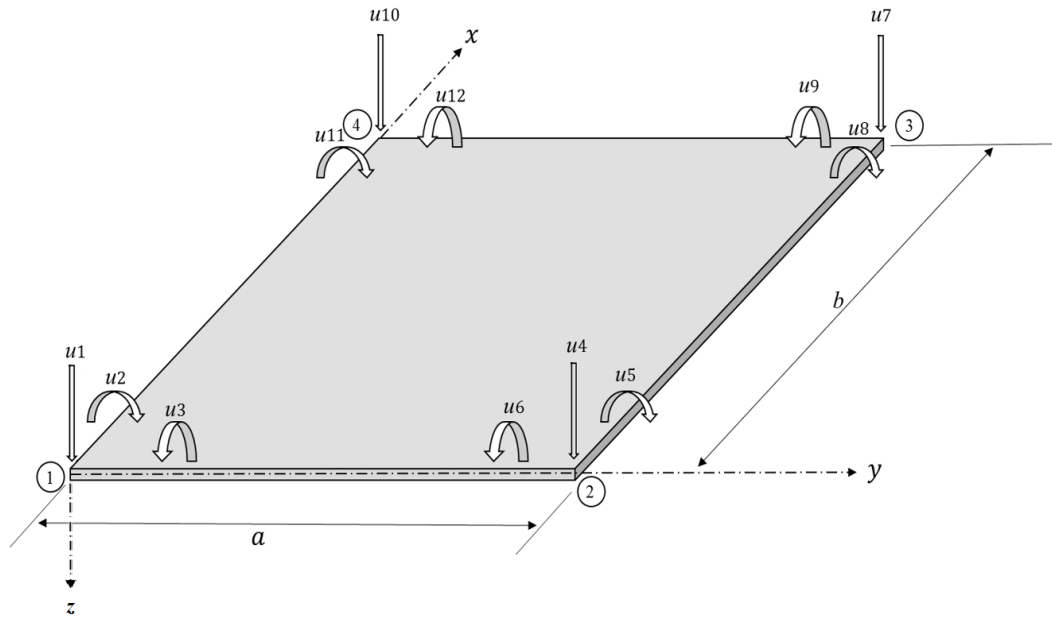


Figure 5-2 Rectangular plate element showing displacements and sign conventions [66].

5.1.2 Equivalent mass matrix for rectangular plate element

An equivalent mass matrix for unassembled elements is calculated using the local coordinate system shown in Figure 5-2. Eq. (5.2) shows the mass matrix for an unassembled element and its derivation is given in Appendix 2.

Table 5-1 Stiffness matrix for rectangular plate in bending: submatrix $\mathbf{k}_{I,I}$ based on compatible deflections [all coefficients to be multiplied by $[E t^3 / (12 (1-\nu^2) ab)]$ [66].

$\frac{156}{35}(\beta^2 + \beta^{-2}) + \frac{72}{25}$					
$\left[\frac{22}{35}\beta^2 + \frac{78}{35}\beta^{-2} + \frac{6}{25}(1 + 5\nu) \right] b$	$\left(\frac{4}{35}\beta^2 + \frac{52}{35}\beta^{-2} + \frac{8}{25} \right) b^2$				
$-\left[\frac{78}{35}\beta^2 + \frac{22}{35}\beta^{-2} + \frac{6}{25}(1 + 5\nu) \right] a$	$-\left[\frac{11}{35}(\beta^2 + \beta^{-2}) + \frac{1}{50}(1 + 60\nu) \right] ab$	$\left(\frac{52}{35}\beta^2 + \frac{4}{35}\beta^{-2} + \frac{8}{25} \right) a^2$	Symmetric		
$\frac{54}{35}\beta^2 - \frac{156}{35}\beta^{-2} - \frac{72}{25}$	$\left(\frac{13}{35}\beta^2 - \frac{78}{35}\beta^{-2} - \frac{6}{25} \right) b$	$\left[-\frac{27}{35}\beta^2 + \frac{22}{35}\beta^{-2} + \frac{6}{25}(1 + 5\nu) \right] a$	$\frac{156}{35}(\beta^2 + \beta^{-2}) + \frac{72}{25}$		
$\left(-\frac{13}{35}\beta^2 + \frac{78}{35}\beta^{-2} + \frac{6}{25} \right) b$	$\left(-\frac{3}{35}\beta^2 + \frac{26}{35}\beta^{-2} - \frac{2}{25} \right) b^2$	$\left[\frac{13}{70}\beta^2 - \frac{11}{35}\beta^{-2} - \frac{1}{50}(1 + 5\nu) \right] ab$	$-\left[\frac{22}{35}\beta^2 + \frac{78}{35}\beta^{-2} + \frac{6}{25}(1 + 5\nu) \right] b$	$\left(\frac{4}{35}\beta^2 + \frac{52}{35}\beta^{-2} + \frac{8}{25} \right) b^2$	
$\left[-\frac{27}{35}\beta^2 + \frac{22}{35}\beta^{-2} + \frac{6}{25}(1 + 5\nu) \right] a$	$\left[-\frac{13}{70}\beta^2 + \frac{11}{35}\beta^{-2} + \frac{1}{50}(1 + 5\nu) \right] ab$	$\left(\frac{18}{35}\beta^2 - \frac{4}{35}\beta^{-2} - \frac{8}{25} \right) a^2$	$-\left[\frac{78}{35}\beta^2 + \frac{22}{35}\beta^{-2} + \frac{6}{25}(1 + 5\nu) \right] a$	$\left[\frac{11}{35}(\beta^2 + \beta^{-2}) + \frac{1}{50}(1 + 60\nu) \right] ab$	$\left(\frac{52}{35}\beta^2 + \frac{4}{35}\beta^{-2} + \frac{8}{25} \right) a^2$

Table 5-2: Stiffness matrix for rectangular plate in bending: submatrix $\mathbf{k}_{II,I}$ based on compatible deflections [all coefficients to be multiplied by $[E t^3 / (12 (1-\nu^2) ab)]$ [66].

$-\frac{156}{35}(\beta^2 + \beta^{-2})$ $+\frac{72}{25}$	$(-\frac{13}{35}\beta^2 - \frac{27}{35}\beta^{-2} + \frac{6}{25})b$	$(\frac{27}{35}\beta^2 + \frac{13}{35}\beta^{-2} - \frac{6}{25})a$	$-\frac{156}{35}\beta^2 + \frac{54}{35}\beta^{-2} - \frac{72}{25}$	$[\frac{22}{35}\beta^2 - \frac{27}{35}\beta^{-2}$ $+\frac{6}{25}(1+5\nu)]b$	$(\frac{78}{35}\beta^2 - \frac{13}{35}\beta^{-2} + \frac{6}{25})a$
$(\frac{13}{35}\beta^2 + \frac{27}{35}\beta^{-2} - \frac{6}{25})b$	$(\frac{3}{35}\beta^2 + \frac{9}{35}\beta^{-2} + \frac{2}{25})b^2$	$[-\frac{13}{70}(\beta^2 + \beta^{-2}) + \frac{1}{50}]ab$	$[\frac{22}{35}\beta^2 - \frac{27}{35}\beta^{-2} + \frac{6}{25}(1$ $+ 5\nu)]b$	$(-\frac{4}{35}\beta^2 + \frac{18}{35}\beta^{-2} - \frac{8}{25})b^2$	$[-\frac{11}{35}\beta^2 + \frac{13}{70}\beta^{-2}$ $-\frac{1}{50}(1+5\nu)]ab$
$(-\frac{27}{35}\beta^2 - \frac{13}{35}\beta^{-2}$ $+\frac{6}{25})a$	$[\frac{13}{70}(\beta^2 + \beta^{-2}) + \frac{1}{50}(1$ $+ 60\nu)]ab$	$(\frac{9}{35}\beta^2 + \frac{3}{35}\beta^{-2} + \frac{2}{25})a^2$	$(-\frac{78}{35}\beta^2 + \frac{13}{35}\beta^{-2} - \frac{6}{25})a$	$[\frac{11}{35}\beta^2 - \frac{13}{70}\beta^{-2} + \frac{1}{50}(1$ $+ 5\nu)]ab$	$(\frac{26}{35}\beta^2 - \frac{3}{35}\beta^{-2} - \frac{2}{25})a^2$
$-\frac{156}{35}\beta^2 - \frac{54}{35}\beta^{-2}$ $-\frac{72}{25}$	$[-\frac{22}{35}\beta^2 + \frac{27}{35}\beta^{-2} - \frac{6}{25}(1$ $+ 5\nu)]b$	$(\frac{78}{35}\beta^2 + \frac{13}{35}\beta^{-2} + \frac{6}{25})a$	$\frac{54}{35}(\beta^2 + \beta^{-2}) + \frac{72}{25}$	$(\frac{13}{35}\beta^2 + \frac{27}{35}\beta^{-2} - \frac{6}{25})b$	$(\frac{27}{35}\beta^2 + \frac{13}{35}\beta^{-2} - \frac{6}{25})a$
$[-\frac{22}{35}\beta^2 + \frac{27}{35}\beta^{-2}$ $-\frac{6}{25}(1+5\nu)]b$	$(-\frac{4}{35}\beta^2 + \frac{18}{35}\beta^{-2} - \frac{8}{25})b^2$	$[\frac{11}{35}\beta^2 - \frac{13}{70}\beta^{-2} - \frac{1}{50}(1$ $+ 5\nu)]ab$	$(\frac{13}{35}\beta^2 + \frac{27}{35}\beta^{-2} + \frac{6}{25})b$	$(\frac{3}{35}\beta^2 + \frac{9}{35}\beta^{-2} + \frac{2}{25})b^2$	$[\frac{13}{70}(\beta^2 + \beta^{-2}) - \frac{1}{50}]ab$
$(-\frac{78}{35}\beta^2 + \frac{13}{35}\beta^{-2}$ $-\frac{6}{25})a$	$[-\frac{11}{35}\beta^2 + \frac{13}{70}\beta^{-2} - \frac{1}{50}(1$ $+ 5\nu)]ab$	$(\frac{26}{35}\beta^2 - \frac{3}{35}\beta^{-2} - \frac{2}{25})a^2$	$(-\frac{27}{35}\beta^2 + \frac{13}{35}\beta^{-2} + \frac{6}{25})a$	$[\frac{13}{70}(\beta^2 + \beta^{-2}) - \frac{1}{50}]ab$	$(\frac{9}{35}\beta^2 + \frac{3}{35}\beta^{-2} + \frac{2}{25})a^2$

Table 5-3: Stiffness matrix for rectangular plate in bending: submatrix $\mathbf{k}_{II,II}$ based on compatible deflections [all coefficients to be multiplied by $[E t^3 / (12 (1-\nu^2) ab)]$ [66].

$\frac{156}{35}(\beta^2 + \beta^{-2}) + \frac{72}{25}$				
$-\left[\frac{22}{35}\beta^2 + \frac{78}{35}\beta^{-2} + \frac{6}{25}(1 + 5\nu)\right]b$	$\left(\frac{4}{35}\beta^2 + \frac{52}{35}\beta^{-2} + \frac{8}{25}\right)b^2$			
$\left[\frac{78}{35}\beta^2 + \frac{22}{35}\beta^{-2} + \frac{6}{25}(1 + 5\nu)\right]a$	$-\left[\frac{11}{35}(\beta^2 + \beta^{-2}) + \frac{1}{50}(1 + 60\nu)\right]ab$	$\left(\frac{52}{35}\beta^2 + \frac{4}{35}\beta^{-2} + \frac{8}{25}\right)a^2$	Symmetric	
$\frac{54}{35}\beta^2 - \frac{156}{35}\beta^{-2} - \frac{72}{25}$	$\left(-\frac{13}{35}\beta^2 + \frac{78}{35}\beta^{-2} + \frac{6}{25}\right)b$	$\left[\frac{27}{35}\beta^2 - \frac{22}{35}\beta^{-2} - \frac{6}{25}(1 + 5\nu)\right]a$	$\frac{156}{35}(\beta^2 + \beta^{-2}) + \frac{72}{25}$	
$\left(\frac{13}{35}\beta^2 - \frac{78}{35}\beta^{-2} - \frac{6}{25}\right)b$	$\left(-\frac{3}{35}\beta^2 + \frac{26}{35}\beta^{-2} - \frac{2}{25}\right)b^2$	$\left[\frac{13}{70}\beta^2 - \frac{11}{35}\beta^{-2} - \frac{1}{50}(1 + 5\nu)\right]ab$	$\left[\frac{22}{35}\beta^2 + \frac{78}{35}\beta^{-2} + \frac{6}{25}(1 + 5\nu)\right]b$	$\left(\frac{4}{35}\beta^2 + \frac{52}{35}\beta^{-2} + \frac{8}{25}\right)b^2$
$\left[\frac{27}{35}\beta^2 - \frac{22}{35}\beta^{-2} - \frac{6}{25}(1 + 5\nu)\right]a$	$\left[\frac{13}{70}\beta^2 + \frac{11}{35}\beta^{-2} + \frac{1}{50}(1 + 5\nu)\right]ab$	$\left(\frac{18}{35}\beta^2 - \frac{4}{35}\beta^{-2} - \frac{8}{25}\right)a^2$	$\left[\frac{78}{35}\beta^2 + \frac{22}{35}\beta^{-2} + \frac{6}{25}(1 + 5\nu)\right]a$	$\left[\frac{11}{35}(\beta^2 + \beta^{-2}) + \frac{1}{50}(1 + 60\nu)\right]ab$
				$\left(\frac{52}{35}\beta^2 + \frac{4}{35}\beta^{-2} + \frac{8}{25}\right)a^2$

5.2 Theory and formulation for VFM

VICONOPT incorporates two earlier programs, VIPASA and VICON. VIPASA provides a powerful analysis for vibration and buckling of prismatic plate assemblies with simply supported ends. However, if the structure is under in-plane shear loading, the mode shapes will be skewed and the end conditions will not be satisfied. Thus, the applicability of VIPASA is limited. VICON [52] provides a solution to this problem by coupling the VIPASA stiffness matrices for different wavelength responses through the Lagrangian Multiplier Method [52]. The complete VIPASA generality and capability are thus retained in the VICON program, which satisfies the end conditions through point constraints and also permits attachments to a supporting structure [45]. Thus the VICON stiffness matrix comprises a series of VIPASA stiffness matrices which are coupled by the constraints.

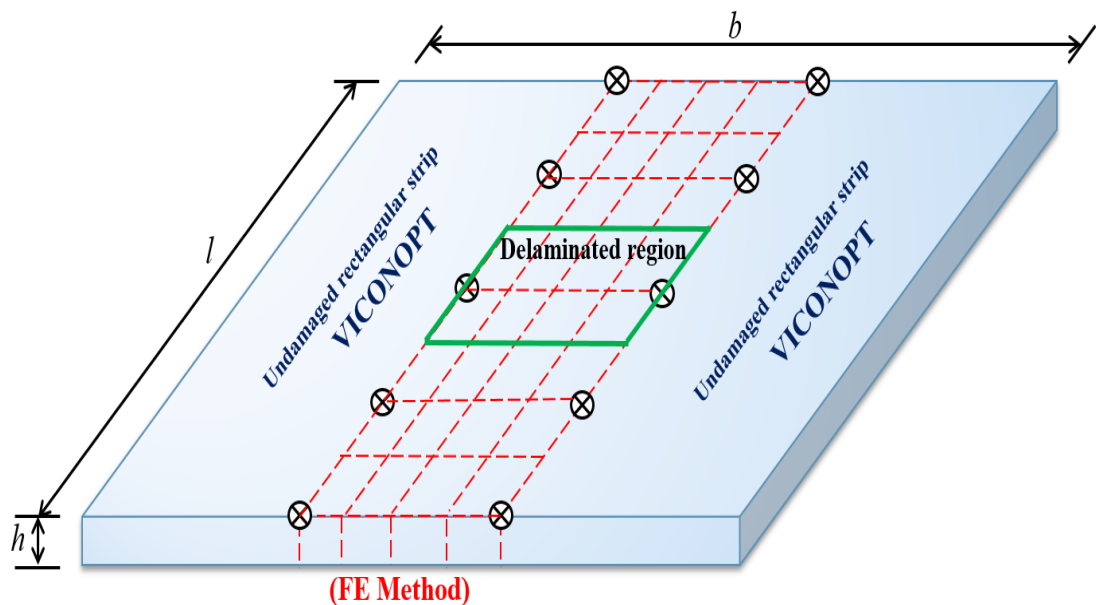


Figure 5-3: Damaged plate modelled by VFM.

VFM is based on using the FE method to model the longitudinal portion of the plate containing the damage as shown in Figure 5-3. However, the FE method has been merged with the VICONOPT process to model the whole plate. The Wittrick-Williams algorithm is used to find the critical buckling loads and natural frequencies for the damaged plates. Thus VICON is used to calculate the dynamic stiffness matrices for the undamaged regions, while the FE method is used to calculate the static stiffness and equivalent mass matrices for the damaged rectangular strip. Embedded damage is modelled by including elements with different stiffness properties within this strip, see Figure 5-3.

VICON assumes that the deflections of a plate assembly of length l can be expressed as a Fourier series, see Equation (3.9).

$$\mathbf{D}_a = \sum_{m=-\infty}^{\infty} \mathbf{D}_m \exp (i\pi x / \lambda_m) \quad (5.3)$$

where \mathbf{D}_a is the nodal displacement amplitude vector of the plate assembly, \mathbf{D}_m are the displacement amplitude vectors from a series of VIPASA analyses with half-wavelengths

$$\lambda_m = \frac{l}{\xi + 2m} , (0 \leq \xi \leq 1; m = 0, \pm 1, \pm 2, \dots, \pm q) \quad (5.4)$$

Here λ_{-m} represents the same contributions as the positive half-wavelength λ_m to the mode shape but having a 180° phase difference. The structure is modelled as infinitely long with a mode shape that repeats at intervals of $L = 2l / \xi$. The perturbation force vectors \mathbf{P}_a are similarly defined as

$$\mathbf{P}_a = \sum_{m=-\infty}^{\infty} \mathbf{K}_m \mathbf{D}_m \exp (i\pi x / \lambda_m) \quad (5.5)$$

where \mathbf{K}_m is the VIPASA dynamic stiffness matrix corresponding to responses at half-wavelength λ_m . The VICON stiffness equations relating \mathbf{K}_m , \mathbf{D}_m , the perturbation forces \mathbf{P}_m and the Lagrangian multipliers \mathbf{P}_L are thus expressed as

$$\begin{bmatrix} lK_0 & \mathbf{0} & \mathbf{0} & \mathbf{0} & \mathbf{0} & \dots & \mathbf{0} & \mathbf{E}_0^H \\ \mathbf{0} & lK_1 & \mathbf{0} & \mathbf{0} & \mathbf{0} & \dots & \mathbf{0} & \mathbf{E}_1^H \\ \mathbf{0} & \mathbf{0} & lK_{-1} & \mathbf{0} & \mathbf{0} & \dots & \mathbf{0} & \mathbf{E}_{-1}^H \\ \mathbf{0} & \mathbf{0} & \mathbf{0} & lK_2 & \mathbf{0} & \dots & \mathbf{0} & \mathbf{E}_2^H \\ \mathbf{0} & \mathbf{0} & \mathbf{0} & \mathbf{0} & lK_{-2} & \dots & \mathbf{0} & \mathbf{E}_{-2}^H \\ \vdots & \vdots & \vdots & \vdots & \vdots & \ddots & \vdots & \vdots \\ \mathbf{0} & \mathbf{0} & \mathbf{0} & \mathbf{0} & \mathbf{0} & \dots & lK_n & \mathbf{E}_n^H \\ \mathbf{E}_0 & \mathbf{E}_1 & \mathbf{E}_{-1} & \mathbf{E}_2 & \mathbf{E}_{-2} & \dots & \mathbf{E}_n & \mathbf{0} \end{bmatrix} \begin{bmatrix} \mathbf{D}_0 \\ \mathbf{D}_1 \\ \mathbf{D}_{-1} \\ \mathbf{D}_2 \\ \mathbf{D}_{-2} \\ \vdots \\ \mathbf{D}_n \\ \mathbf{P}_L \end{bmatrix} = \begin{bmatrix} \mathbf{P}_0 \\ \mathbf{P}_1 \\ \mathbf{P}_{-1} \\ \mathbf{P}_2 \\ \mathbf{P}_{-2} \\ \vdots \\ \mathbf{P}_n \\ \mathbf{0} \end{bmatrix} \quad (5.6)$$

The stiffness matrix in Eq. (5.6) may be partitioned as

$$\mathbf{K}_{VICON} = \begin{bmatrix} \mathbf{K}^{Global\ VIPASA} & \mathbf{C}^H \\ \mathbf{C} & \mathbf{0} \end{bmatrix} \quad (5.7)$$

where

$$\mathbf{K}_{Global\ VIPASA} = \begin{bmatrix} \lambda \mathbf{K}_0 & \mathbf{0} & \mathbf{0} & \mathbf{0} & \mathbf{0} & \dots & \mathbf{0} \\ \mathbf{0} & \lambda \mathbf{K}_1 & \mathbf{0} & \mathbf{0} & \mathbf{0} & \dots & \mathbf{0} \\ \mathbf{0} & \mathbf{0} & \lambda \mathbf{K}_{-1} & \mathbf{0} & \mathbf{0} & \dots & \mathbf{0} \\ \mathbf{0} & \mathbf{0} & \mathbf{0} & \lambda \mathbf{K}_2 & \mathbf{0} & \dots & \mathbf{0} \\ \mathbf{0} & \mathbf{0} & \mathbf{0} & \mathbf{0} & \lambda \mathbf{K}_{-2} & \dots & \mathbf{0} \\ \vdots & \vdots & \vdots & \vdots & \vdots & \ddots & \mathbf{0} \\ \mathbf{0} & \mathbf{0} & \mathbf{0} & \mathbf{0} & \mathbf{0} & \dots & \lambda \mathbf{K}_n \end{bmatrix} \quad (5.8)$$

$$\mathbf{C} = [\mathbf{E}_0 \quad \mathbf{E}_1 \quad \mathbf{E}_{-1} \quad \mathbf{E}_2 \quad \mathbf{E}_{-2} \quad \dots \quad \mathbf{E}_n] \quad (5.9)$$

and superscript H denotes Hermitian transpose. $\mathbf{K}_{Global\ VIPASA}$ is a series of VIPASA matrices \mathbf{K}_m at different values of λ_m . The matrix \mathbf{K}_m can be partitioned as

$$\mathbf{K}_m = \begin{bmatrix} \mathbf{k}_{11} & \mathbf{k}_{12} \\ \mathbf{k}_{21} & \mathbf{k}_{22} \end{bmatrix} \quad (5.10)$$

where

$$\mathbf{k}_{11} = \begin{bmatrix} s_{MM} & -s_{MQ} & 0 & 0 \\ -\bar{s}_{MQ} & s_{QQ} & 0 & 0 \\ 0 & 0 & s_{NN} & -s_{NT} \\ 0 & 0 & -s_{NT} & s_{TT} \end{bmatrix} \quad (5.11)$$

$$\mathbf{k}_{22} = \begin{bmatrix} s_{MM} & \bar{s}_{MQ} & 0 & 0 \\ s_{MQ} & s_{QQ} & 0 & 0 \\ 0 & 0 & s_{NN} & s_{NT} \\ 0 & 0 & s_{NT} & s_{TT} \end{bmatrix} \quad (5.12)$$

$$\mathbf{k}_{12} = \bar{\mathbf{k}}_{21}^T = \begin{bmatrix} f_{MM} & f_{MQ} & 0 & 0 \\ -f_{MQ} & -f_{QQ} & 0 & 0 \\ 0 & 0 & -f_{NN} & -f_{NT} \\ 0 & 0 & f_{NT} & f_{TT} \end{bmatrix} \quad (5.13)$$

Here, s_{MM} , s_{MQ} , s_{QQ} , f_{MM} , f_{MQ} and f_{QQ} are the out-of-plane stiffness coefficients while s_{NN} , s_{NT} , s_{TT} , f_{NN} , f_{NT} and f_{TT} are the in-plane stiffness coefficients. The derivation of these coefficients is illustrated in reference [42]. However, the current work considers only out-of-plane plate deformations, and thus the calculation procedure for finding the values of the out-of-plane stiffness coefficients is detailed in Appendix 3.

\mathbf{C} in Eq. (5.7) is the global constraint matrix comprising submatrices \mathbf{E}_m as in Eq. (5.9), where \mathbf{E}_m is the constraint matrix for responses corresponding to half-wavelength λ_m in the bay $0 \leq x < l$ and contains terms of the form $e^{(i\pi x/\lambda_m)}$.

The hybrid dynamic stiffness matrix of the plate is formed by using Lagrangian multipliers to couple the VICON and FE components, as follows.

$$\mathbf{K}_{Global} = \begin{bmatrix} \mathbf{K}_{Global\ VIPASA} & \mathbf{0} & \mathbf{C}_1^H \\ \mathbf{0} & \mathbf{K}_{FE} & \mathbf{C}_2^T \\ \mathbf{C}_1 & \mathbf{C}_2 & \mathbf{0} \end{bmatrix} \quad (5.14)$$

Here, $\mathbf{K}_{Global\ VIPASA}$ is given in Eq. (5.8). The constraint matrices \mathbf{C}_1 and \mathbf{C}_2 enforce equal displacements and rotations at the nodes connecting the undamaged and damaged strips. \mathbf{C}_1 also includes any support conditions in the undamaged regions. \mathbf{C}_2^T

is the transpose of \mathbf{C}_2 . \mathbf{K}_{FE} is the FE dynamic stiffness matrix for the damaged rectangular strip. In the case of vibration problems \mathbf{K}_{FE} takes the form

$$\mathbf{K}_{FE} = \mathbf{k} - n^2 \mathbf{m} \quad (5.15)$$

where n is the frequency. \mathbf{k} and \mathbf{m} are the static stiffness matrix and equivalent mass matrix of the damaged rectangular strip, and they can be calculated based on the Eqs. (5.1) and (5.2) respectively.

The Wittrick-Williams algorithm of Eq. (3.1) [46] has been extended to cover VICON analysis and takes the form

$$J = \sum_m (J_{0m} + s\{\mathbf{K}_m\} + s\{\mathbf{R}\} - r) \quad (5.16)$$

where J_{0m} is the number of eigenvalues which would be exceeded for $\lambda = \lambda_m$ if all the degrees of freedom at the nodes of the plate assembly were to be clamped, r is the number of constraints applied and

$$\mathbf{R} = \mathbf{R}_0 - \frac{1}{L} \sum_{-\infty}^{\infty} \mathbf{E}_m \mathbf{K}_m^{-1} \mathbf{E}_m^H \quad (5.17)$$

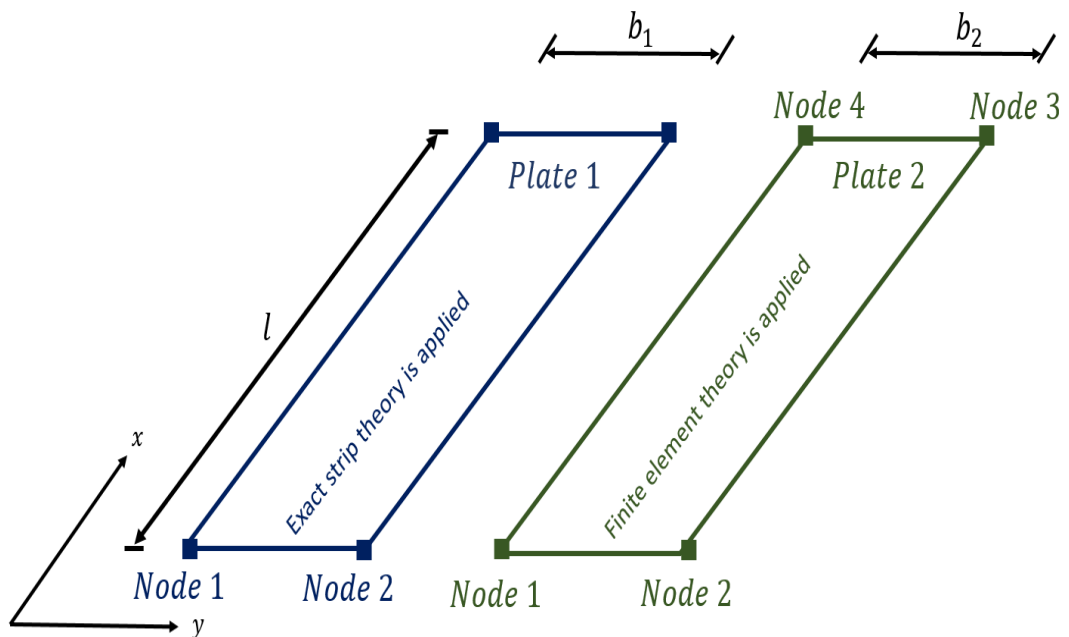
Here, \mathbf{R} has an order equal to the number of constraints (r) and it replaces the null matrix at the bottom right of \mathbf{K}_{Global} in Eq. (5.14) when Gauss elimination is applied.

It will be obtained after all rows except those in \mathbf{R} have been pivotal. $\mathbf{R}_0 = \mathbf{0}$ when all the constraints are rigid [42, 45, 68-70].

5.2.1 Example of plate assembly using VFM

A simple example of a plate assembly is chosen to illustrate the theory and formulation used by VFM to model an assembled plate structure consisting of two or more plates. Figure 5-4 (a) includes two plates with the same length l and widths b_1 and b_2 . The exact strip method is used to model plate 1 as a single strip with nodes (numbered 1 and 2) at the longitudinal edges of the plate. Only out-of-plane degrees of freedom, i.e. vertical displacements and rotations about the x axis, are considered. Finite element theory is applied to model plate 2. For the purpose of illustrating the concept of VFM and minimizing the size of the matrices in the following equations, it is modelled using only one element as shown in Figure 5-4 (a). The degrees of freedom at the nodes are vertical displacements and rotations about the x and y axes.

(a)



(b)

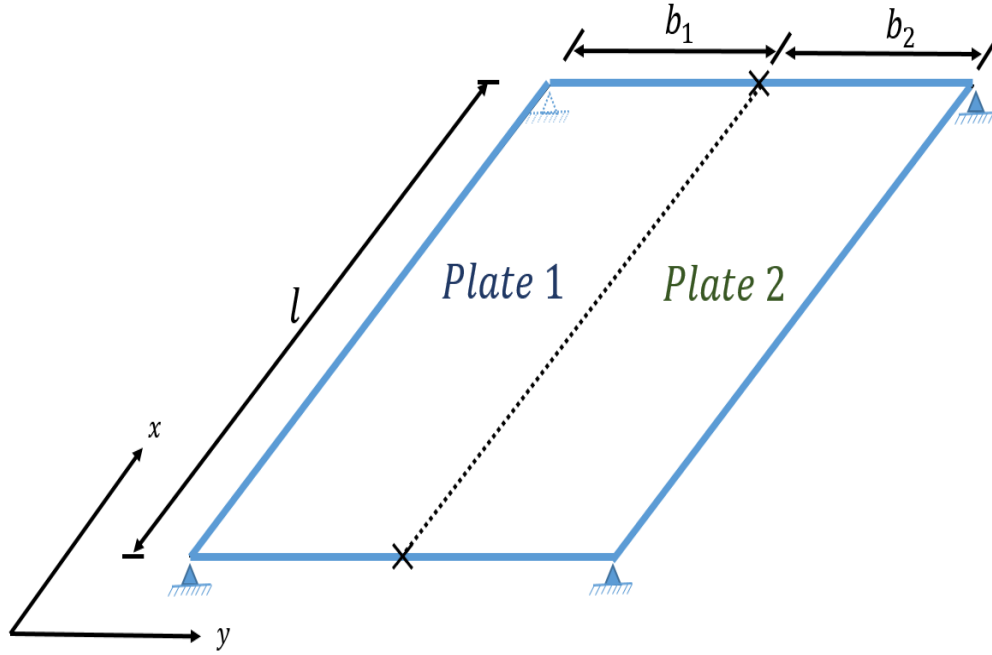


Figure 5-4 Assembling two plates using VFM. (a) exact strip and FE components. (b) the assembled structure.

Plate 1 is modelled using the exact strip method and the first step is specifying the value of the response parameter ξ , which was introduced in section 3.2.2. Based on Eq. (5.4), when $\xi = 1$ the half-wavelengths (λ_m) considered will be $\lambda_0 = l/1$, $\lambda_{-1} = -l/1$, $\lambda_1 = l/3$, $\lambda_{-2} = -l/3$, $\lambda_2 = l/5$, ... etc. In this example, only the first two of these values are included in the following equations, in order to keep the size of the matrices manageable. Using Eqs. (5.8) and (5.10)-(5.13), the stiffness matrix of plate 1 can be obtained as follows:

$$\mathbf{K}_{Global\ VIPASA} = \begin{bmatrix} l\mathbf{K}_0 & 0 \\ 0 & l\mathbf{K}_{-1} \end{bmatrix} \quad (5.18)$$

where

$$\mathbf{K}_0 = \begin{bmatrix} S_{MM\lambda=l} & -S_{MQ\lambda=l} & f_{MM\lambda=l} & f_{MQ\lambda=l} \\ -\bar{S}_{MQ\lambda=l} & S_{QQ\lambda=l} & -f_{MQ\lambda=l} & -f_{QQ\lambda=l} \\ \bar{f}_{MM\lambda=l} & -\bar{f}_{MQ\lambda=l} & S_{MM\lambda=l} & \bar{S}_{MQ\lambda=l} \\ \bar{f}_{MQ\lambda=l} & -\bar{f}_{QQ\lambda=l} & S_{MQ\lambda=l} & S_{QQ\lambda=l} \end{bmatrix} \quad (5.19)$$

$$\mathbf{K}_{-1} = \begin{bmatrix} S_{MM\lambda=-l} & -S_{MQ\lambda=-l} & f_{MM\lambda=-l} & f_{MQ\lambda=-l} \\ -\bar{S}_{MQ\lambda=-l} & S_{QQ\lambda=-l} & -f_{MQ\lambda=-l} & -f_{QQ\lambda=-l} \\ \bar{f}_{MM\lambda=-l} & -\bar{f}_{MQ\lambda=-l} & S_{MM\lambda=-l} & \bar{S}_{MQ\lambda=-l} \\ \bar{f}_{MQ\lambda=-l} & -\bar{f}_{QQ\lambda=-l} & S_{MQ\lambda=-l} & S_{QQ\lambda=-l} \end{bmatrix} \quad (5.20)$$

Here, the coefficients in Eqs. (5.19) and (5.20) are calculated based on the values of λ .

The stiffness matrix of plate 2 will be represented as \mathbf{K}_{FE} and can be calculated using

Eqs. (5.1), (5.2) and (5.15) to form the following equation

$$\mathbf{K}_{FE} = \begin{bmatrix} \mathbf{k}_{11} - n^2 \mathbf{m}_{11} & \mathbf{k}_{12} - n^2 \mathbf{m}_{12} & \mathbf{k}_{13} - n^2 \mathbf{m}_{13} & \mathbf{k}_{14} - n^2 \mathbf{m}_{14} \\ \mathbf{k}_{21} - n^2 \mathbf{m}_{21} & \mathbf{k}_{22} - n^2 \mathbf{m}_{22} & \mathbf{k}_{23} - n^2 \mathbf{m}_{23} & \mathbf{k}_{24} - n^2 \mathbf{m}_{24} \\ \mathbf{k}_{31} - n^2 \mathbf{m}_{31} & \mathbf{k}_{32} - n^2 \mathbf{m}_{32} & \mathbf{k}_{33} - n^2 \mathbf{m}_{33} & \mathbf{k}_{34} - n^2 \mathbf{m}_{34} \\ \mathbf{k}_{41} - n^2 \mathbf{m}_{41} & \mathbf{k}_{42} - n^2 \mathbf{m}_{42} & \mathbf{k}_{43} - n^2 \mathbf{m}_{43} & \mathbf{k}_{44} - n^2 \mathbf{m}_{44} \end{bmatrix} \quad (5.21)$$

where the subscripts refer to node numbers and the size of each term in this matrix is

3×3 , based on the number of the degrees of freedom for each node. By applying Eq.

(5.9), the constraint matrices \mathbf{C}_1 and \mathbf{C}_2 which represent the connections between

plates 1 and 2 will take the following forms

$$\mathbf{C}_1 = [\mathbf{C}_{1\lambda=l} \quad \mathbf{C}_{1\lambda=-l}] \quad (5.22)$$

where

$$\mathbf{C}_{1\lambda=l} = \begin{bmatrix} 0 & 0 & 1 & 0 \\ 0 & 0 & 0 & 1 \\ 0 & 0 & e^{i\pi} & 0 \\ 0 & 0 & 0 & e^{i\pi} \end{bmatrix} \quad (5.23)$$

$$\mathbf{C}_{1\lambda=-l} = \begin{bmatrix} 0 & 0 & 1 & 0 \\ 0 & 0 & 0 & 1 \\ 0 & 0 & e^{-i\pi} & 0 \\ 0 & 0 & 0 & e^{-i\pi} \end{bmatrix} \quad (5.24)$$

$$\mathbf{C}_2 = \begin{bmatrix} 0 & -1 & 0 & 0 & 0 & 0 & 0 & 0 & 0 & 0 & 0 & 0 \\ -1 & 0 & 0 & 0 & 0 & 0 & 0 & 0 & 0 & 0 & 0 & 0 \\ 0 & 0 & 0 & 0 & 0 & 0 & 0 & 0 & 0 & 0 & -1 & 0 \\ 0 & 0 & 0 & 0 & 0 & 0 & 0 & 0 & 0 & -1 & 0 & 0 \end{bmatrix} \quad (5.25)$$

Since all the submatrices of the overall stiffness matrix are now defined, Eq. (5.14) is applied to form the assembled plate structure stiffness matrix as follows

$$\mathbf{K}_{Global} = \begin{bmatrix} l\mathbf{K}_0 & \mathbf{0} & \mathbf{0} & \mathbf{C}_{1\lambda=l}^H \\ \mathbf{0} & l\mathbf{K}_{-1} & \mathbf{0} & \mathbf{C}_{1\lambda=-l}^H \\ \mathbf{0} & \mathbf{0} & \mathbf{K}_{FE} & \mathbf{C}_2^T \\ \mathbf{C}_{1\lambda=l} & \mathbf{C}_{1\lambda=-l} & \mathbf{C}_2 & \mathbf{0} \end{bmatrix} \quad (5.26)$$

It should be explained here that the calculated matrix \mathbf{K}_{Global} depends on frequency, so that the eigenvalues can be found by trying successive trial frequencies and using the Wittrick-Williams algorithm. However, for the present work we have simply searched for the lowest frequency where the determinant goes to zero, i.e. assuming that the J_{0m} terms in the W-W algorithm are zero.

5.2.2 Solution time

Due to dissimilarities in the programming language used in the methods presented where VFM is coded using MATLAB, VICON is coded in FORTRAN and ABAQUS is coded in C++, the solution times can be difficult to compare directly. Anderson et al [45] demonstrated the computational efficiency of the VICON analysis over finite element analysis. Williams and Anderson [71] further demonstrated that the approach used in VICON shows significant computational savings for point symmetric structures and lateral cross-sections. Kennedy et al. [72] again detailed the computational efficiency of the exact strip theory, comparing the program VICONOPT with the finite element method (using the STAGS finite element code), using examples including a composite blade stiffened panel and a ring-stiffened laminated cylinder. This study numerically confirmed that for comparably converged solutions, VICONOPT is typically between 100 and 10^4 times faster. The conclusions from these papers apply to the standard VICON analysis, which can only be applied to damaged structures when the damage is through the length. However Damghani et al. [50] compared the computational efficiency of SM against FEA. A similar assessment will now be made for VFM.

Based on the computational time requirements previously established for VICON analysis [71, 72] and considering only out-of-plane behaviour, the solution time required for one iteration of the Wittrick-Williams algorithm is proportional to

$$W_L = \frac{1}{2} C' \mu N \left(B^2 \times 2^3 + Br \times 2^2 + \frac{4}{3} r^2 \right) + \frac{1}{2} C N_{FE} \left(B_{FE}^2 + B_{FE} r + \frac{1}{3} r^2 \right) + \frac{1}{6} C r^3 \quad (6.2)$$

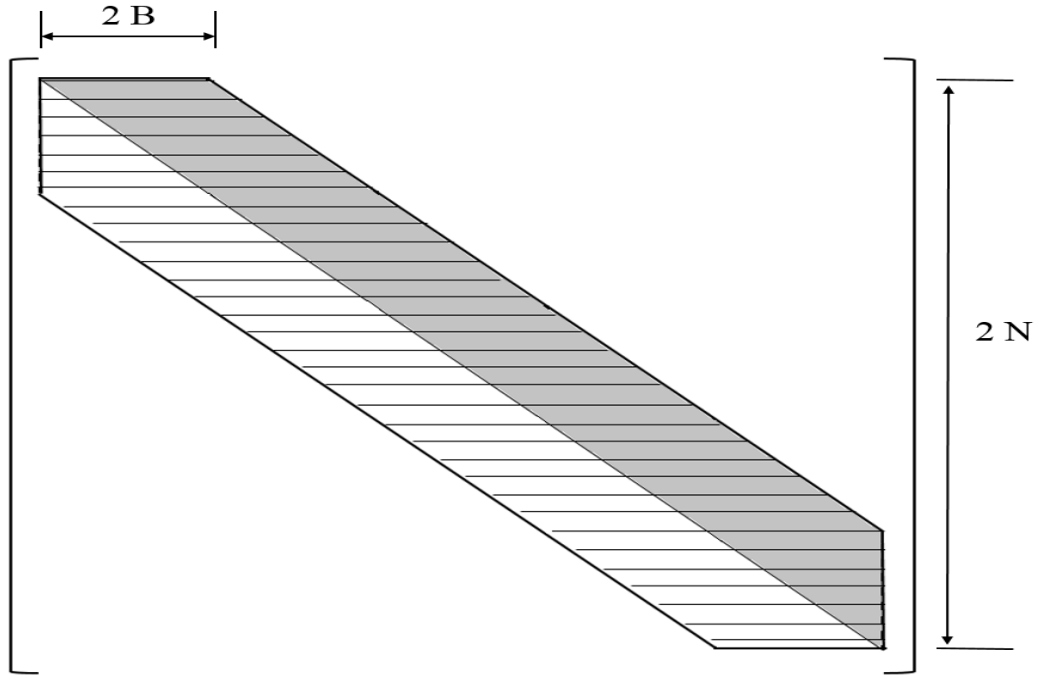


Figure 5-5: An example of a banded, symmetric VIPASA matrix

C and C' are time constants for real and complex arithmetic respectively, μ is the number of VIPASA matrices used in equation (5.6) and r is the number of constraints applied. The nodes are assumed to be numbered to minimise the bandwidth of the VIPASA and FE matrices, as illustrated in Figure 5-5 where only the elements in the shaded region need to be stored and manipulated. N and B are the order and bandwidth of each VIPASA matrix, while N_{FE} and B_{FE} are the order and bandwidth of the FE matrix.

6 Modelling the effect of damage in natural frequencies using the VFM method

In this chapter the results obtained using the VFM approach outlined in Chapter 5 to examine the behaviour of a series of damaged plates are compared with those from existing techniques in order to validate the method. Results of a study carried out to look at the natural frequencies of isotropic and composite plates containing through-the-length and embedded damage, including delaminations and areas of reduced stiffness, for instance due to matrix cracking, of different sizes and severities are presented. A comparison is then made between those obtained using VFM, the Smeared Method (SM) [50], VICON analysis and the FE software ABAQUS [20] Figure 6-1 illustrates the types of damage modelled and Figure 6-2 details which techniques have been used to model which damage case. ABAQUS and VFM are used to model all cases of damage. Due to the prismatic requirements of VICON analysis, it is only used when the damage is through the length while the SM is used to model embedded rectangular damage.

For the case of a plate containing centrally located through the length and embedded rectangular damage (shown in Figure 6-3), Chapter 5 detailed the mechanisms for modelling this in VFM. The way in which the same damage has been modelled using the other methods is described in the following sections. A series of numerical analyses and a study of the solution times for each method are then presented.

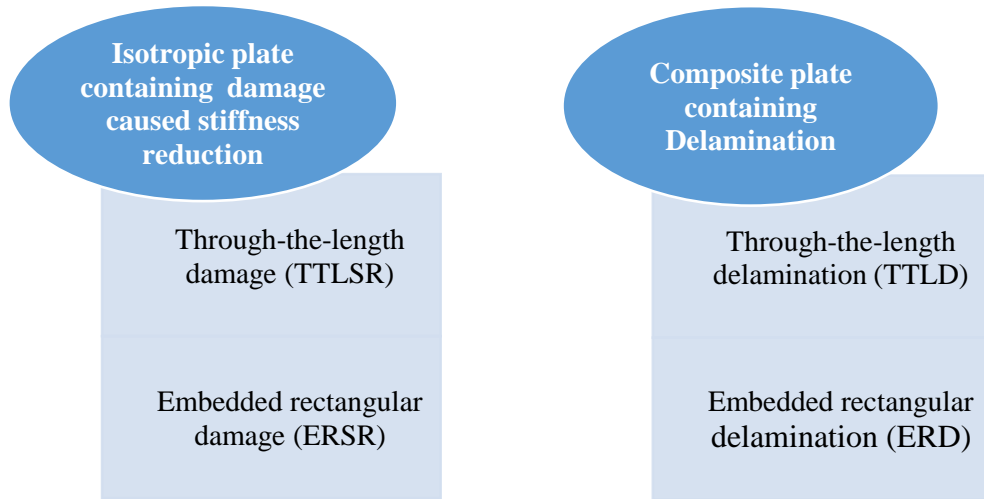


Figure 6-1 Types of damage studied.

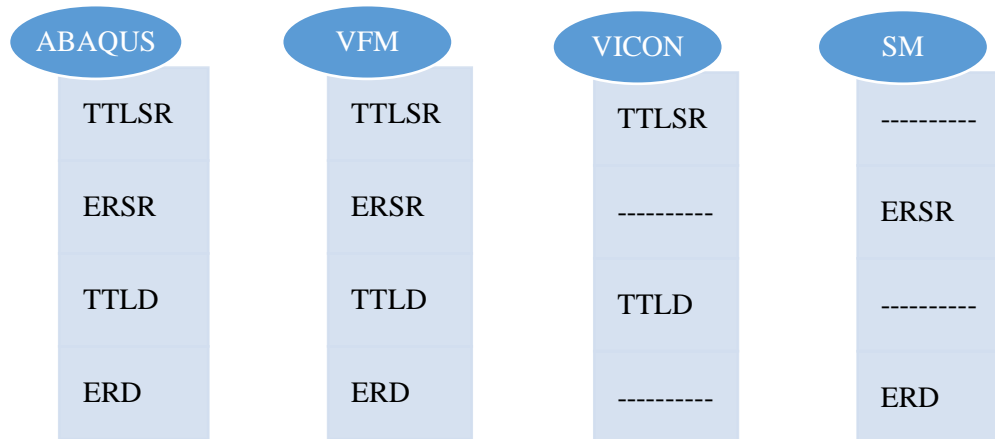
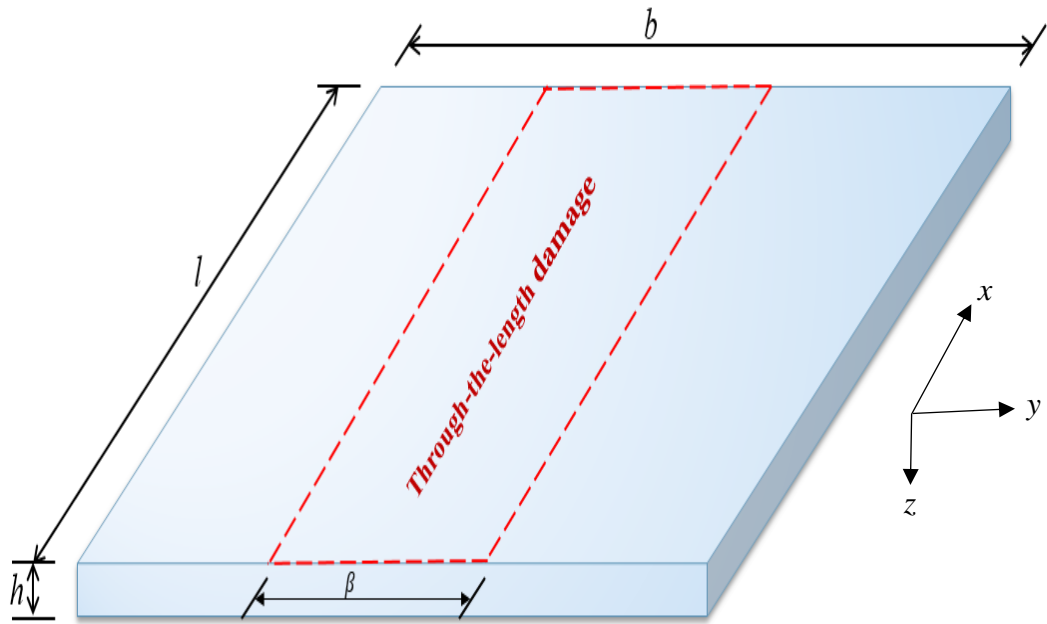


Figure 6-2 Methods used to model different types of damage.

(a)



(b)

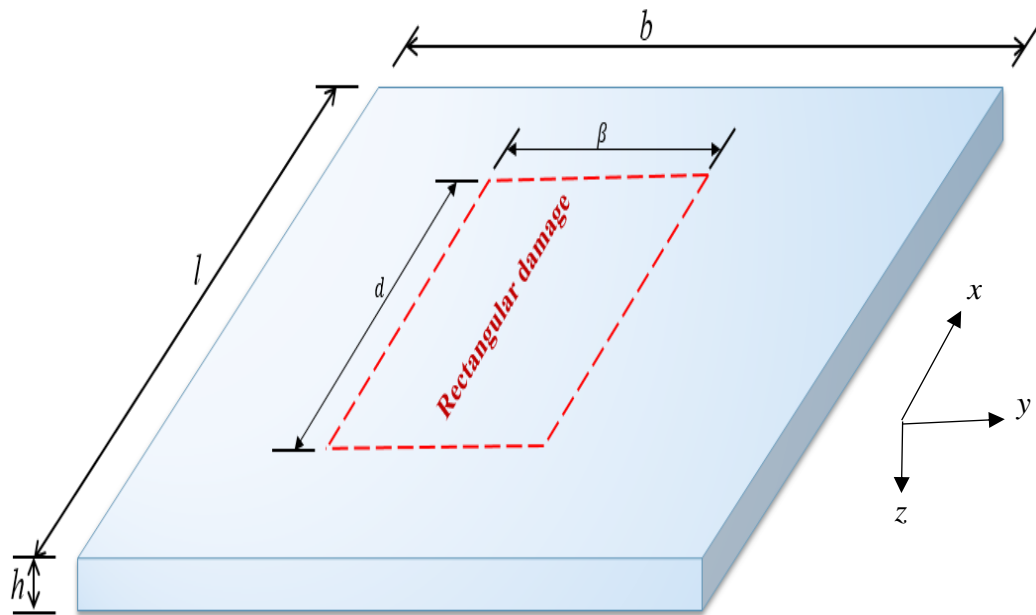


Figure 6-3: Plate containing centrally located (a) through-the-length damage (b) embedded rectangular damage.

6.1 VICON model

VICON analysis was used to model isotropic plates with through the length damage. For this case, VICON is able to model this kind of damage directly as shown in Figure 6-4. To do this, it is assumed that the damage reduces the stiffness of the area affected. In the VICON input data, the properties of each strip are used to represent whether the strip is perfect or damaged as well as the severity of the damage.

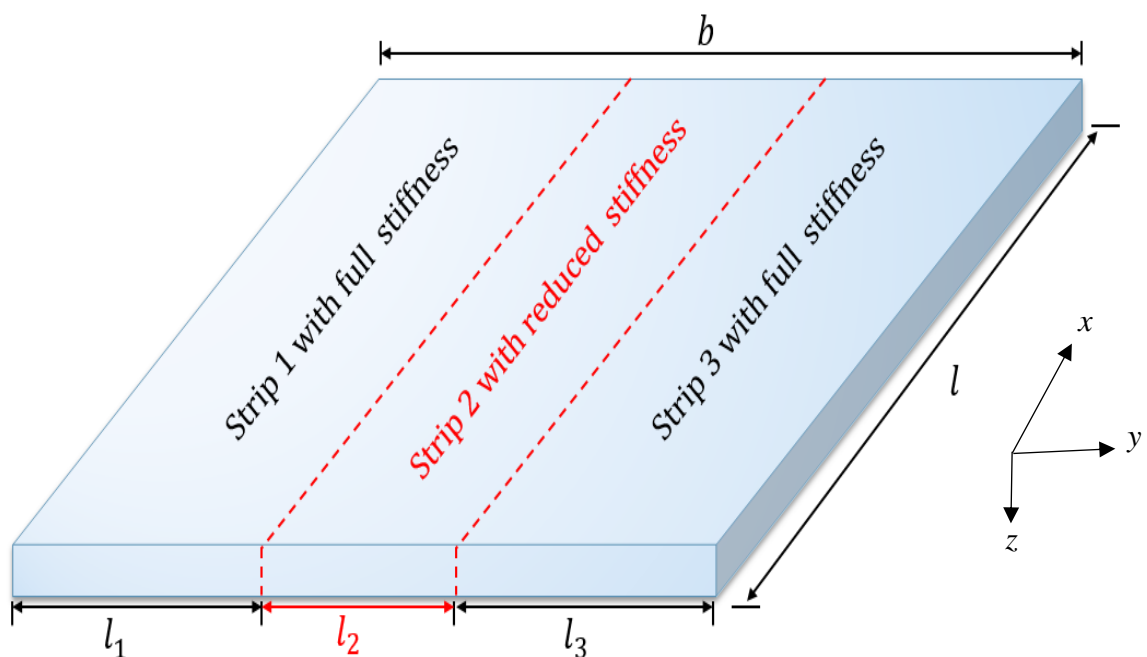


Figure 6-4: Isotropic plate with through the length damage modelled by VICON.

6.2 ABAQUS models

ABAQUS/Standard [20] was used in all cases to validate the results obtained from VFM. Models were constructed using a four noded shell element with reduced integration and using five degrees of freedom per node (S4R5) homogeneous continuum shell elements. A rectangular mesh was used with the same number and size of elements to model the strip containing the centrally located rectangular

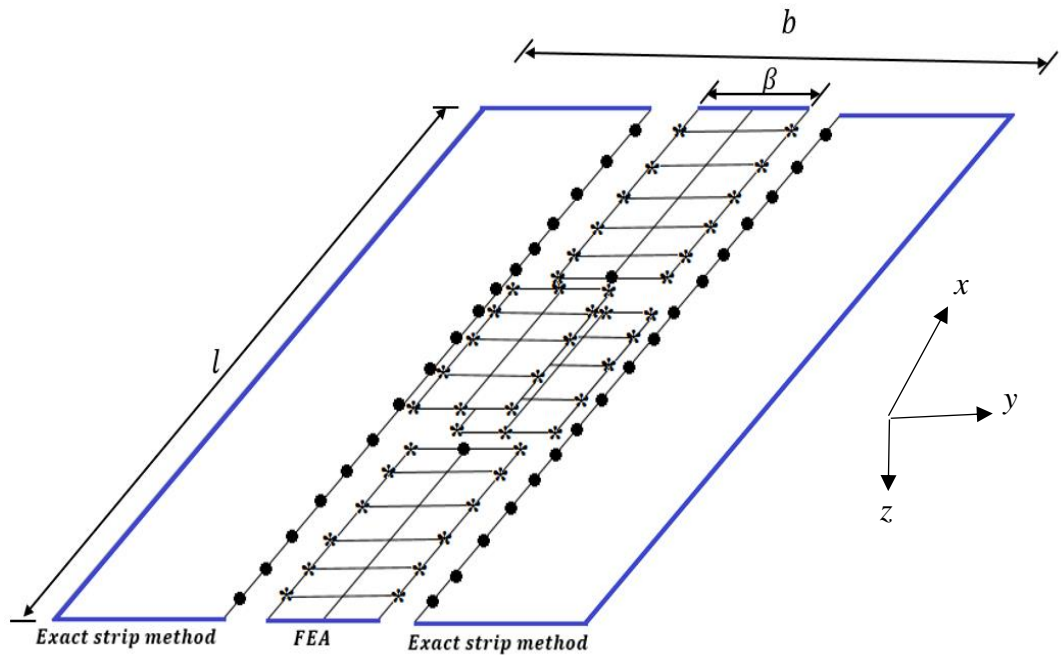
delamination as was used for the VFM model, in order to achieve the maximum possible equivalence between the two. The element size is specified based on the minimum mesh density needed for accurate results. Figure 6-5 (a) shows how VFM is used to model a plate with a centrally located embedded rectangular delamination. The nodes marked with circles (●) at the boundaries between the VICON and FE regions, and at the boundary of the delamination, are treated as master nodes. Those at the same locations and marked with stars (*) are treated as slave node whose displacements and rotations are constrained to match those of the master nodes., The blue line shows the regions where boundary conditions are applied. Figure 6-5 (b) is an example of the way ABAQUS is used to model a plate to include the same number and size of elements that VFM used to model the strip containing centrally located rectangular delamination. In both methods the displacements at the edges of the plates are constrained to apply the simply supported boundary condition of the plates, i.e. in-plane displacements on the x and y axes and vertical out-of-plane displacement.

6.3 Smearred method (SM)

Damghani et al. [50] developed the Smearred Method to model plates with embedded damage. In the case of an isotropic plate with embedded rectangular damage, application of the SM results in the substitution of the strip containing the damage with an equivalent strip with averaged stiffness to satisfy the prismatic requirement of the exact strip method that the SM is based on, see Figure 6-6. The stiffness of the equivalent strip is assumed according to:

$$K_v = \left(k_r \times \frac{d}{l} \right) + \left(k_f \times \frac{l-d}{l} \right) \quad (6.1)$$

(a)



(b)

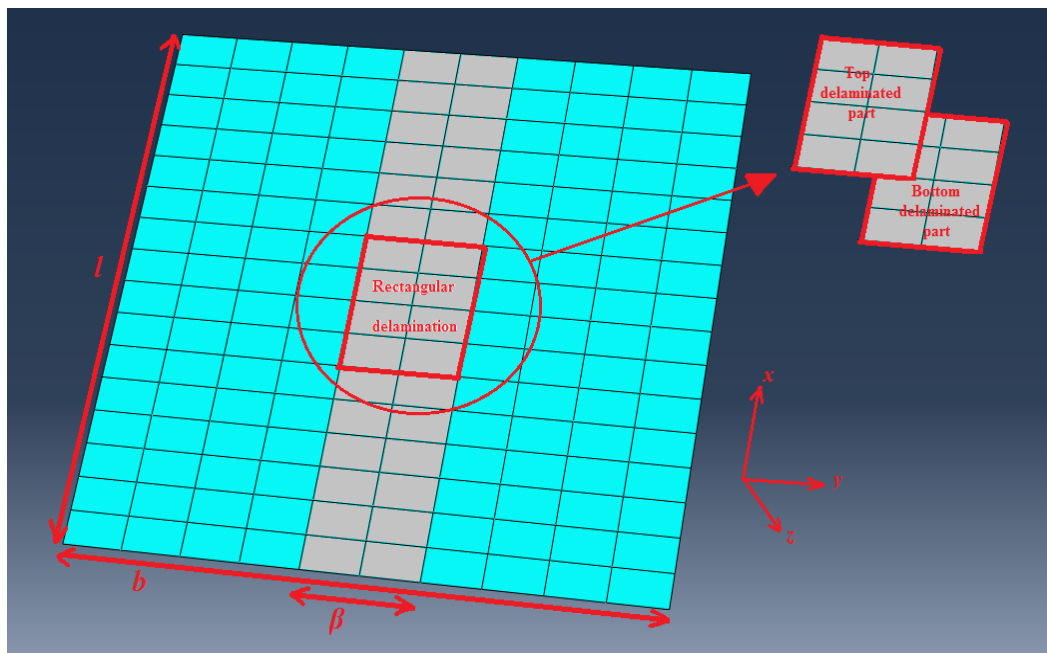


Figure 6-5 Identical plates containing embedded delaminations modelled by (a) VFM (b) ABAQUS.

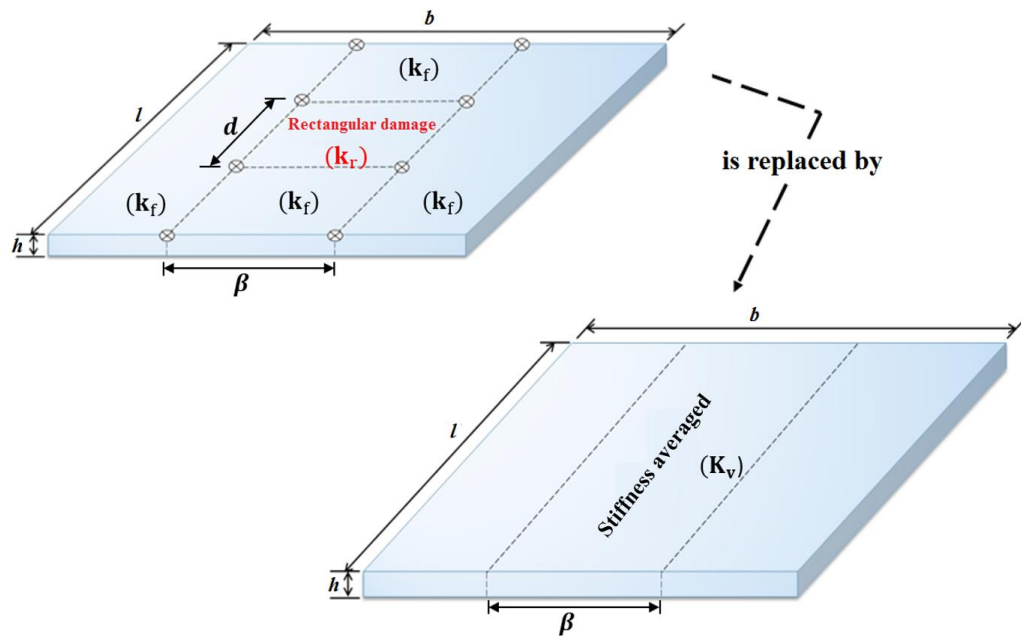


Figure 6-6 Smearing method for modelling embedded reduced stiffness damage.

where \mathbf{K}_v is the averaged stiffness of the damaged strip. \mathbf{k}_f is the stiffness of a perfect strip, calculated using the correct value of Young's modulus (E) and \mathbf{k}_r is the reduced stiffness, calculated using a reduced value of Young's modulus (fE) to represent the effect of damage (i.e. applying a stiffness reduction factor f). Since the stiffness of the strip including the embedded damage is averaged, VICON analysis can be used as described in section 6.1.

For embedded delaminations, the strip containing the rectangular delamination is divided into four different regions as shown in Figure 6-7. Regions 1 and 2 represent the top and bottom portions of the delaminated area and 3a and 3b are the perfect areas of the same strip. By manipulating the properties of the sub-laminates, regions 1 and 2 are re-modelled as strips 1 and 2 with length l instead of d to satisfy the prismatic

requirements of the method, while regions 3a and 3b are remodelled as strip 3 using Eq. (6.1) [50].

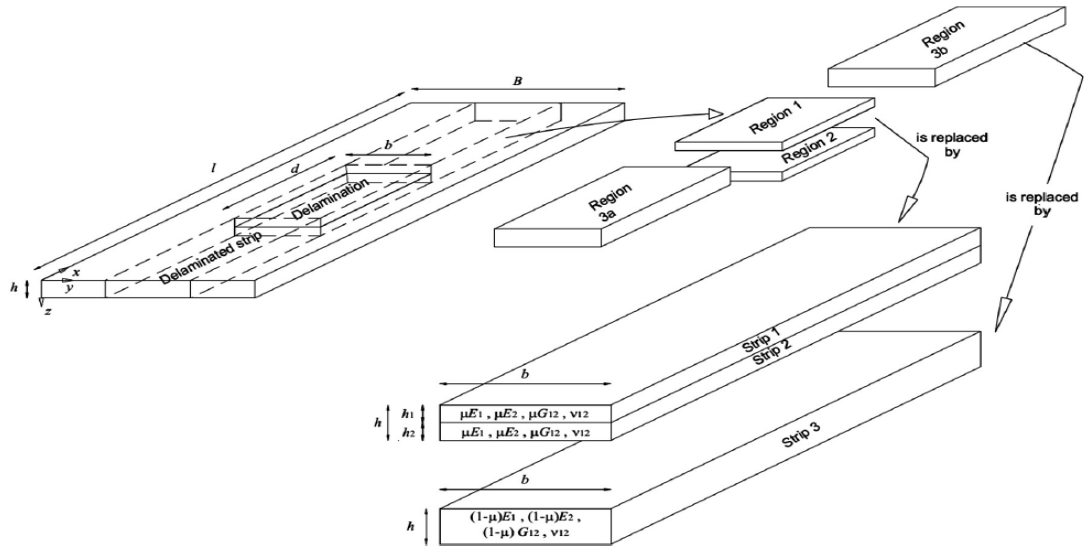


Figure 6-7 Sketch of VICONOPT model for a laminate of length l , width B and thickness h , having an embedded rectangular delamination of length $d (= \mu l)$ and width b , (Figure reproduced from Damghani et al. (2014)).

6.4 Numerical study

The VFM method was then validated by comparing the natural frequencies of a range of isotropic and composite plates containing through the length and embedded damage obtained using VFM, SM, VICON analysis and ABAQUS as detailed in Figure 6-2.

6.4.1 Reduced stiffness isotropic plates

The first plates to be examined were isotropic plates with (i) through the length and (ii) embedded damage. Plates had length $l = 100\text{mm}$, width $b = 100\text{mm}$ and thickness $h = 1\text{mm}$. Material properties were: Young's modulus $E = 110 \text{ kN.mm}^{-2}$, density $\rho = 2300 \text{ kg.mm}^{-3}$ and Poisson's ratio $\nu = 0.3$. Different values of stiffness reduction factor (f) were considered for the effect of damage: $f = 0.25$, $f = 0.3$, $f = 0.67$ and $f = 0.75$.

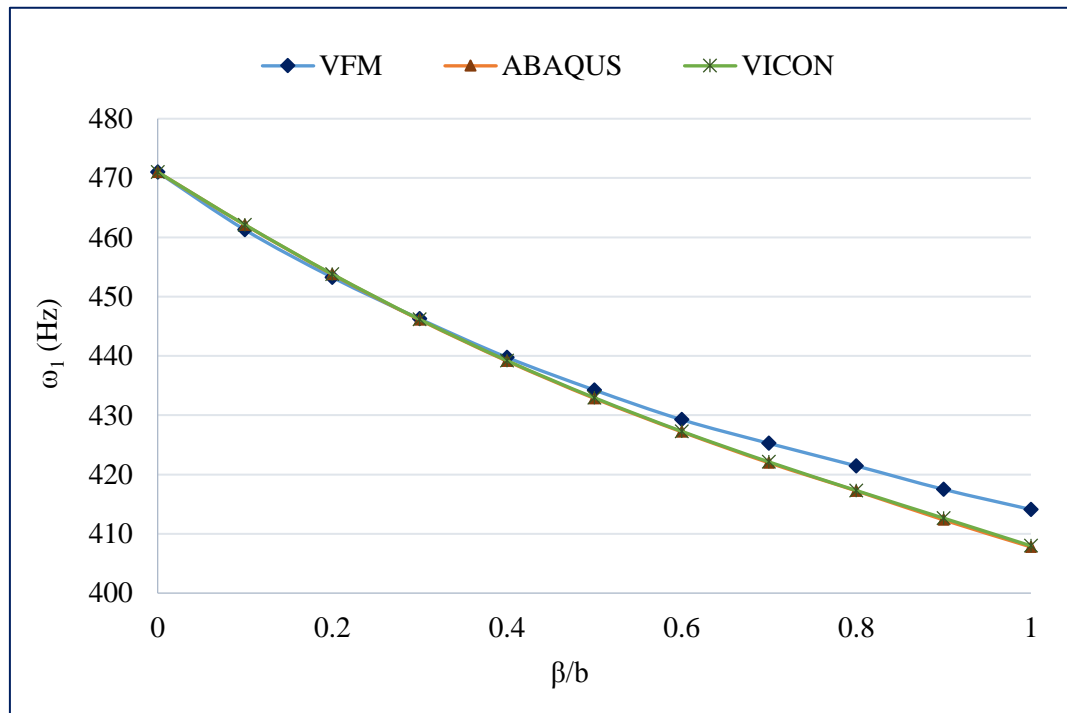
6.4.1.1 Through the length damage (TTLSR)

Figure 6-8 shows the first natural frequencies of isotopic plates containing different sizes of through the length damage (β/b) with different stiffness reduction factors ($f=0.25, 0.75$). Figure 6-8 (a) that there is a perfect match between the VICON and ABAQUS results for a range of different widths of through the length damage. For $0 \leq \beta/b \leq 0.4$, VFM is also seen to match these results. However, as the damage width increases i.e. for $\beta/b > 0.4$, VFM predicts higher natural frequencies than both VICON and ABAQUS albeit with a maximum difference of only 1.55% at $\beta/b = 1$ and $f = 0.75$. This is due to the number of elements used in the finite element part of the VFM being slightly too small to accurately model the vibration mode shape leading to the model being over-constrained and as a result of this raising the natural frequencies. In Figure 6-8 (b), $f=0.25$, VFM results perfectly match VICON and ABAQUS results for $0 \leq \beta/b \leq 0.8$. For $\beta/b > 0.8$, VFM predicts higher natural frequencies than both VICON and ABAQUS with a maximum difference of 2.55% at $\beta/b = 1$.

6.4.1.2 Embedded rectangular damage (ERSR)

Figure 6-9 presents the first natural frequencies of isotopic plates containing embedded rectangular damage ($d=l/2$) with different stiffness reduction factors ($f=0.67, 0.3$), as calculated using VFM, ABAQUS and SM. Excellent agreement is demonstrated between the VFM and ABAQUS results demonstrating that VFM is a significant improvement on the smeared method, which gives good results when the damaged plate vibrates globally, $0 \leq \beta/b \leq 0.3$, but conservative results when the plate vibrates locally, $\beta/b > 0.3$, since this mode is not adequately represented, see Figure 6 6.

(a)



(b)

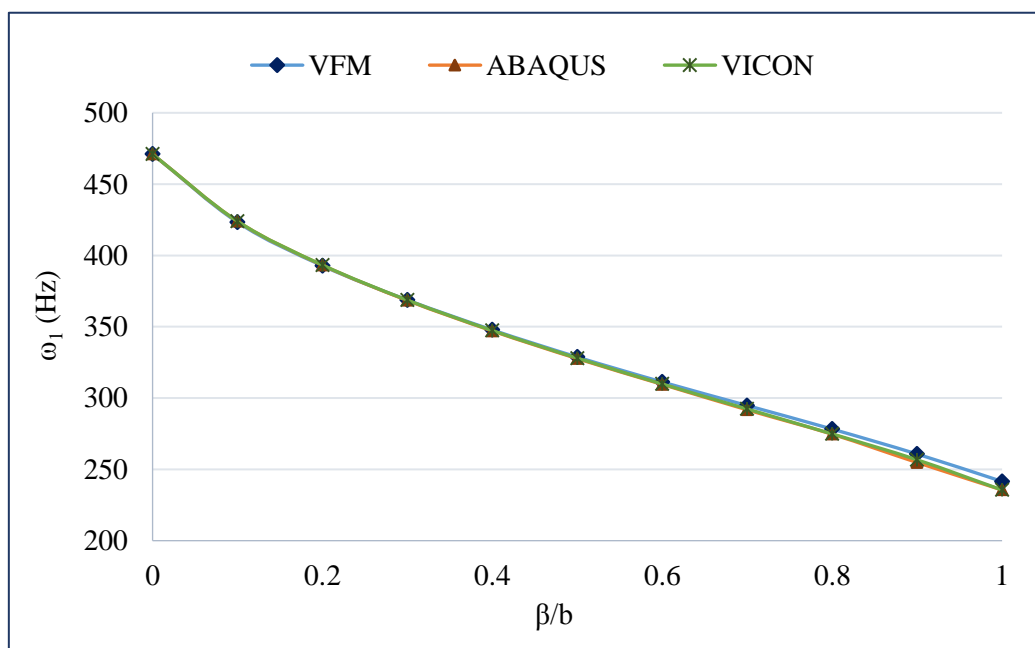
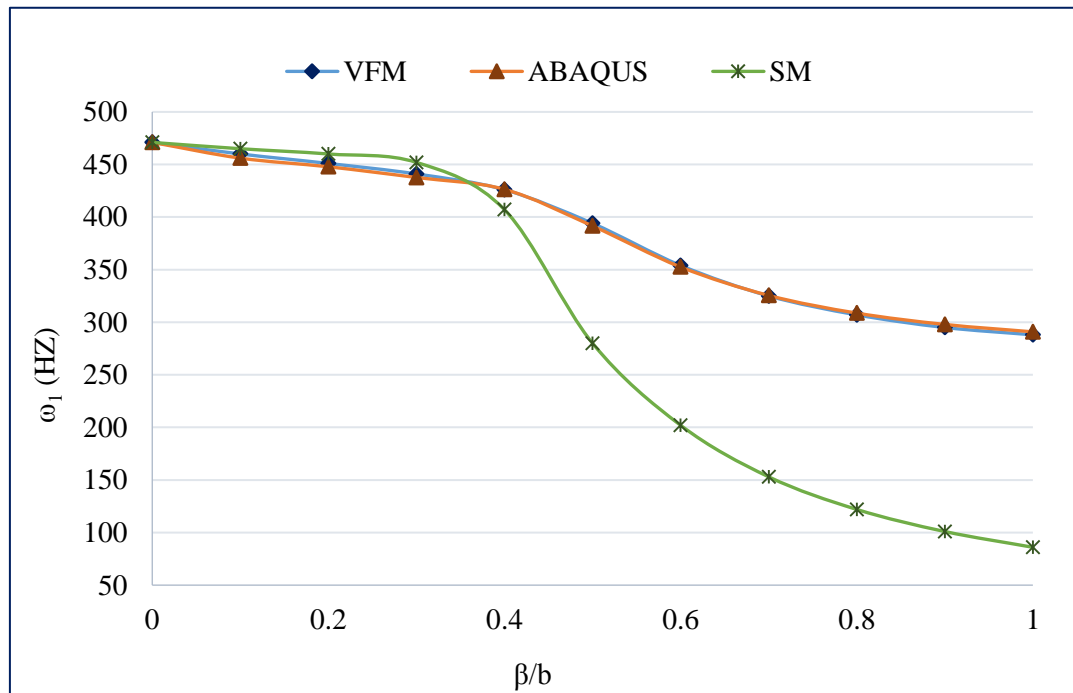


Figure 6-8: Lowest natural frequency for isotropic plates (ω_1) against width β/b for centrally located damage using the three techniques, Smearing Method (SM), ABAQUS and VFM. (a) through-the-length damage and $f = 0.75$. (b) through-the-length damage and $f = 0.25$.

(a)



(b)

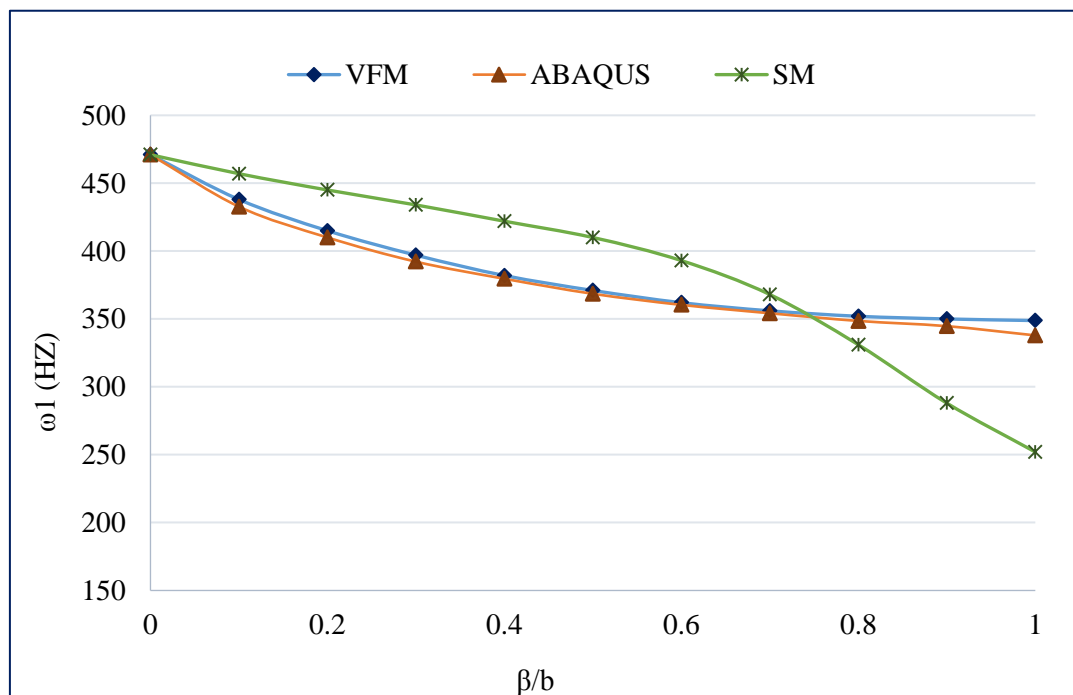


Figure 6-9: Lowest natural frequency of isotropic plates (ω_1) against width β/b for centrally located damage using the three techniques, Smearing Method (SM), ABAQUS and VFM. (a) embedded rectangular damage, $d = 50\text{mm}$ and $f = 0.67$. (b) embedded rectangular damage, $d = 50\text{mm}$ and $f = 0.3$.

6.4.2 Delaminated composite plates

The VFM, ABAQUS, VICON and SM techniques were then used to study the first natural frequencies of through the length delaminated composite plates and composite plates containing embedded rectangular delaminations. The plates examined had length $l = 100\text{mm}$, width $b = 100\text{ mm}$, thickness $h = 4\text{mm}$, delaminations at two different depths ($h/2$ and $h/4$) and material properties: Young's moduli $E_1 = 110\text{ kN.mm}^{-2}$, $E_2 = 10\text{ kN.mm}^{-2}$, shear moduli $G_{12} = G_{13} = G_{23} = 5\text{ kN.mm}^{-2}$, Poisson's ratio $\nu_{12} = 0.33$ and density $\rho = 4480\text{ kg.mm}^{-3}$. They each comprised of 32 unidirectional plies of thickness 0.125mm in the sequence [0/45/-45/90/90/-45/45/0/0/45/-45/90/90/-45/45/0]s.

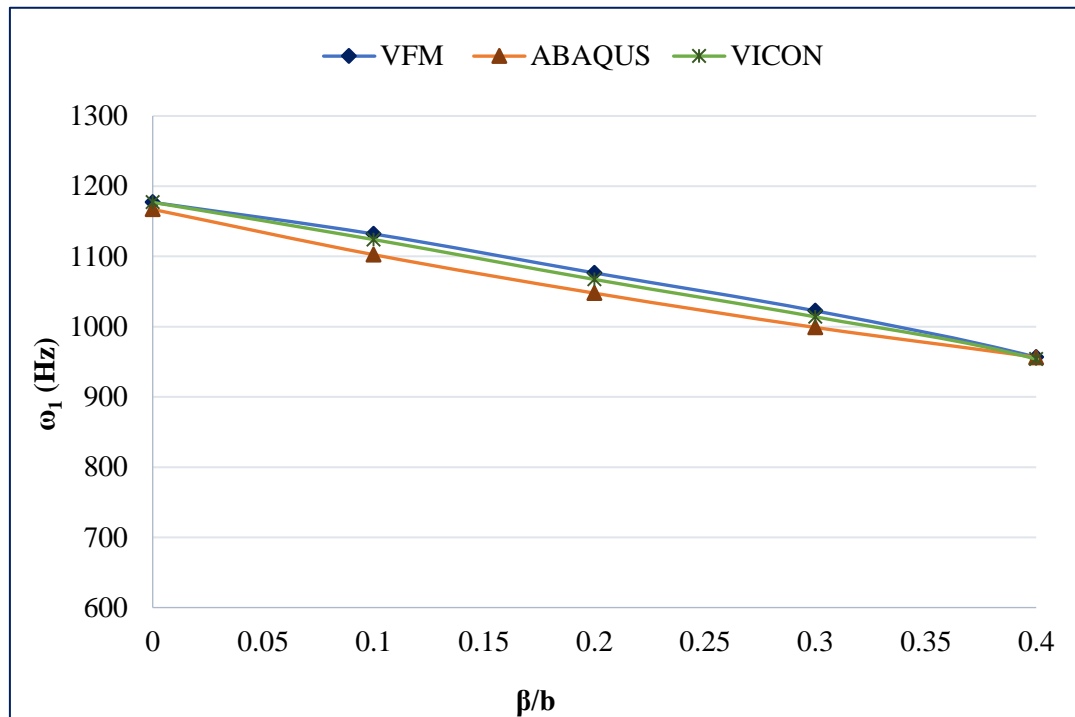
6.4.2.1 Through-the-length delaminations (TTLD)

Figure 6-10 shows how the lowest natural frequencies of composite plates varies with delamination size. It can be seen that there is a very good match between VFM, VICON and ABAQUS in handling this kind of damage. The graphs show a decrease in the value of the first natural frequency when the width of the delamination is increased. However, moving the delamination towards the mid thickness of the plate causes more reduction in the value of the first natural frequency for the different delamination widths studied. The VICON results are slightly higher than the ABAQUS results, with maximum differences of 1.95% and 1.67% for delamination depths of $h/4$ and $h/2$ respectively. Due to the presence of constraint regions in VFM, the maximum differences between VFM and ABAQUS are 2.68% and 2.38% for delamination depths of $h/4$ and $h/2$ respectively.

6.4.2.2 Embedded rectangular delamination (ERD)

Variations in the lowest natural frequencies of composite plates against the size and depth of centrally located embedded rectangular delaminations were then examined. Figure 6-11 studies the reduction in the lowest natural frequency of a composite plate containing embedded rectangular delaminations of various sizes and through the thickness locations. Figure 6-11 (a) and (b) show the variations for a delamination of length 25mm, showing very good agreement between VFM and ABAQUS for both delamination depths with maximum differences between results of 1.88% and 3.4% for delamination depths of $h/4$ and $h/2$ respectively occurring when $\beta/b = 1$. In Figure 6-11 (c) and (d) where the delamination length is 50mm, the maximum difference between the two models is less than 3.3% when $0 \leq \beta/b \leq 0.7$ for both cases of delamination depth. This reaches 3.8%, 5.6% and 6.3% when $\beta/b = 0.8, 0.9$ and 1.0 respectively for plates with a delamination depth of $h/4$, with a slightly smaller difference when the delamination is at depth of $h/2$. Since VFM uses finite element theory based on a fixed number of elements to model the damaged part of the plate, as the size of the damage increases the mesh becomes coarser and hence the error is larger.

(a)



(b)

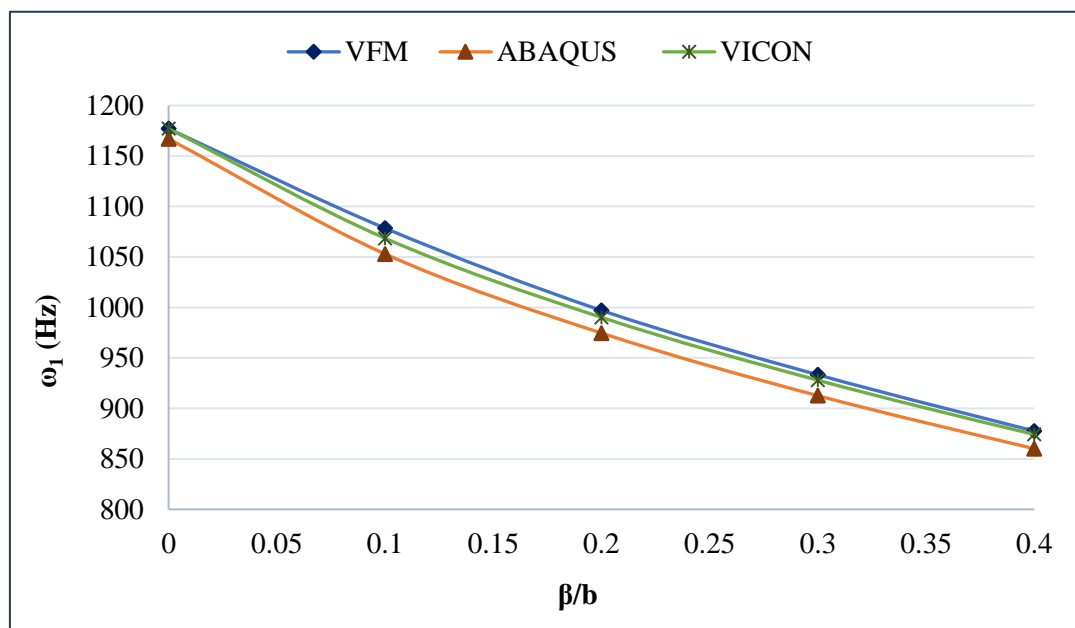
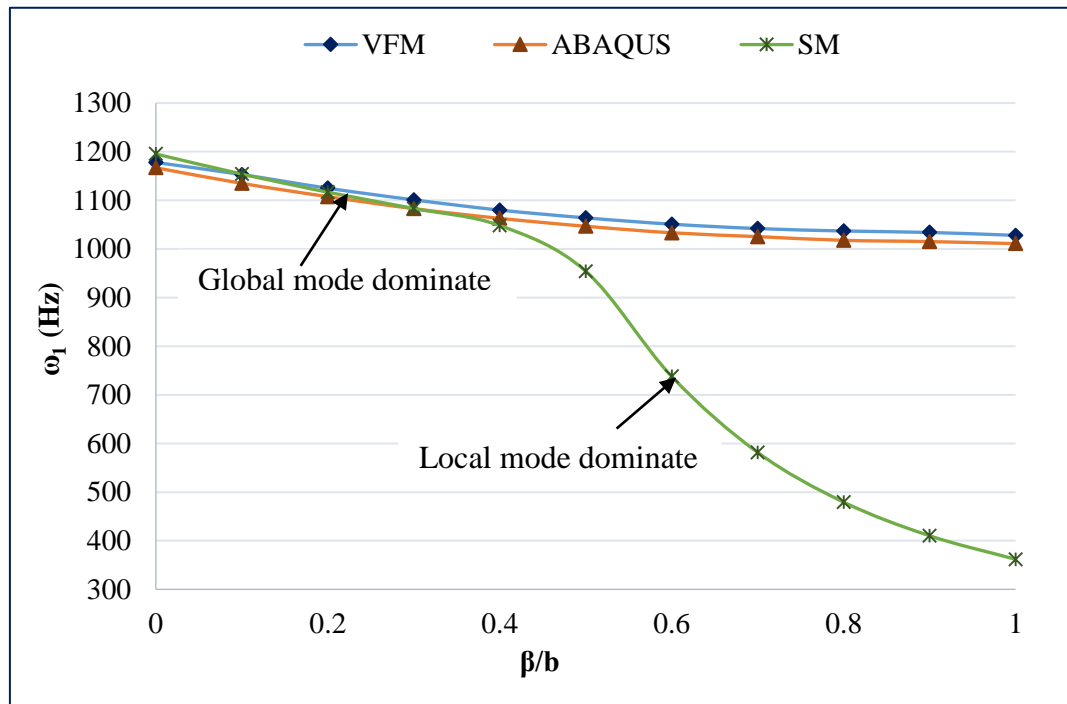
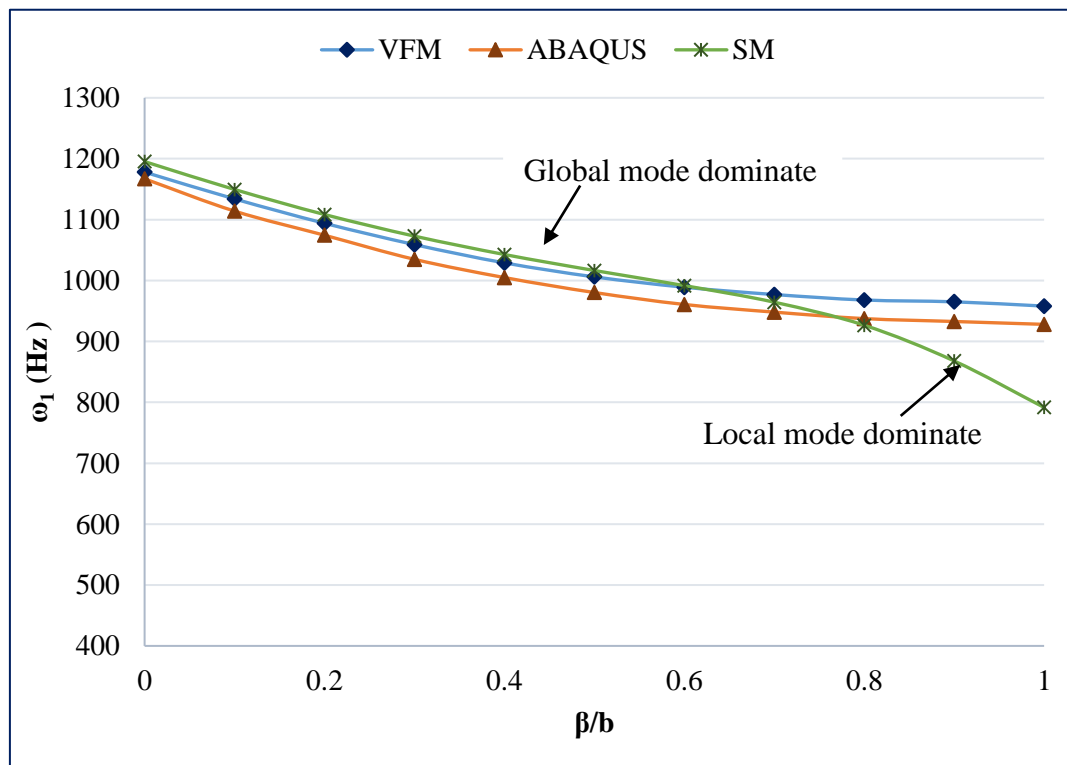


Figure 6-10: Lowest natural frequency of composite plates (ω_1) against width β/b for centrally located through the length delamination using ABAQUS and VFM. (a) Delamination depth is at $h/4$ from the plate top surface (b) Delamination depth is at $h/2$ from the plate top surface.

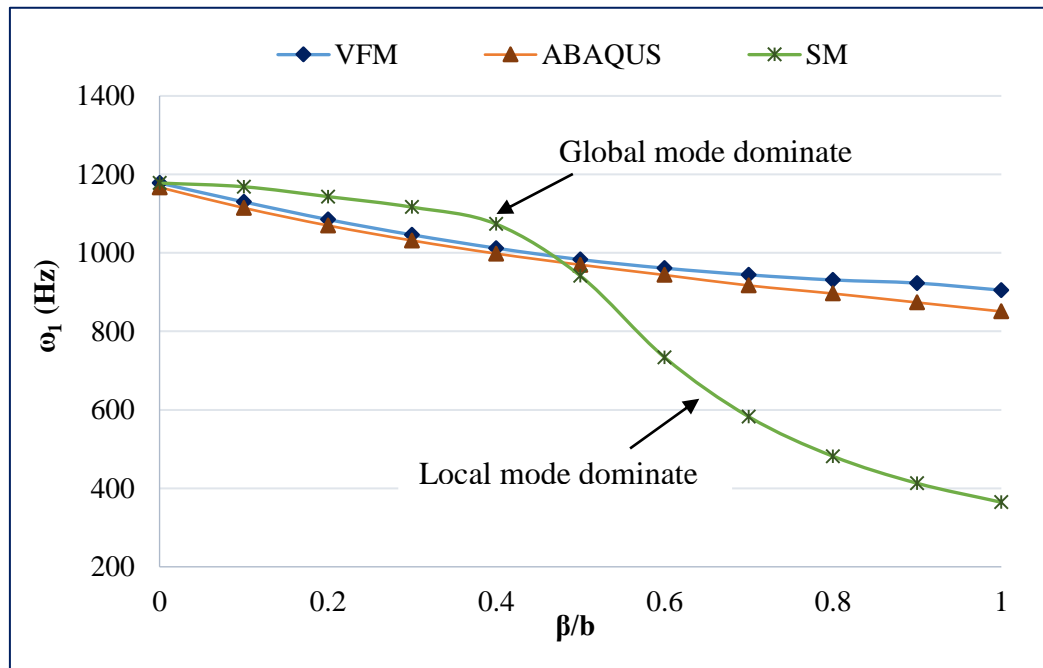
(a)



(b)



(c)



(d)

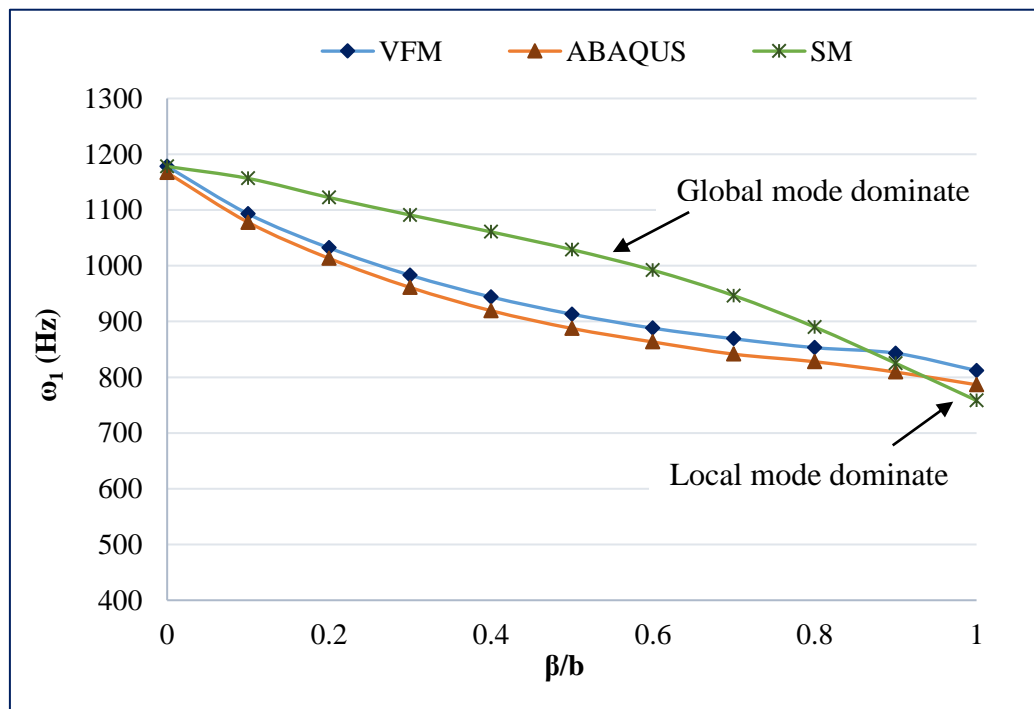


Figure 6-11: Lowest natural frequencies of composite plates (ω_1) against width β/b for centrally located embedded rectangular delaminations, using the Smearing Method (SM), ABAQUS and VFM. (a) delamination depth = $h/4$, $d = 25$ mm. (b) delamination depth = $h/2$, $d = 25$ mm. (c) delamination depth = $h/4$, $d = 50$ mm. (d) delamination depth = $h/2$, $d = 50$ mm.

In terms of the SM results, as explained in section 6.3, the embedded rectangular damage is modelled indirectly, see Figure 6-7. This leads to very good agreement with the other methods when the plate vibrates globally, (when $0 \leq \beta/b \leq 0.3$ and $0 \leq \beta/b \leq 0.6$) as seen in Figure 6-11 (a) and (b) respectively, but with increasing differences between predicted natural frequencies when the panel vibrates locally as seen in Figure 6-11 (c). These more conservative results are due to the SM method predicting a conservative local behaviour, see Figure 6-12, not seen in the VFM and ABAQUS models for the reasons explained in section 4.1.

As the delamination is moved to the mid-thickness (Figure 6-11 (b) and (d)), the SM only models global vibration modes for all delamination sizes and therefore agrees well with other techniques only for geometries where the global mode is dominant.

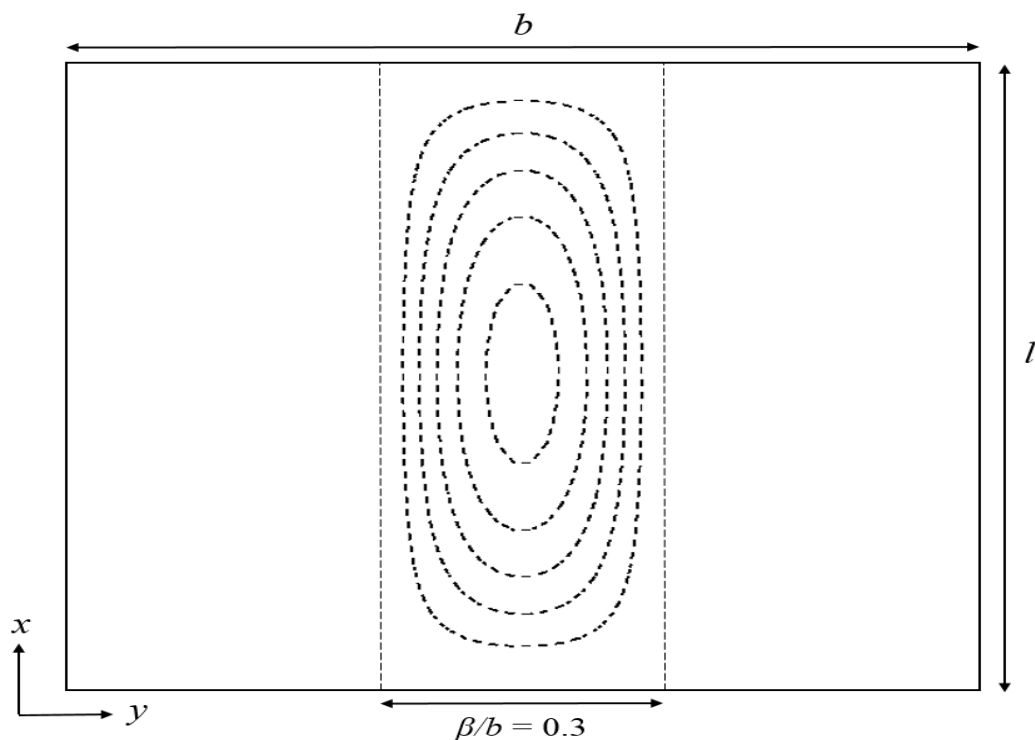
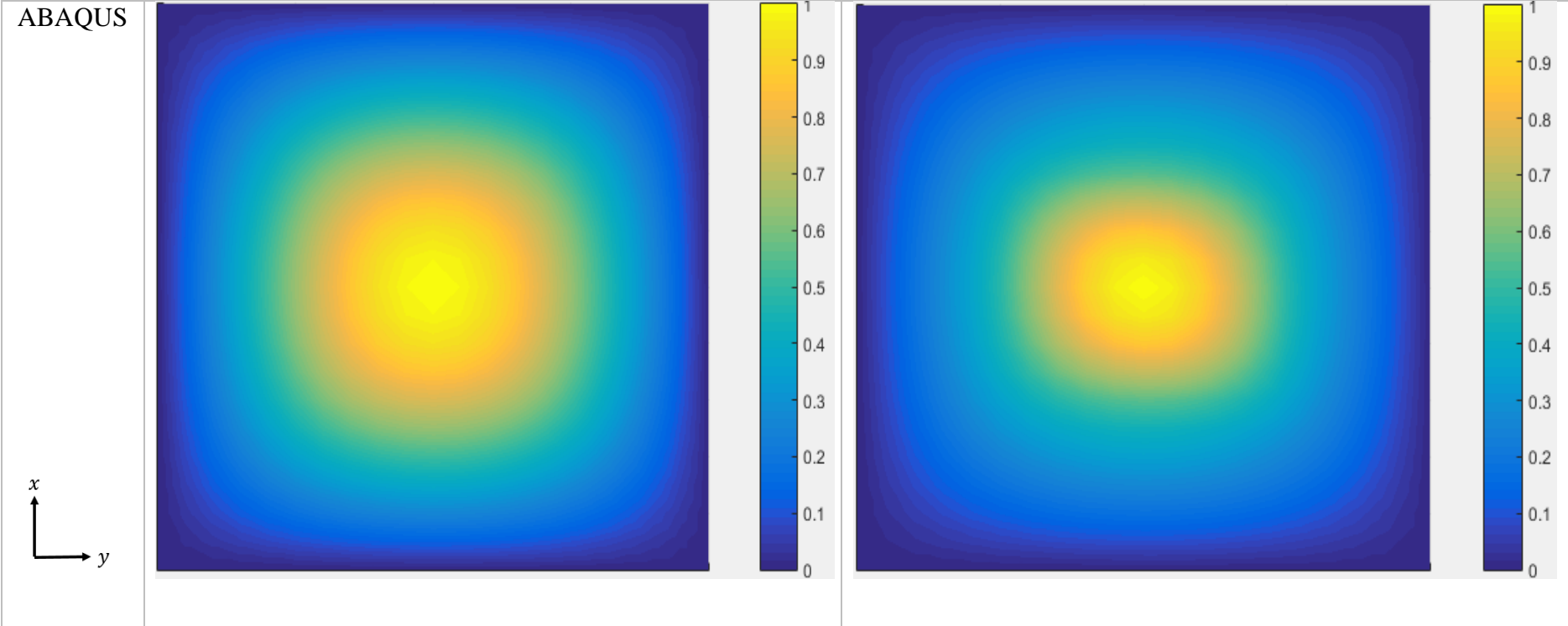
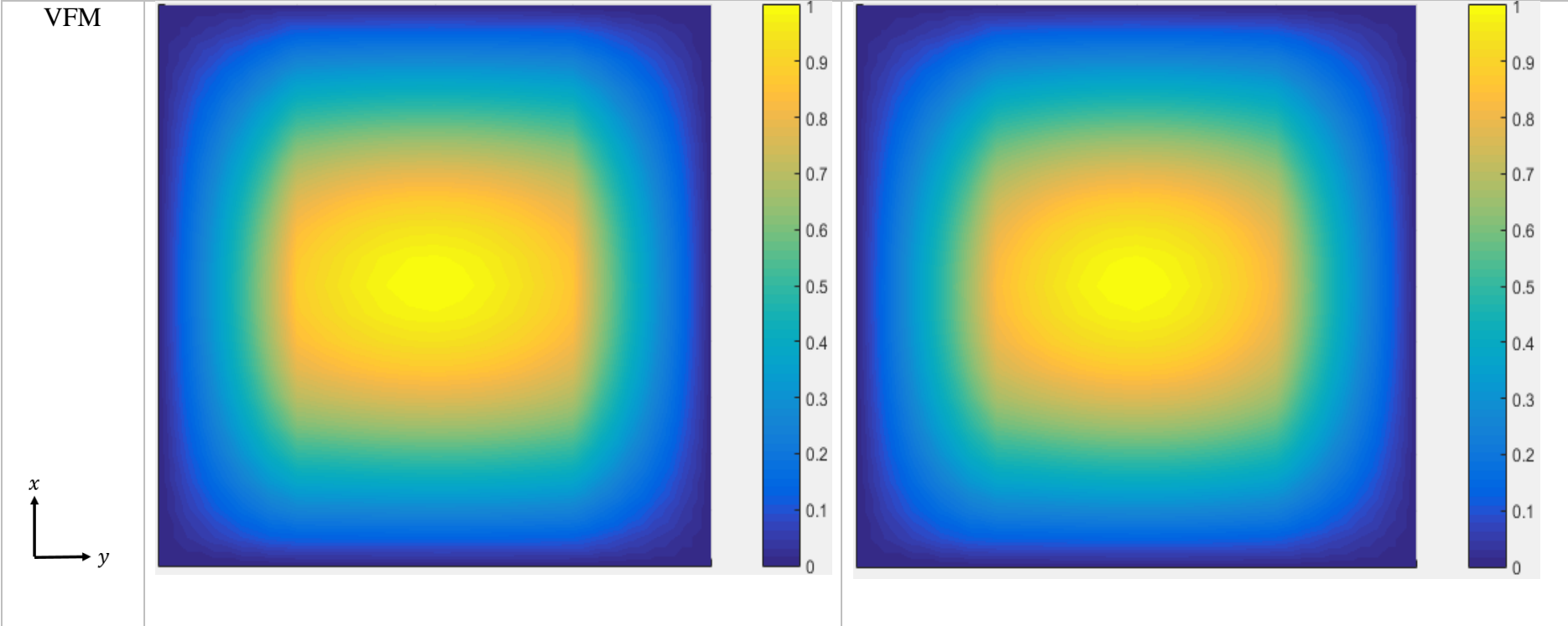


Figure 6-12: Mode shape corresponding to the lowest natural frequency of a composite plate having a centrally located embedded rectangular delamination with depth = $h/4$, $d = 50\text{mm}$ and $\beta/b=0.3$ obtained using the Smearing Method (SM).

Figure 6-13 shows normalised mode shape plots, obtained from ABAQUS, VFM and SM, of the lowest natural frequency for two cases from Figure 6-11. For the mid-thickness delamination in Figure 6-11 (a), the three methods give almost identical mode shapes. But in Figure 6-11 (b), where the delamination is closer to the top surface, ABAQUS and VFM show good agreement with a maximum difference of 3% in the magnitude of the out of plane displacement, while SM gives a fictitious through-the-length local mode.





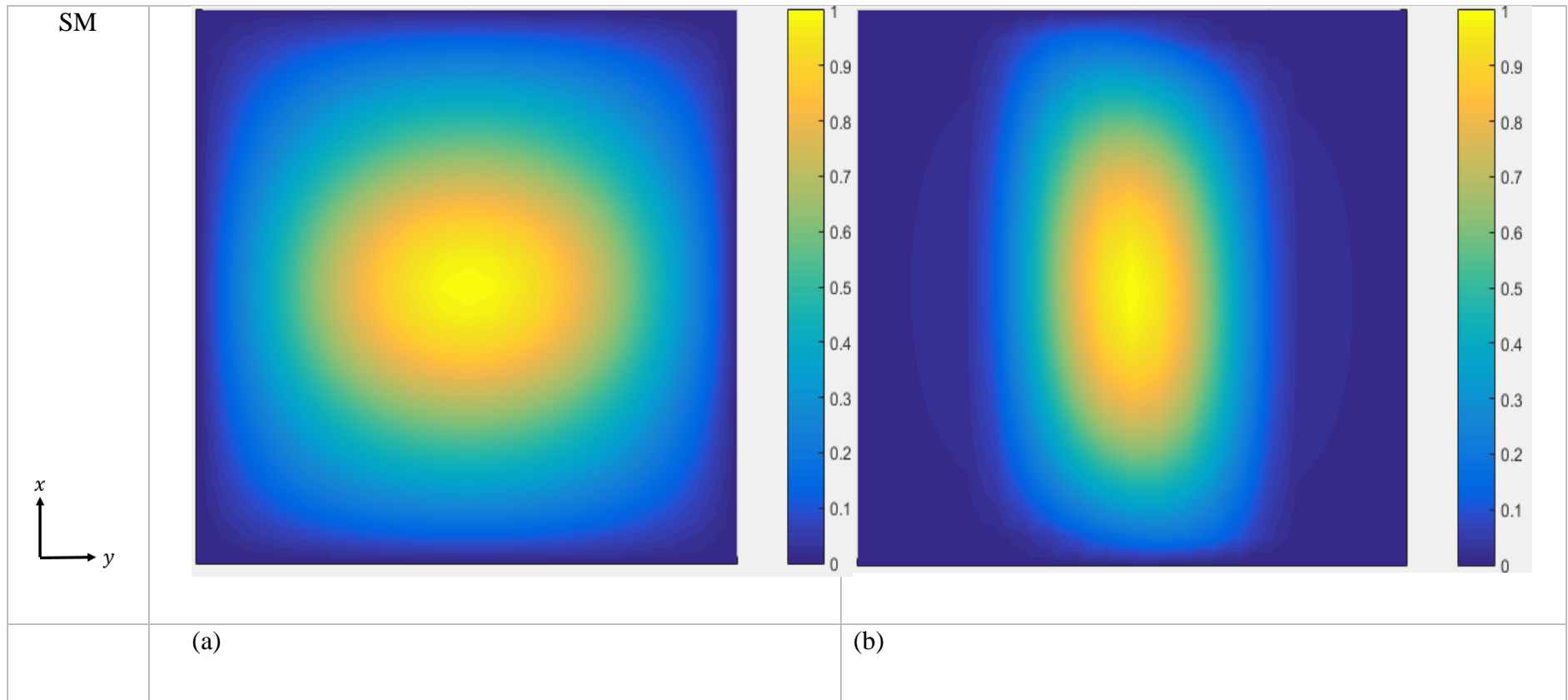


Figure 6-13: ABAQUS, VFM and SM plots of the out-of-plane deflection in the normalised mode shape of the lowest natural frequency for a composite plate containing an embedded rectangular delamination. (a) Delamination length $d=0.5l$, depth $0.5h$, width $\beta=0.5b$, see Figure 6-11(d). (b) Delamination length $d = 0.5l$, depth $0.25h$, width $\beta = 0.6b$, Figure 6-11 (c).

6.4.2.3 Effect of delamination location.

Having validated the VFM method for modelling damage, the effects of widthwise/lengthwise position and the depth of a delamination on the first natural frequency of a damaged plate were studied using VFM and ABAQUS. Figure 6-14 shows a plate containing embedded delaminations D1 (located at $(a_x, a_y=b/2)$), and D2 (located at $(a_x=l/2, a_y)$). However, it is aimed to investigate the effects of location of delamination, lengthwise (D1) and widthwise (D2) respectively.

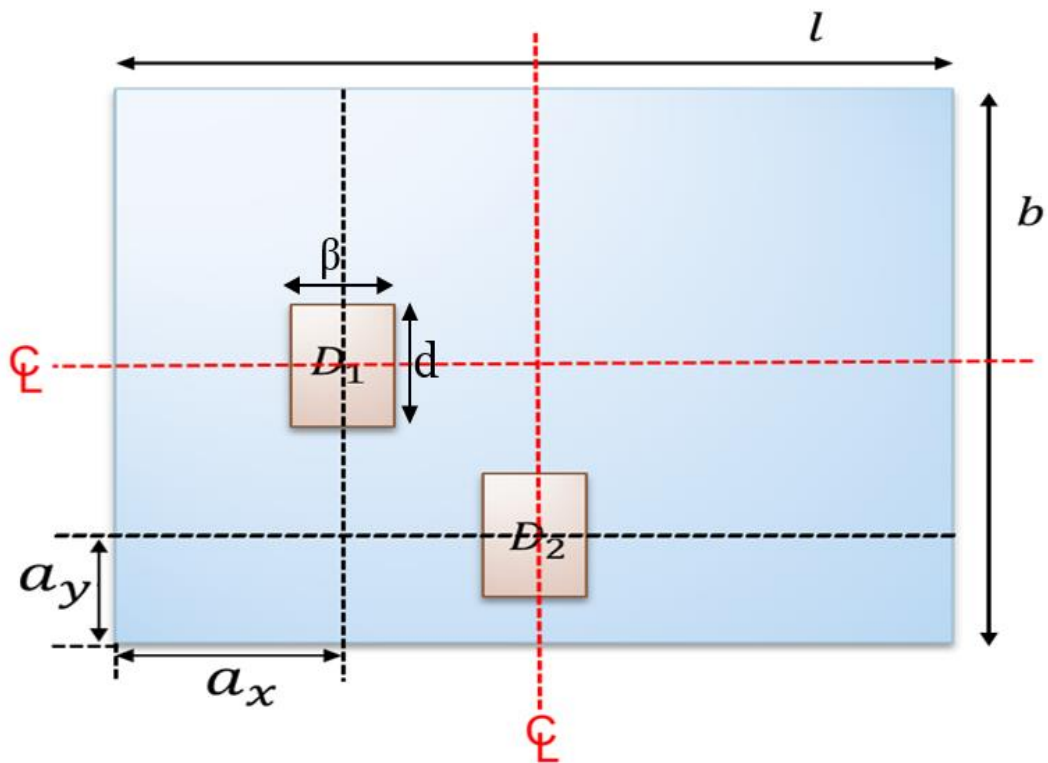
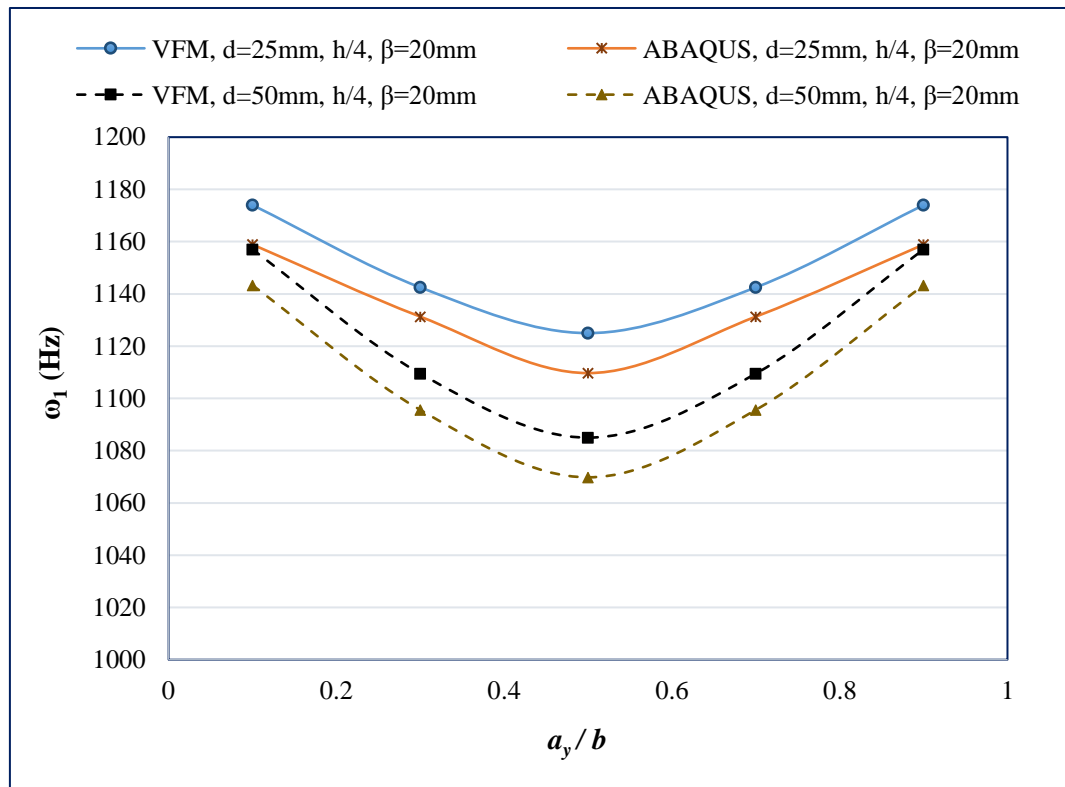


Figure 6-14 Plate containing embedded delaminations.

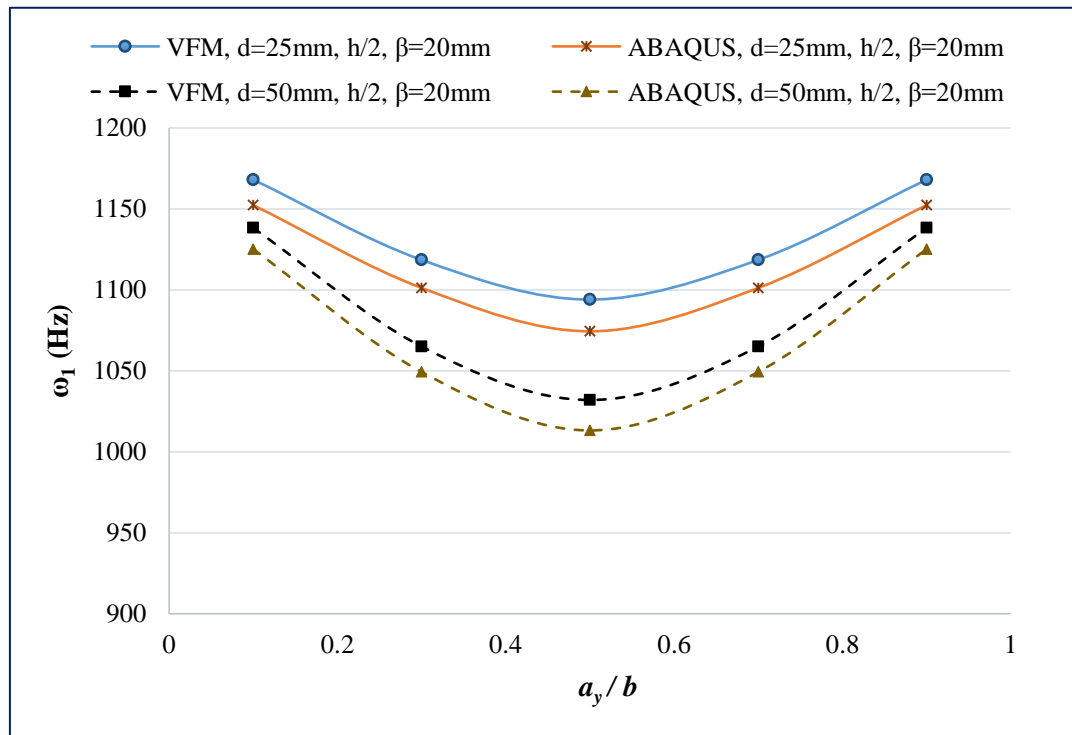
Figure 6-15 (a) to (c) show the results of this analysis for composite plates containing embedded delaminations with length 25mm, 50mm and 75mm at depths of $h/4$ and $h/2$ as their location varies widthwise (β/b). Figure 6-16 (a) to (d) demonstrate the effect

of changing the lengthwise position of delaminations of length $d=25\text{mm}$ and 50mm , and width $\beta=20\text{mm}$ and 40mm , at depths of $h/4$ and $h/2$. All cases clearly show a reduction in the first natural frequency as the delamination moves toward the centre of the plate.

(a)



(b)



(c)

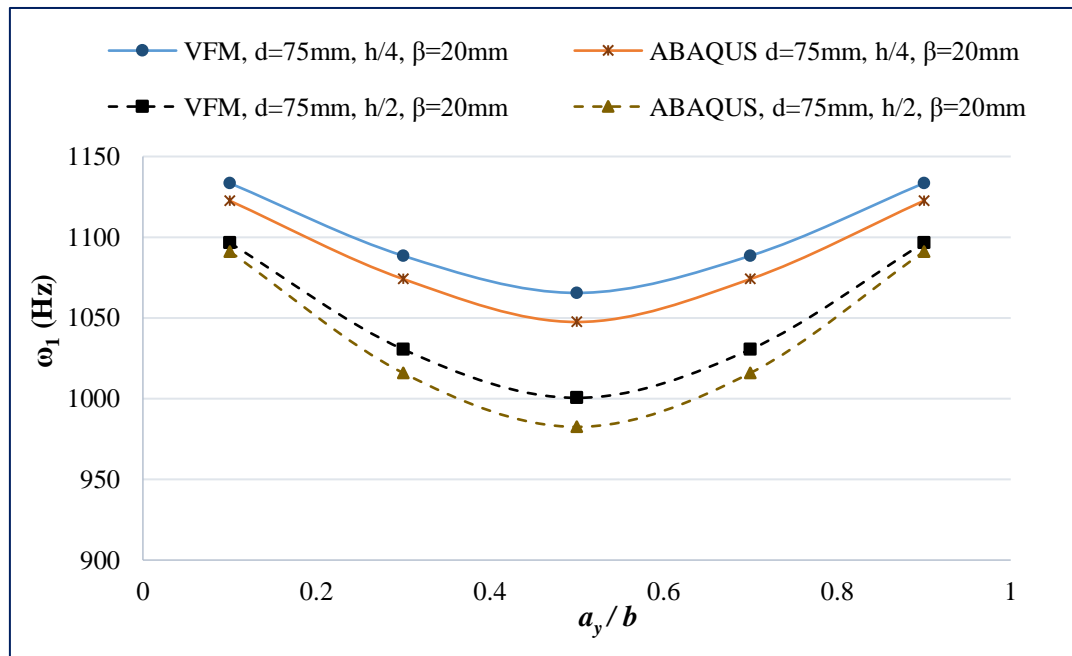
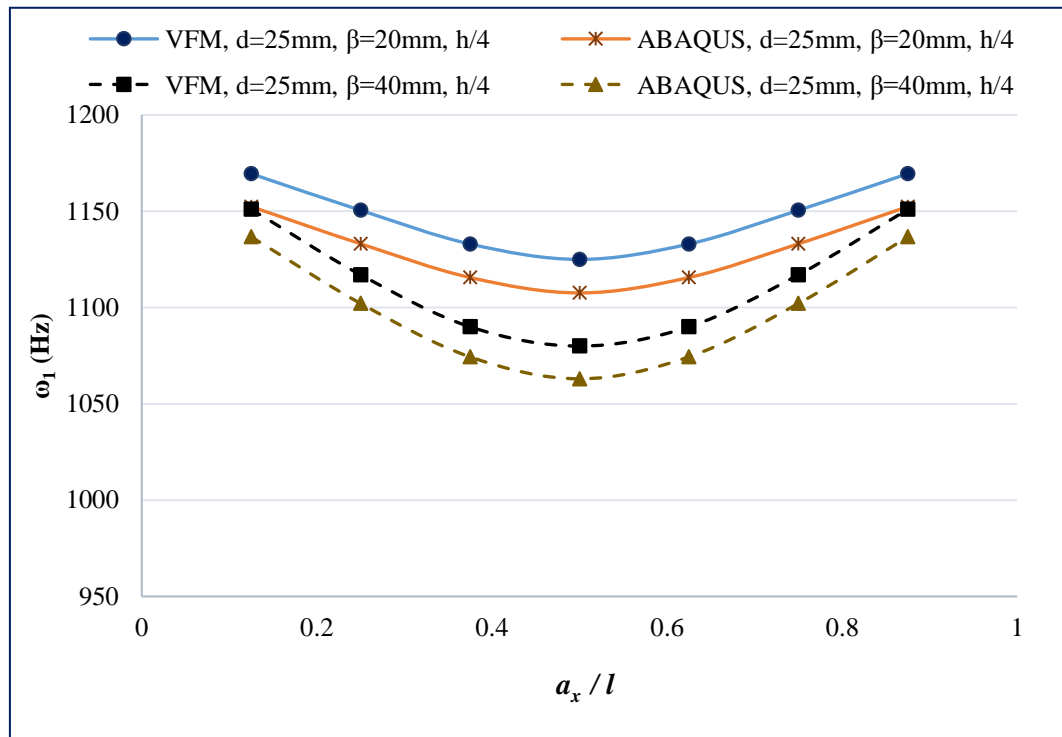
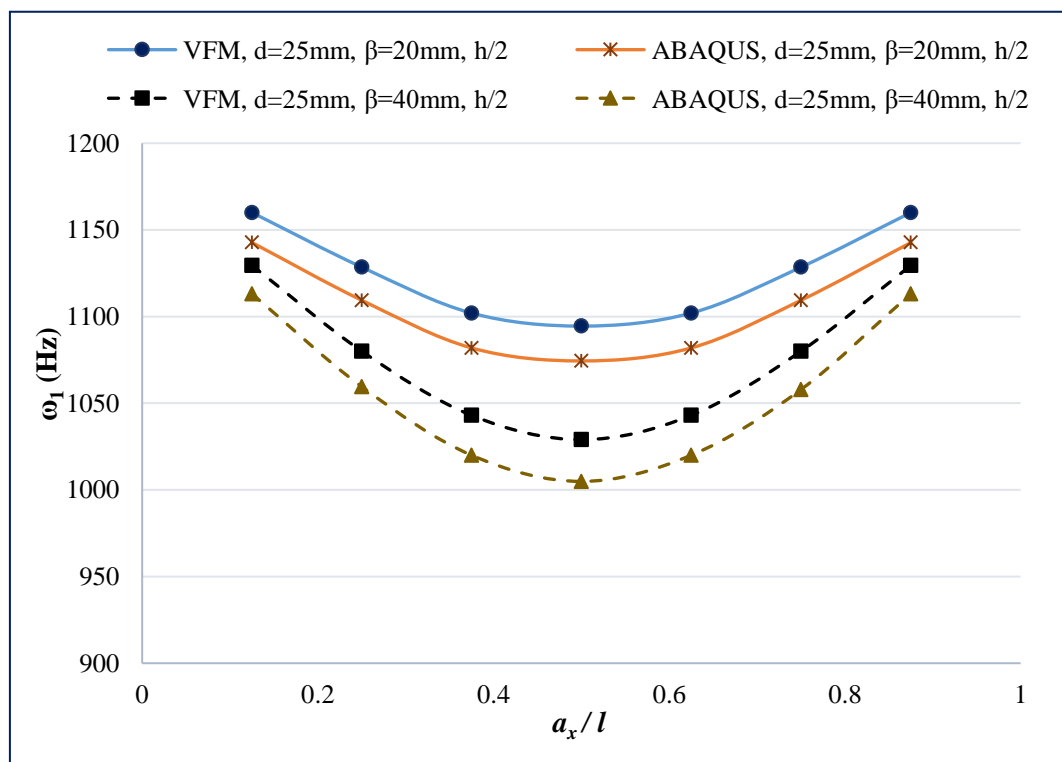


Figure 6-15: Lowest natural frequency of composite plates (ω_1) against widthwise position and depth of embedded rectangular delaminations.

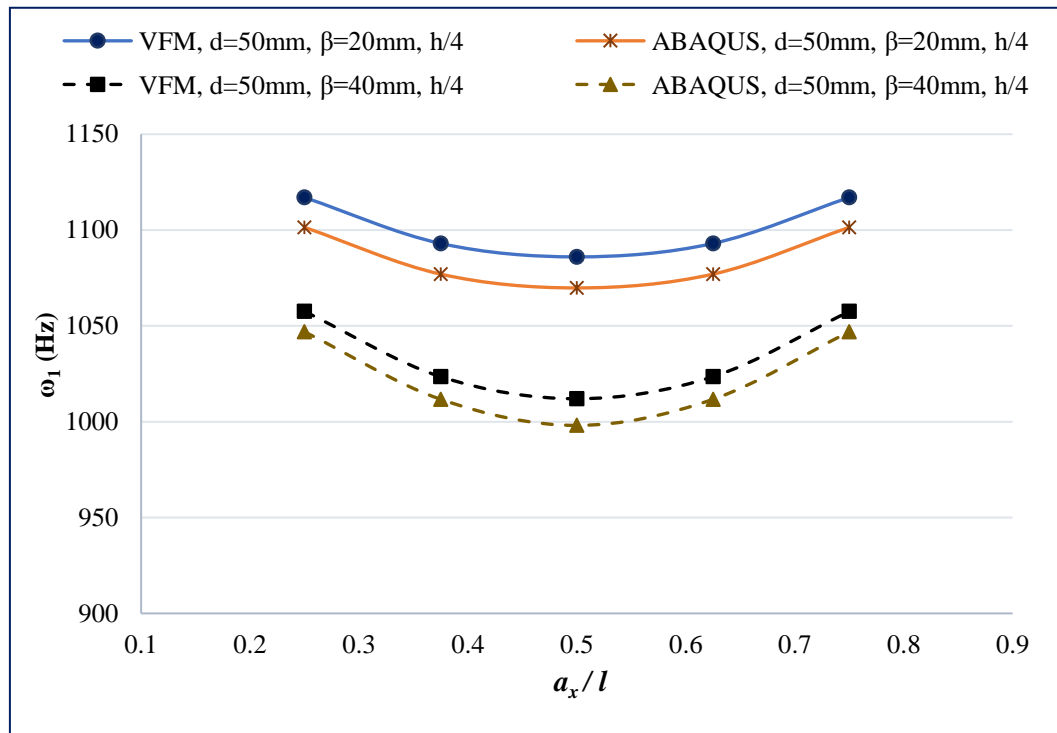
(a)



(b)



(c)



(d)

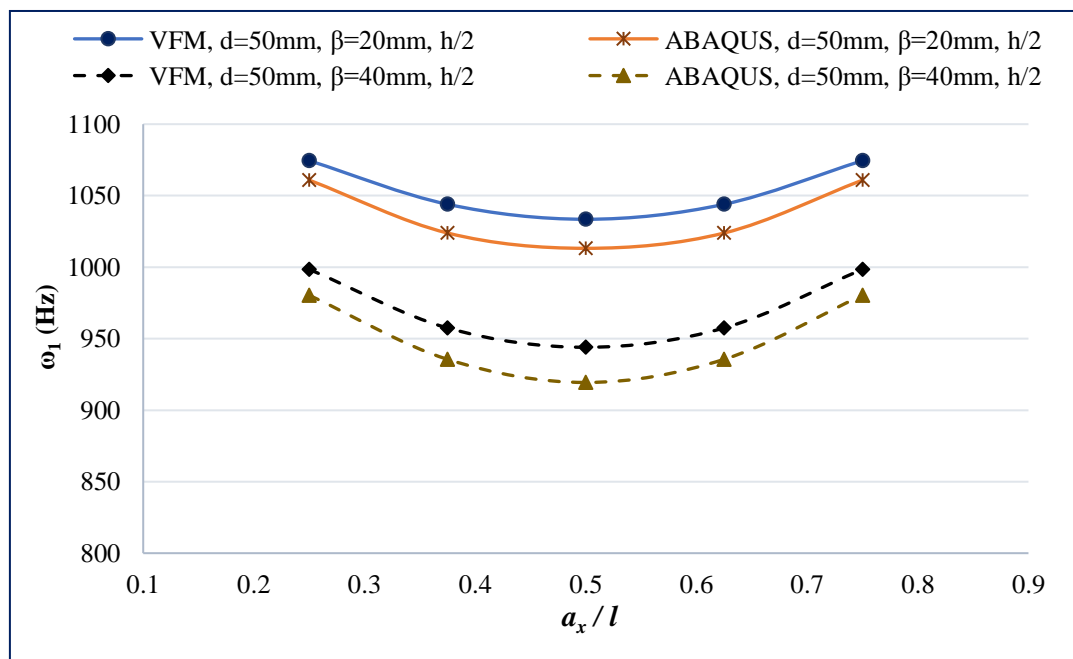


Figure 6-16: Lowest natural frequency of composite plates (ω_1) against lengthwise position and depth of embedded rectangular delaminations.

These analyses demonstrate the capability of VFM in handling all possible locations and depths of delamination, for through the length and embedded damage. Excellent agreement is seen between VFM and FE (ABAQUS) results for all cases of damage studied with the maximum difference found being 2.67% for the case when the plate has a delamination with $d=50$ mm, $b=40$ mm, a delamination depth of $h/2$ and the delamination located at the centre of the plate.

6.4.2.4 Effect of aspect ratio

Finally the relationship is studied between the aspect ratio (b/l) and the lowest natural frequencies of simply supported laminated plates with centrally located embedded delaminations of increasing size, length $d = 25$ mm and 50mm located at depth $h/4$. Plates examined had length $l = 100$ mm width $b = 50$ mm, 100 mm, 150 mm, 200 mm, 250 mm and 300 mm, thickness $h = 2$ mm and material properties: Young's moduli $E_1 = 110$ kNmm², $E_2 = 10$ kNmm², shear moduli $G_{12} = G_{13} = G_{23} = 5$ kN/mm², Poisson's ratio $\nu_{12} = 0.33$ and density $\rho = 4480$ kg/mm³. The plates comprised 32 plies of thickness 0.0625mm in the sequence [0/45/-45/90/90/-45/45/0/0/45/-45/90/90/-45/45/0],s. Only results from VFM are presented in this analytical study, however graphs for the same study comparing results from VFM and ABAQUS are included in Appendix 4

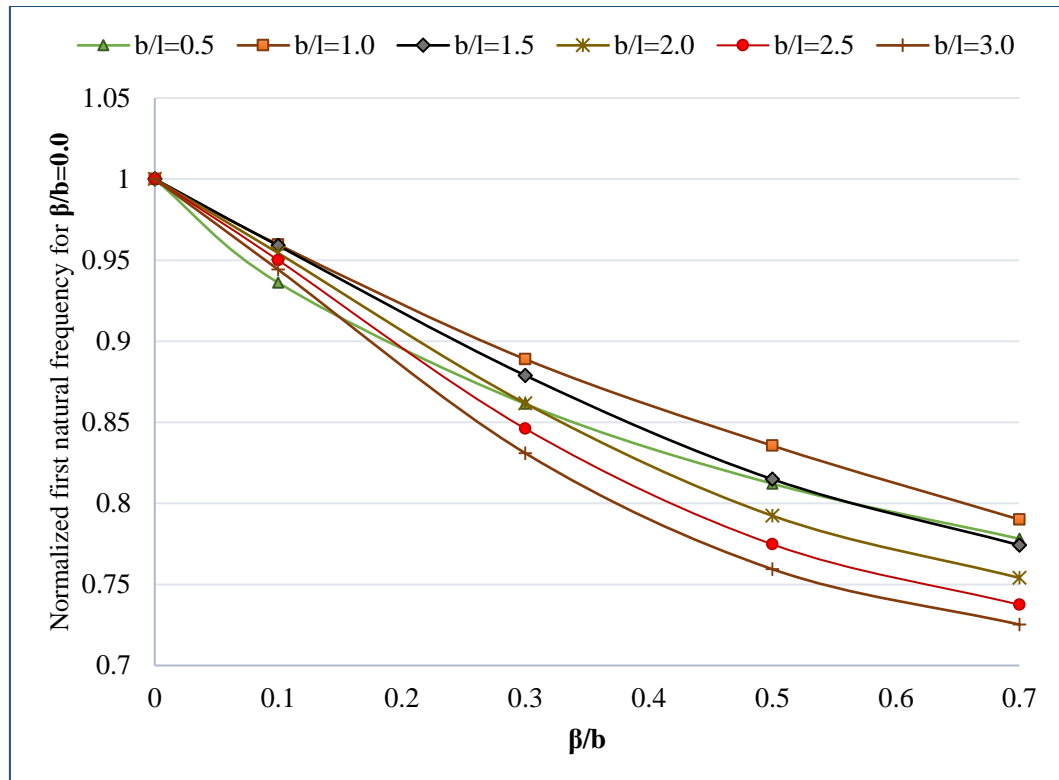


Figure 6-17: The effect of aspect ratio (b/l) on the lowest natural frequency for different delamination sizes, $d = 50\text{mm}$.

Figure 6-17 illustrates the effect of changing the delamination size for plates with different aspect ratios b/l , while Figure 6-18 plots the reductions in the lowest natural frequency against the aspect ratio. In these figures the natural frequencies have been normalized relative to those of undamaged plates, i.e. having $\beta = 0$. The maximum difference between VFM and ABAQUS results is just 2.84%, see Appendix 9.4. The figures show decreased natural frequencies with increased delamination size and for larger aspect ratios. The degradations in natural frequency tend to be smaller for square plates.

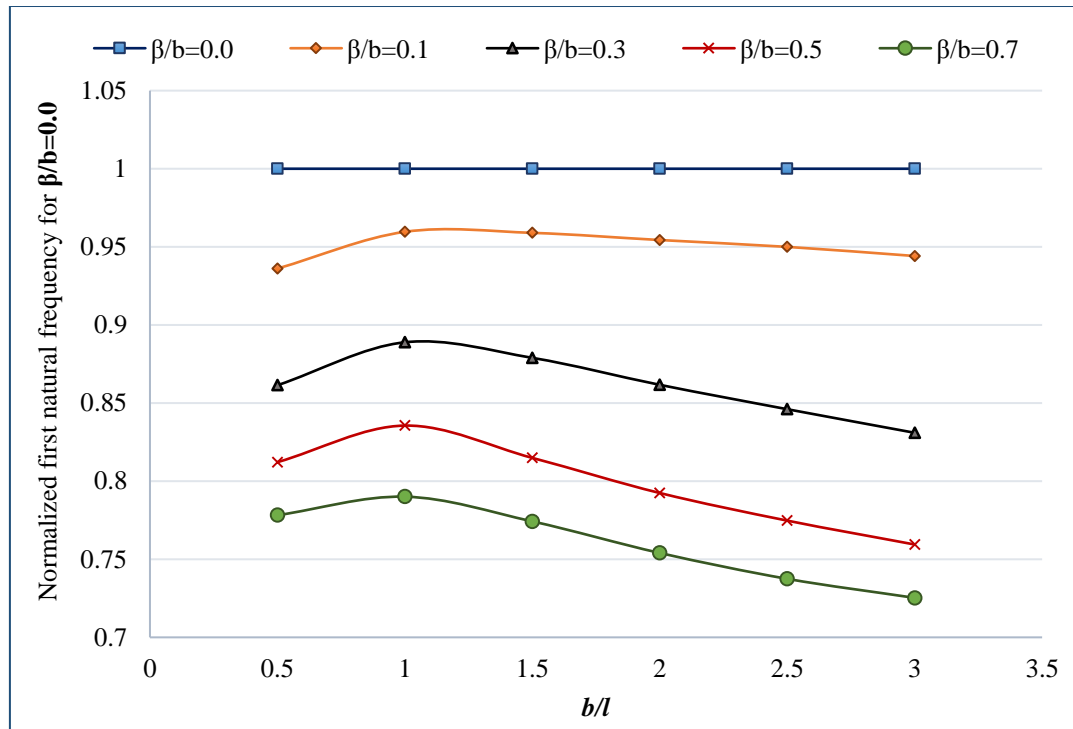
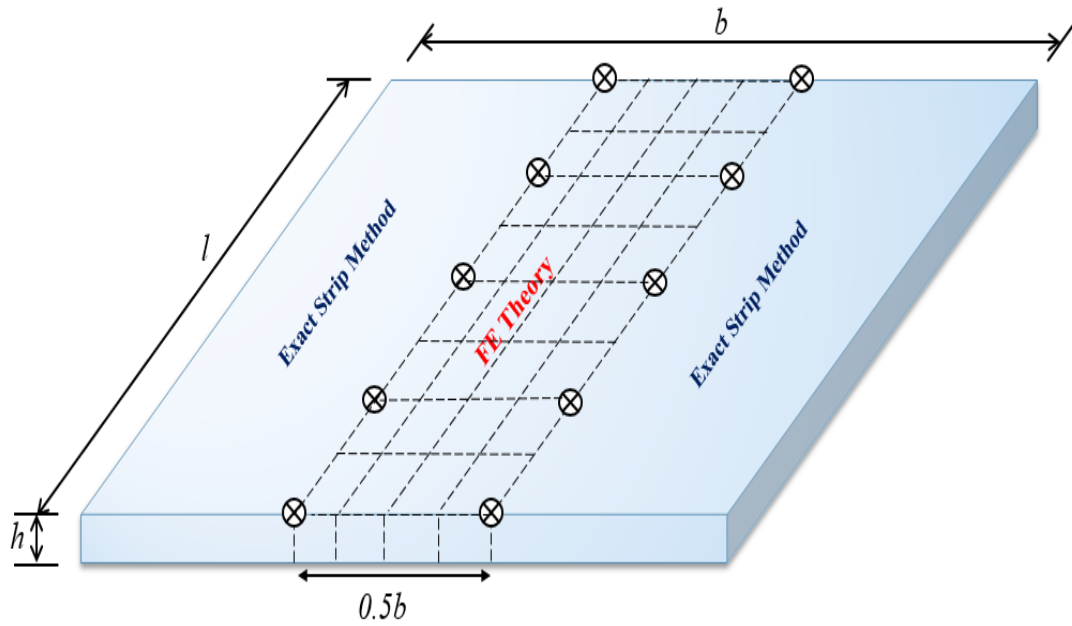


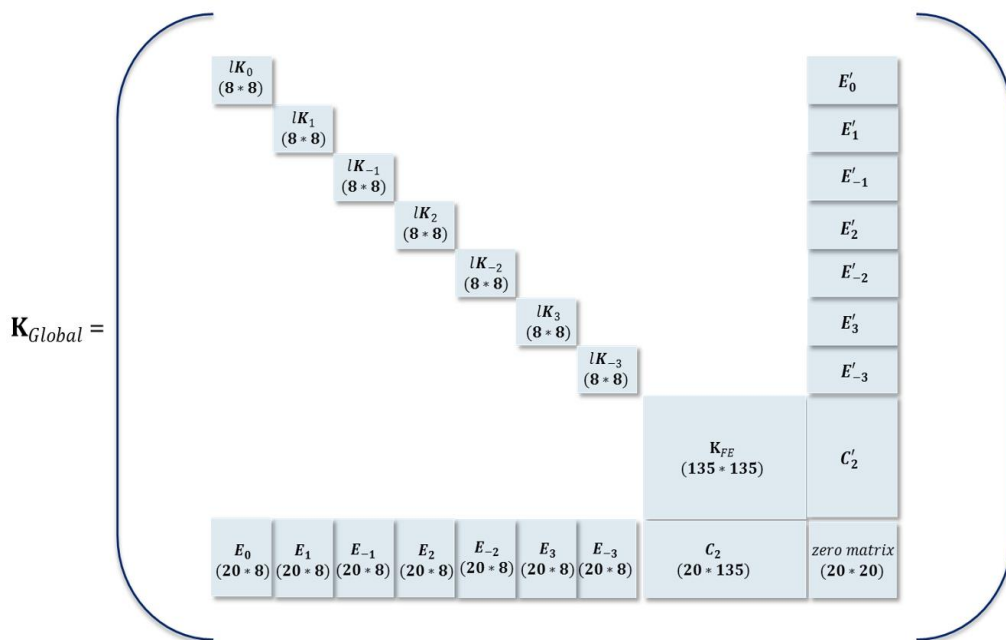
Figure 6-18 Plots of normalized first natural frequency against aspect ratios for different delamination width with $d=50\text{mm}$.

6.5 Solution time application to VFM

Figure 6-19 (a) shows a plate modelled using VFM. The central portion of the plate is modelled using a finite element mesh of 32 elements (4×8). The edge portions are modelled using the exact strip method. The form of the global dynamic stiffness matrix is shown in Figure 6-19 (b). Applying equation (6.2) shows that the VFM and pure FE analysis times are, respectively, 7.02 and 29.85 times longer than that of the pure VICON analysis. Thus for through-the-length damage there is a clear computational advantage in using VICON analysis over FE analysis. In the case of embedded damage, for which pure VICON analysis cannot be used, VFM provides an accurate alternative to pure FE and is about 4 times faster.



(a)



(b)

Figure 6-19 (a) Damaged plate modelled in VFM. (b) form of the global dynamic stiffness matrix.

7 Overall conclusions and future works

7.1 Conclusions

An extended hybrid model VFM has been developed by combining the exact strip method with the finite element method. This model can be applied to modelling a change of properties in a local region such as delamination of a composite laminate. This method is of the potential to deal with a plate of irregular shape and complex boundary conditions where the exact strip method is limited.

In Chapter 4, aspects such as different stacking sequences of the plies, through-the-length and through-the-width delaminations, single and multi-delamination zones at the same and varying depths and the delamination effect on the global buckling load are studied and the following conclusions are obtained:

- The simplicity of the VICONOPT program allows the analysis of laminate plates with various ply arrangements in a seamless manner. Consequently, the effects of the size and location of delaminations on the critical buckling load and buckling mode shapes can be easily studied.
- As delamination width increases, a reduction in the critical buckling load accompanied by a transition from a global mode to a local mode of the delaminated layer takes place.
- The critical buckling load of a delaminated plate is very sensitive to the ply orientations of the delaminated layer with respect to the direction of the in-plane force system.

Chapter 7: Overall conclusions and future works

- Composite plates with on-axis and off-axis plies which buckle at smaller half-wavelengths witness higher critical buckling loads.
- It is observed that a through-the-length and through-the-width delaminated portion has effectively clamped boundary conditions, so that the buckling half-wavelength will be less than the plate length, for delamination at any depth except at mid-thickness.
- The global buckling load for a delaminated composite plate is predicted for any delamination width. A relationship is established between the global buckling load and the delamination ratio, which can be considered in the design process when only global buckling is the concern.

From chapter 6, it can be summarized that

1. VFM has been shown to efficiently handle geometries of damage that the previous VICON models could not.
2. A near perfect match is achieved between VICON and ABAQUS results when analysing isotropic plates containing through-the-length stiffness reduction. VFM is also seen to match these results. However, as the damage width increases VFM predicts higher natural frequencies than both VICON and ABAQUS albeit with a maximum difference of only 1.55% for damage extending over the whole plate.
3. Excellent agreement between VFM and ABAQUS is demonstrated in modelling an embedded rectangular stiffness reduction. The smeared method gives good results for narrow delaminations when the plate vibrates globally,

but conservative results for wider delaminations when the damaged plate vibrates locally since this type of mode is not adequately represented.

4. A very good match is observed between VFM, VICON and ABAQUS in handling through-the-length delaminations in a composite plate, with the maximum differences between VFM and ABAQUS being 1.95% and 1.67% for delaminations at 25% and 50% of the plate thickness, respectively.
5. There is very good agreement between VFM and ABAQUS results for composite plates containing an embedded rectangular delamination, with the maximum differences between VFM and ABAQUS being 1.88% and 3.4%, for delaminations at 25% and 50% of the plate thickness, respectively. These errors increase slightly if the length of the damage is increased, because VFM uses finite element theory based on a fixed number of elements to model the damaged part of the plate, so that as the size of the damage increases the mesh becomes coarser.
6. The smeared method models the embedded damage indirectly and this leads to good agreement with the other methods when the composite plate vibrates globally but with increasing differences when it vibrates locally.
7. VFM is used to study the effects of widthwise and lengthwise position and depth of rectangular delamination on the first natural frequency of a composite plate, and the results are validated with ABAQUS.
8. VFM is used to illustrate the effect of aspect ratio on the lowest natural frequency of a simply supported laminated plate containing a rectangular delamination. It is noted that the degradation in natural frequency tends to be smaller for square plates and to increase with increasing width to length ratio.

9. Due to dissimilarity in the computer programming languages used in the methods presented, only an approximate assessment of the solution time could be carried out. It was found that VFM and finite element analysis times for a typical problem are, respectively, 7.02 and 29.85 times that of the exact strip method.
10. It is concluded that VFM has extended the capability of the exact strip method by modelling embedded delaminations and other damage, while still having a computational advantage over finite element analysis.

7.2 Future works

Based on work executed in this thesis the following topics can be recommended for future study:

1. Fully incorporating VFM into VICONOPT so it can be used on a wide range of plates and stiffened panels. The combined code will be able to handle all kinds of embedded damages, in contrast to the existing VICONOPT code which can only handle problems which satisfy the prismatic requirements of the exact strip method i.e. plates with through the length damage.
2. The VFM approach will then be available for vibration, buckling and postbuckling analysis for a wide range of damaged plates and stiffened panels, and for making allowance for damage in optimum design.
3. Using a more robust finite element model, so as to model other sorts of damage, e.g. cracks and various shapes of delamination, including circular, triangular and elliptical delaminations.

4. A current PhD student is already extending the novel hybrid approach presented in this thesis (VFM) to model plates containing cracks of arbitrary length and alignment, with a view to detecting the location and extent of damage in plate assemblies.

8 References

- [1] *General introduction*, D. Hull and T. W. Clyne, 1996.
- [2] D. Gay, *Composite materials : design and applications*, 2nd ed. ed. Boca Raton, FL: Boca Raton, FL : CRC Press, 2007.
- [3] J. R. Vinson, *Composite materials and their use in structures*. London: London : Applied Science Publishers, 1975.
- [4] R. F. Gibson, *Principles of composite material mechanics*: CRC press, 2016.
- [5] J. N. Reddy, *Mechanics of laminated composite plates and shells: theory and analysis*: CRC press, 2004.
- [6] R. M. Jones, *Mechanics of composite materials*, 2nd ed. ed. Philadelphia, PA: Philadelphia, PA : Taylor & Francis, 1999.
- [7] H. Altenbach, "Theories for laminated and sandwich plates. A review," *Mechanics Of Composite Materials*, vol. 34, pp. 243-252, 1998.
- [8] D. Gay and S. V. Hoa, *Composite materials: design and applications*: CRC press, 2007.
- [9] BOEING, "Boeing 787 from the Ground Up," *AERO Magazine*, vol. 04, pp. 17-24, 2006 2006.
- [10] F. C. Campbell, *Structural composite materials*: ASM international, 2010.
- [11] O. M. E. S. Khayal, "Literature review on imperfection of composite laminated plates," *Journal of Microscopy and Ultrastructure*, vol. 5, pp. 119-122, 2017/09/01/ 2017.
- [12] R. Smith, "Composite defects and their detection," *Materials science and engineering*, vol. 3, pp. 103-143, 2009.
- [13] R. Spoonire, "Void defect modeling in carbon epoxy composites Part I: Stiffness," in *19th AIAA Non-Deterministic Approaches Conference, 2017*, 2017.
- [14] V. V. Bolotin, "Mechanics of Delaminations in Laminate Composite Structures," *Mechanics of Composite Materials*, vol. 37, pp. 367-380, September 01 2001.
- [15] T. K. O'BRIEN, "Delamination of composite materials," in *Composite Materials Series*. vol. 4, ed: Elsevier, 1991, pp. 181-198.
- [16] R. B. Pipes and N. Pagano, "Interlaminar stresses in composite laminates under uniform axial extension," *Journal of Composite Materials*, vol. 4, pp. 538-548, 1970.
- [17] A. K. Noor, M. Shuart, J. Starnes Jr, and J. Williams, "Failure analysis and mechanisms of failure of fibrous composite structures," 1983.
- [18] W. Gong, J. Chen, and E. A. Patterson, "Buckling and delamination growth behaviour of delaminated composite panels subject to four-point bending," *Composite Structures*, vol. 138, pp. 122-133, 2016.
- [19] S. Y. Lee and D. Y. Park, "Buckling analysis of laminated composite plates containing delaminations using the enhanced assumed strain solid element," *International Journal of Solids and Structures*, vol. 44, pp. 8006-8027, 2007.
- [20] W. Ding, *Delamination analysis of composite laminates*: University of Toronto, 2000.
- [21] V. V. Bolotin, "Delaminations in composite structures: Its origin, buckling, growth and stability," *Composites Part B: Engineering*, vol. 27, pp. 129-145, 1996/01/01/ 1996.
- [22] R. Hosseinzadeh, M. M. Shokrieh, and L. Lessard, "Damage behavior of fiber reinforced composite plates subjected to drop weight impacts," *Composites science and technology*, vol. 66, pp. 61-68, 2006.
- [23] V. M. Sreehari and D. K. Maiti, "Buckling and post buckling characteristics of laminated composite plates with damage under thermo-mechanical loading," *Structures*, vol. 6, pp. 9-19, 2016.

Chapter 8: References

- [24] R. A. M. Santos, P. N. B. Reis, F. G. A. Silva, and M. F. S. F. de Moura, "Influence of inclined holes on the impact strength of CFRP composites," *Composite Structures*, vol. 172, pp. 130-136, 2017.
- [25] D. Li, "Delamination and transverse crack growth prediction for laminated composite plates and shells," *Computers & Structures*, vol. 177, pp. 39-55, 2016.
- [26] Y. Pekbey and O. Sayman, "A numerical and experimental investigation of critical buckling load of rectangular laminated composite plates with strip delamination," *Journal of Reinforced Plastics and Composites*, vol. 25, pp. 685-697, 2006.
- [27] ANSYS, "User's manual.," *ANSYS Inc.*, 2002.
- [28] F. Cappello and D. Tumino, "Numerical analysis of composite plates with multiple delaminations subjected to uniaxial buckling load," *Composites Science and Technology*, vol. 66, pp. 264-272, 2006.
- [29] B. L. Karihaloo and H. Stang, "Buckling-driven delamination growth in composite laminates: Guidelines for assessing the threat posed by interlaminar matrix delamination," *Composites Part B: Engineering*, vol. 39, pp. 386-395, 2008.
- [30] P. F. Liu, S. J. Hou, J. K. Chu, X. Y. Hu, C. L. Zhou, Y. L. Liu, *et al.*, "Finite element analysis of postbuckling and delamination of composite laminates using virtual crack closure technique," *Composite Structures*, vol. 93, pp. 1549-1560, 2011.
- [31] P. F. Liu and J. Y. Zheng, "On the through-the-width multiple delamination, and buckling and postbuckling behaviors of symmetric and unsymmetric composite laminates," *Applied Composite Materials*, vol. 20, pp. 1147-1160, 2013.
- [32] S. F. Nikrad, S. Keyoursangari, H. Asadi, A. H. Akbarzadeh, and Z. T. Chen, "Computational study on compressive instability of composite plates with off-center delaminations," *Computer Methods in Applied Mechanics and Engineering*, vol. 310, pp. 429-459, 2016.
- [33] S. Yazdani, W. J. H. Rust, and P. Wriggers, "Delamination growth in composite laminates of variable stiffness," *International Journal for Numerical Methods in Engineering*, vol. 108, pp. 1406-1424, 2016.
- [34] A. Szekrényes, "Application of Reddy's third-order theory to delaminated orthotropic composite plates," *European Journal of Mechanics, A/Solids*, vol. 43, pp. 9-24, 2014.
- [35] X. W. Wang, I. Pont-Lezica, J. M. Harris, F. J. Guild, and M. J. Pavier, "Compressive failure of composite laminates containing multiple delaminations," *Composites Science and Technology*, vol. 65, pp. 191-200, 2005.
- [36] Z. Aslan and M. Şahin, "Buckling behavior and compressive failure of composite laminates containing multiple large delaminations," *Composite Structures*, vol. 89, pp. 382-390, 2009.
- [37] T. Park, S. Y. Lee, and G. Z. Voyiadjis, "Finite element vibration analysis of composite skew laminates containing delaminations around quadrilateral cutouts," *Composites Part B: Engineering*, vol. 40, pp. 225-236, 2009.
- [38] I. N. Jayatilake, W. Karunasena, and W. Lokuge, "Finite element based dynamic analysis of multilayer fibre composite sandwich plates with interlayer delaminations," *Advances in Aircraft and Spacecraft Science*, vol. 3, pp. 15-28, 2016.
- [39] S. Devendiran, K. Manivannan, K. Venkatesan, A. T. Mathew, A. Thakur, and V. Ashish Chauhan, "Free vibration of damaged and undamaged hybrid CFRP/GFRP composite laminates," *International Journal of Mechanical Engineering and Technology*, vol. 8, pp. 349-360, 2017.
- [40] Z.-X. Wang, P. Qiao, and J. Xu, "Vibration analysis of laminated composite plates with damage using the perturbation method," *Composites Part B: Engineering*, vol. 72, pp. 160-174, 2015/04/01/ 2015.
- [41] D. Kennedy, M. Fischer, and C. A. Featherston, "Recent developments in exact strip analysis and optimum design of aerospace structures," *Proceedings of the Institution of Mechanical Engineers, Part C: Journal of Mechanical Engineering Science*, vol. 221, pp. 399-413, 2007.

Chapter 8: References

- [42] W. H. Wittrick and F. W. Williams, "Buckling and vibration of anisotropic or isotropic plate assemblies under combined loadings," *International Journal of Mechanical Sciences*, vol. 16, pp. 209-239, 1974.
- [43] F. W. Williams, D. Kennedy, M. S. Anderson, and R. Butler, "VICONOPT - Program for exact vibration and buckling analysis or design of prismatic plate assemblies," *AIAA Journal*, vol. 29, pp. 1927-1928, 1991.
- [44] M. S. Anderson, K. W. Hennessy, and W. Heard Jr, "Vibration and Instability of Plate-Assemblies including Shear and Anisotropy (VIPASA) user's guide, addendum," 1976.
- [45] M. S. Anderson, F. W. Williams, and C. J. Wright, "Buckling and vibration of any prismatic assembly of shear and compression loaded anisotropic plates with an arbitrary supporting structure," *International Journal of Mechanical Sciences*, vol. 25, pp. 585-596, 1983/01/01/ 1983.
- [46] Y. K. Cheung, *Finite strip method in structural analysis*: Elsevier, 2013.
- [47] Y. K. Cheung and J. Kong, "The application of a new finite strip to the free vibration of rectangular plates of varying complexity," *Journal of Sound and Vibration*, vol. 181, pp. 341-353, 1995.
- [48] S. J. Guo, A. J. Keane, and M. Moshrefi-Torbati, "Vibration analysis of stepped thickness plates," *Journal of Sound and Vibration*, vol. 204, pp. 645-656, 1997.
- [49] M. Damghani, D. Kennedy, and C. Featherston, "Critical buckling of delaminated composite plates using exact stiffness analysis," *Computers and Structures*, vol. 89, pp. 1286-1294, 2011.
- [50] M. Damghani, D. Kennedy, and C. Featherston, "Global buckling of composite plates containing rectangular delaminations using exact stiffness analysis and smearing method," *Computers and Structures*, vol. 134, pp. 32-47, 2014.
- [51] S. M. Powell, D. Kennedy, and F. W. Williams, "Efficient multi-level substructuring with constraints for buckling and vibration analysis of prismatic plate assemblies," *International Journal of Mechanical Sciences*, vol. 39, pp. 795-805, 1997.
- [52] F. W. Williams and M. S. Anderson, "Incorporation of Lagrangian Multipliers into an algorithm for finding exact natural frequencies or critical buckling loads," *International Journal of Mechanical Sciences*, vol. 25, pp. 579-584, 1983.
- [53] W. H. Wittrick and F. W. Williams, "A general algorithm for computing natural frequencies of elastic structures," *Quarterly Journal of Mechanics and Applied Mathematics*, vol. 24, pp. 263-284, 1971.
- [54] W. H. Wittrick and F. W. Williams, "An Algorithm for Computing Critical Buckling Loads of Elastic Structures," *Journal of Structural Mechanics*, vol. 1, pp. 497-518, 1973.
- [55] F. W. Williams and W. H. Wittrick, "An automatic computational procedure for calculating natural frequencies of skeletal structures," *International Journal of Mechanical Sciences*, vol. 12, pp. 781-791, 1970.
- [56] M. S. Anderson and D. Kennedy, "Transverse shear deformation in exact buckling and vibration of composite plate assemblies," *AIAA journal*, vol. 31, pp. 1963-1965, 1993.
- [57] M. S. Anderson and D. Kennedy, "Inclusion of transverse shear deformation in the exact buckling and vibration analysis of composite plate assemblies," 1993.
- [58] F. W. Williams, M. Anderson, D. Kennedy, R. Butler, and G. Aston, "User manual for VICONOPT: An exact analysis and optimum design program covering the buckling and vibration of prismatic assemblies of flat in-plane loaded, anisotropic plates, with approximations for discrete supports, and transverse stiffeners," 1990.
- [59] C. A. Featherston and A. Watson, "Buckling of optimised flat composite plates under shear and in-plane bending," in *Composites Science and Technology* vol. 65, ed, 2005, pp. 839-853.

Chapter 8: References

- [60] A. Ghaehri, A. Keshmiri, and F. Taheri-Behrooz, "Buckling and vibration of symmetrically laminated composite elliptical plates on an elastic foundation subjected to uniform in-plane force," *Journal of Engineering Mechanics*, vol. 140, 2014.
- [61] N. J. Kumar, P. R. Babu, and R. Pandu, "Investigations on buckling behaviour of laminated curved composite stiffened panels," *Applied Composite Materials*, vol. 21, pp. 359-376, 2014.
- [62] K. Cox and A. Echtermeyer, "Effects of composite fiber orientation on wind turbine blade buckling resistance," *Wind Energy*, vol. 17, pp. 1925-1943, 2014.
- [63] H. A. Rasheed, R. Al-Masri, and B. Alali, "Closed form stability solution of simply supported anisotropic laminated composite plates under axial compression compared with experiments," *Engineering Structures*, vol. 151, pp. 327-336, 2017.
- [64] S. Metoui, E. Pruliere, A. Ammar, and F. Dau, "A reduced model to simulate the damage in composite laminates under low velocity impact," *Computers & Structures*, vol. 199, pp. 34-45, 2018/04/01/ 2018.
- [65] X. Chen, Z. Wu, G. Nie, and P. Weaver, "Buckling analysis of variable angle tow composite plates with a through-the-width or an embedded rectangular delamination," *International Journal of Solids and Structures*, vol. 138, pp. 166-180, 2018/05/01/ 2018.
- [66] J. S. Przemieniecki, *Theory of Matrix Structural Analysis*: Dover, 1985.
- [67] F. Bogner, R. Mallett, M. Minich, and L. Schmit, "DEVELOPMENT AND EVALUATION OF ENERGY SEARCH METHODS OF NONLINEAR STRUCTURAL ANALYSIS," DTIC Document 1965.
- [68] F. Williams, "Natural frequencies of repetitive structures," *The Quarterly Journal of Mechanics and Applied Mathematics*, vol. 24, pp. 285-310, 1971.
- [69] D. Lam, F. Williams, and D. Kennedy, "Critical buckling of stiffened panels with discrete point connections," *International journal of mechanical sciences*, vol. 39, pp. 991-1009, 1997.
- [70] W. J. Stroud, W. H. Greene, and M. S. Anderson, "Buckling loads of stiffened panels subjected to combined longitudinal compression and shear: results obtained with PASCO, EAL, and STAGS computer programs," 1984.
- [71] F. W. Williams and M. S. Anderson, *BUCKLING AND VIBRATION ANALYSIS OF SHEAR-LOADED PRISMATIC PLATE ASSEMBLIES WITH SUPPORTING STRUCTURES, UTILIZING SYMMETRIC OR REPETITIVE CROSS-SECTIONS* vol. in, 1985.
- [72] D. Kennedy, F. W. Williams, and M. S. Anderson, "Buckling and vibration analysis of laminated panels using viconopt," *Journal of Aerospace Engineering*, vol. 7, pp. 245-262, 1994.
- [73] R. W. Clough and J. L. Tocher, "Finite element stiffness matrices for analysis of plates in bending," in *Proceedings of conference on matrix methods in structural analysis*, 1965, pp. 515-545.

9 Appendices

9.1 Appendix 1

The following gives the derivations of the static stiffness matrix of Eq. (5.1) [66].

When a is the plate length on the y axis, b is the plate width on the x axis, t is the plate thickness, E denotes Young's modulus, ρ is the density and ν is Poisson's ratio, the displacement functions used to calculate the stiffness properties of an isotropic rectangular plate in bending are of the form

$$u_z = \mathbf{a} * \mathbf{u} \quad (9.1.1)$$

where \mathbf{a} is a function of the position coordinates and \mathbf{u} is a displacement vector with a positive direction of

$$\mathbf{u} = \{u_1 \ u_2 \ \dots \ u_{12}\} \quad (9.1.2)$$

$$\mathbf{e} = \underline{\mathbf{b}} * \mathbf{u} \quad (9.1.3)$$

where \mathbf{e} is the strain vector and $\underline{\mathbf{b}}$ represents a matrix of the exact strains due to unit displacements \mathbf{u} .

Using the sign convention established in Figure 5-2 (a) chapter 5, the matrix \mathbf{a} for compatible deflections and slopes can be given by

$$\mathbf{a}^T = \begin{bmatrix} (1 + 2\xi) (1 + 2\xi)^2 (1 + 2\eta) (1 - \eta)^2 \\ (1 + 2\xi) (1 - 2\xi)^2 \eta (1 - \eta)^2 b \\ -\xi (1 - \xi)^2 (1 + 2\eta) (1 - \eta)^2 a \\ -(1 + 2\xi) (1 - \xi)^2 (3 - 2\eta) \eta^2 \\ -(1 + 2\xi) (1 - \xi)^2 (1 - \eta) \eta^2 b \\ -\xi (1 - \xi)^2 (3 - 2\eta) \eta^2 a \\ (3 - 2\xi) \xi^2 (3 - 2\eta) \eta^2 \\ -(3 - 2\xi) \xi^2 (1 - \eta) \eta^2 b \\ (1 - \xi) \xi^2 (3 - 2\eta) \eta^2 a \\ (3 - 2\xi) \xi^2 (1 + 2\eta) (1 - \eta)^2 \\ (3 - 2\xi) \xi^2 \eta (1 - \eta)^2 b \\ (1 - \xi) \xi^2 (1 + 2\eta) (1 - \eta)^2 a \end{bmatrix} \quad (9.1.4)$$

Where

$$\xi = x/b \text{ and } \eta = y/a \quad (9.1.5)$$

Based on the assumed deflection function, first introduced by Clough and Tocher [73],

the strains are calculated from the flat-plate theory, using

$$e_{xx} = -z \frac{\partial^2 u_z}{\partial x^2} \quad (9.1.6)$$

$$e_{yy} = -z \frac{\partial^2 u_z}{\partial y^2} \quad (9.1.7)$$

$$e_{xy} = -2z \frac{\partial^2 u_z}{\partial x \partial y} \quad (9.1.8)$$

Chapter 9: Appendices

Eqs. (9.1.6) to (9.1.8) and (9.1.4) can then be used to determine the matrix \mathbf{b} in Eq. (9.1.3) which expresses the total strains due to unit displacement and is given by

$$\mathbf{b}^T = \begin{bmatrix}
 (1 - 2\xi)(1 + 2\eta)(1 - \eta)^2 \frac{6z}{a^2} & (1 + 2\xi)(1 - \xi)^2(1 - 2\eta) \frac{6z}{b^2} & -\xi(1 - \xi)\eta(1 - \eta) \frac{72z}{ab} \\
 (1 - 2\xi)\eta(1 - \eta)^2 \frac{6bz}{a^2} & (1 + 2\xi)(1 - \xi)^2(2 - 3\eta) \frac{2z}{b} & \xi(1 - \xi)(1 - \eta)(1 - 3\eta) \frac{12z}{a} \\
 -(2 - 3\xi)(1 + 2\eta)(1 - \eta)^2 \frac{2z}{a} & -\xi(1 - \xi)^2(1 - 2\eta) \frac{6az}{b^2} & -(1 - \xi)(1 + 3\xi)\eta(1 - \eta) \frac{12z}{b} \\
 (1 - 2\xi)(3 - 2\eta)\eta^2 \frac{6z}{a^2} & -(1 + 2\xi)(1 - \xi)^2(1 - 2\eta) \frac{6z}{b^2} & \xi(1 - \xi)\eta(1 - \eta) \frac{72z}{ab} \\
 -(1 - 2\xi)(1 - \eta)\eta^2 \frac{6bz}{a^2} & (1 + 2\xi)(1 - \xi)^2(1 - 3\eta) \frac{2z}{b} & -\xi(1 - \xi)\eta(2 - 3\eta) \frac{12z}{a} \\
 -(2 - 3\xi)(3 - 2\eta)\eta^2 \frac{2z}{a} & \xi(1 - \xi)^2(1 - 2\eta) \frac{6az}{b^2} & (1 - \xi)(1 + 3\xi)\eta(1 - \eta) \frac{12z}{b} \\
 -(1 - 2\xi)(3 - 2\eta)\eta^2 \frac{6z}{a^2} & -(3 - 2\xi)\xi^2(1 - 2\eta) \frac{6z}{b^2} & -\xi(1 - \xi)\eta(1 - \eta) \frac{72z}{ab} \\
 (1 - 2\xi)(1 - \eta)\eta^2 \frac{6bz}{a^2} & (3 - 2\xi)\xi^2(1 - 3\eta) \frac{2z}{b} & \xi(1 - \xi)\eta(2 - 3\eta) \frac{12z}{a} \\
 -(1 - 3\xi)(3 - 2\eta)\eta^2 \frac{2z}{a} & -(1 - \xi)\xi^2(1 - 2\eta) \frac{6az}{b^2} & -\xi(2 - 3\xi)\eta(1 - \eta) \frac{12z}{a} \\
 -(1 - 2\xi)(1 + 2\eta)(1 - \eta)^2 \frac{6z}{a^2} & (3 - 2\xi)\xi^2(1 - 2\eta) \frac{6z}{b^2} & \xi(1 - \xi)\eta(1 - \eta) \frac{72z}{ab} \\
 -(1 - 2\xi)(1 + 2\eta)(1 - \eta)^2 \frac{6bz}{a^2} & (3 - 2\xi)\xi^2(2 - 3\eta) \frac{2z}{b} & -(1 - \xi)(1 - \xi)\eta(1 - 3\eta) \frac{12z}{a} \\
 -(1 - 3\xi)(1 + 2\eta)(1 - \eta)^2 \frac{2z}{a} & (1 - \xi)\xi^2(1 - 2\eta) \frac{6az}{b^2} & \xi(1 - \xi)\eta(1 - \eta) \frac{12z}{b}
 \end{bmatrix}$$

(9.1.9)

Chapter 9: Appendices

Substituting \mathbf{b} from Eq. (9.1.9) into Eq. (9.1.3) and performing the required integration, the stiffness matrix will be as follows

$$\mathbf{k} = \begin{bmatrix} \mathbf{k}_{I,I} & \mathbf{Symmetric} \\ \mathbf{k}_{II,I} & \mathbf{k}_{II,II} \end{bmatrix} \quad (9.1.10)$$

where the submatrices $\mathbf{k}_{I,I}$, $\mathbf{k}_{II,I}$ and $\mathbf{k}_{II,II}$ are presented in Table 5-1 , 5-2 and 5-3.

9.2 Appendix 2

The equivalent mass matrix is calculated from [66]

$$\mathbf{m} = \int_V \rho \mathbf{a}^T \mathbf{a} dV \quad (9.2.1)$$

where ρ is the density and \mathbf{a} is the deflection matrix which refers to all nodal displacement in local coordinates system shown in Figure 5-2 in chapter 5.

By substituting \mathbf{a} of Eq. (9.1.4) into Eq. (9.2.1) and performing integration over the whole rectangle, the mass matrix is obtained and is given by Eq. (5.2).

9.3 Appendix 3

The calculation procedure for finding the values of the out-of-plane stiffness coefficients in Eq. (5.10) starts with calculating the values of the parameters T , S and L as follows [42]

$$T = \alpha_{12} + 2\alpha_{12} - 3\alpha_{23}^2 - \frac{\lambda^2 N_T}{2\pi^2 D_{22}}$$

$$S = \frac{\lambda^2 N_S}{\pi^2 D_{22}} + 2(\alpha_{23}T + \alpha_{23}^3 - \alpha_{23})$$

$$L = \frac{\lambda^2}{\pi^2 D_{22}} + (N_L + 4m\lambda^2 n^2) - 2\alpha_{23}S + (T + \alpha_{23}^2)^2 - \alpha_{11}$$

where N_L , N_T , N_S and n are the in-plane axial, transverse and shear loads, and the frequency of vibration, respectively, λ is the specified half-wavelength, m is the mass per unit area and $\alpha_{11} = D_{11}/D_{22}$, $\alpha_{12} = D_{12}/D_{22}$, $\alpha_{33} = D_{33}/D_{22}$, $\alpha_{13} = D_{13}/D_{22}$ and $\alpha_{23} = D_{23}/D_{22}$. Here D_{11} , D_{22} , D_{12} , D_{13} and D_{23} are the out-of-plane elastic properties of the plate.

In unloaded vibration problems for isotropic or orthotropic plates $S = 0$ and the calculation path will depend on the value of L as follows

Case (a). $S = 0, L > 0$

1. Calculate α and γ from the equations

Chapter 9: Appendices

$$\alpha^2 = T + L^{\frac{1}{2}},$$

$$\gamma^2 = T - L^{\frac{1}{2}}$$

2. Calculate s_1 , c_1 , s_3 and c_3 from

$$s_1 = (1/\alpha) \sinh \omega \alpha$$

$$c_1 = \cosh \omega \alpha$$

$$s_3 = (1/\gamma) \sinh \omega \gamma$$

$$c_3 = \cosh \omega \gamma$$

where $\omega = \pi b/\lambda$ and b is the plate width.

3. Then calculate

$$Z = T s_1 s_3 - c_1 c_3 + 1$$

$$R_1 = L^{\frac{1}{2}} (c_1 s_3 - c_3 s_1)$$

$$R_2 = L^{\frac{1}{2}} (\alpha^2 c_3 s_1 - \gamma^2 c_1 s_3)$$

$$R_3 = Ls_1s_3$$

$$R_4 = L^{\frac{1}{2}}(s_1 - s_3)$$

$$R_5 = (s_1 + s_3)$$

$$R_6 = L^{\frac{1}{2}}(c_1 - c_3)$$

4. The out of plane stiffness coefficients then calculated as following

$$S_{MM} = \left(\pi D_{22} / \lambda \right) Z^{-1} R_1$$

$$S_{QQ} = \left(\pi^3 D_{22} / \lambda^3 \right) Z^{-1} R_2$$

$$S_{MQ} = \left(\pi^2 D_{22} / \lambda^2 \right) (T - \alpha_{12} - Z^{-1} R_3)$$

$$f_{MM} = \left(\pi D_{22} / \lambda \right) Z^{-1} R_4$$

$$f_{QQ} = \left(\pi^3 D_{22} / \lambda^3 \right) Z^{-1} (T R_4 + LR_5)$$

$$f_{MQ} = \left(\pi^2 D_{22} / \lambda^2 \right) Z^{-1} R_6$$

Case (b). $S = 0, L < 0$

1. Calculate α , γ and β from the equations

$$\alpha = \gamma = \left\{ \frac{1}{2} \left[\sqrt{(T^2 - L)} + T \right] \right\}^{\frac{1}{2}}$$

$$\beta = \left\{ \frac{1}{2} \left[\sqrt{(T^2 - L)} - T \right] \right\}^{\frac{1}{2}}$$

2. Calculate the same equations in *case (a)* stage 3 and

$$s_2 = \sin \omega \beta$$

$$c_2 = \cos \omega \beta$$

3. Calculate

$$A = T + 2\beta^2$$

$$F = L + 8T\beta^2 + 12\beta^4$$

4. Calculate

$$Z = (A + \beta^2)s_1s_3 - c_1c_3 + 2c_2^2 - 1$$

$$R_1 = 2\beta^2(c_1s_3 - c_3s_1) - 4\beta c_2s_2$$

$$R_2 = 4A\beta c_2s_2 + (F - 2\beta^2A)(c_1s_3 + c_3s_1)$$

$$R_3 = F s_1 s_3$$

$$R_4 = 2\beta s_2(c_1 + c_3) - 2\beta^2 c_2(s_3 + s_1)$$

$$R_5 = c_2(s_3 + s_1)$$

$$R_6 = (T + A + 2\beta^2)\beta(s_2 + s_3)$$

5. Then the out-of-plane stiffness coefficients can be calculated using the same equations in *case (a)* stage 5.

Case (b). $S = 0, L = 0$

1. Calculate

$$s_4 = \frac{\sinh \omega \sqrt{T}}{\omega \sqrt{T}}$$

$$c_4 = \cosh \omega \sqrt{T}$$

$$Z = \frac{1}{2} (s_4^2 - 1)$$

2. The out-of-plane stiffness coefficients can be calculated using the following equations

$$S_{MM} = \left(D_{22}/b \right) Z^{-1} (s_4 c_4 - 1)$$

$$S_{QQ} = \left(D_{22}/b^3 \right) \omega^2 Z^{-1} T (s_4 c_4 + 1)$$

$$S_{MQ} = - \left(D_{22}/b^2 \right) \omega^2 (\alpha_{12} + T + T Z^{-1})$$

$$f_{MM} = \left(D_{22}/b \right) Z^{-1} (c_4 - s_4)$$

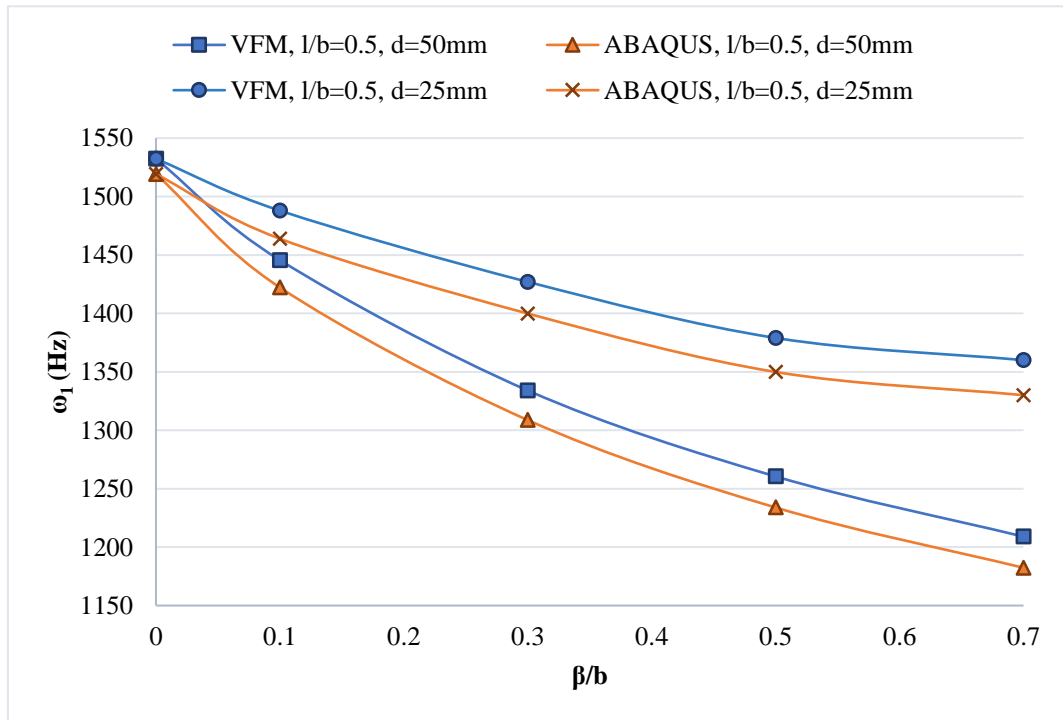
$$f_{QQ} = \left(D_{22}/b^3 \right) Z^{-1} \omega^2 T (c_4 + s_4)$$

$$f_{MQ} = - \left(D_{22}/b^2 \right) Z^{-1} \omega^2 T s_4$$

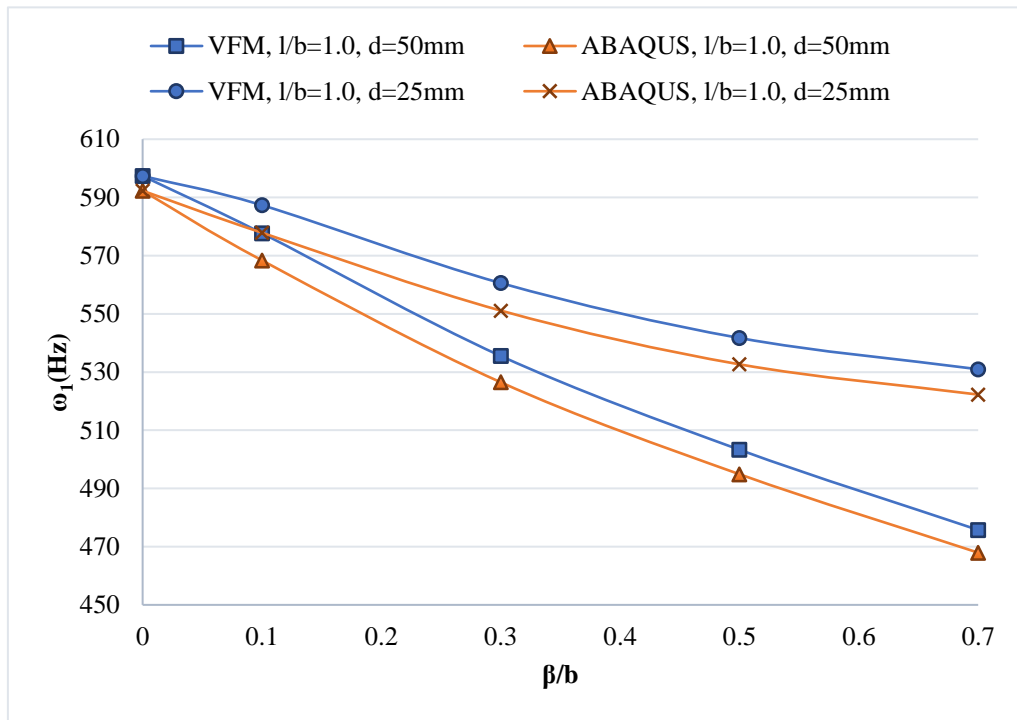
9.4 Appendix 4

Further analytical graphs related to the effect of aspect ratio on a simply supported composite plate containing an embedded delamination (section 6.4.2.4).

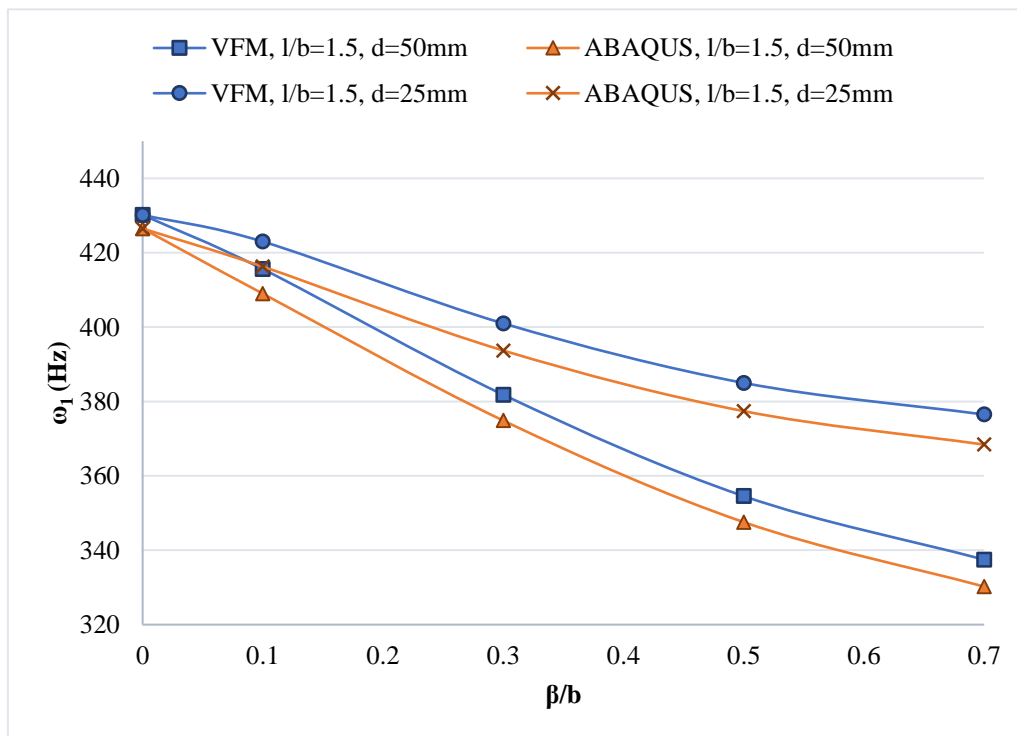
(a)



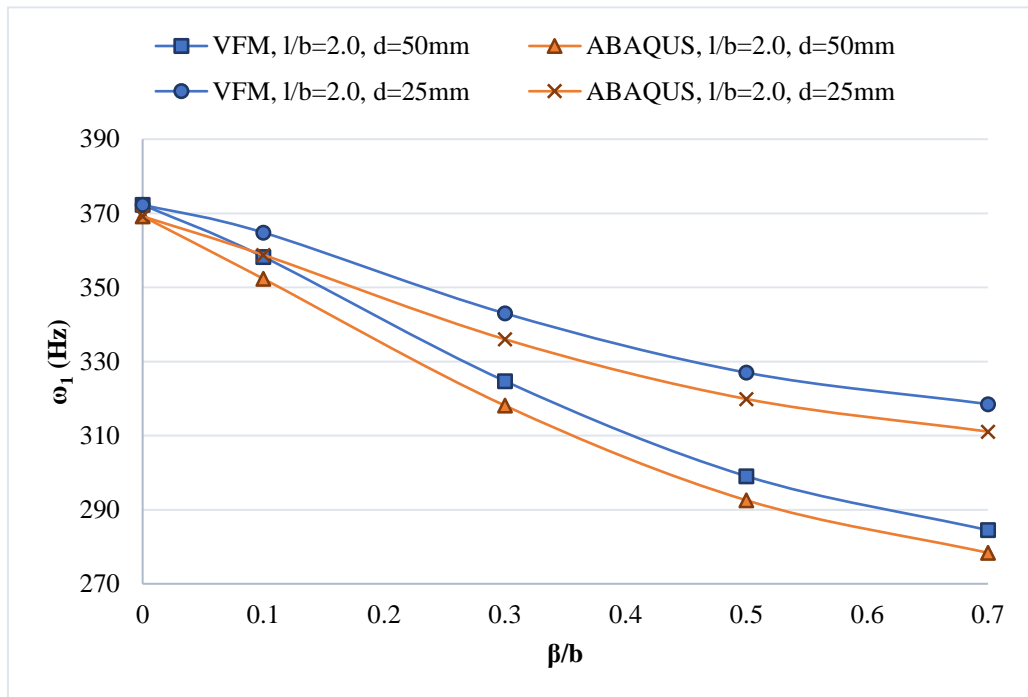
(b)



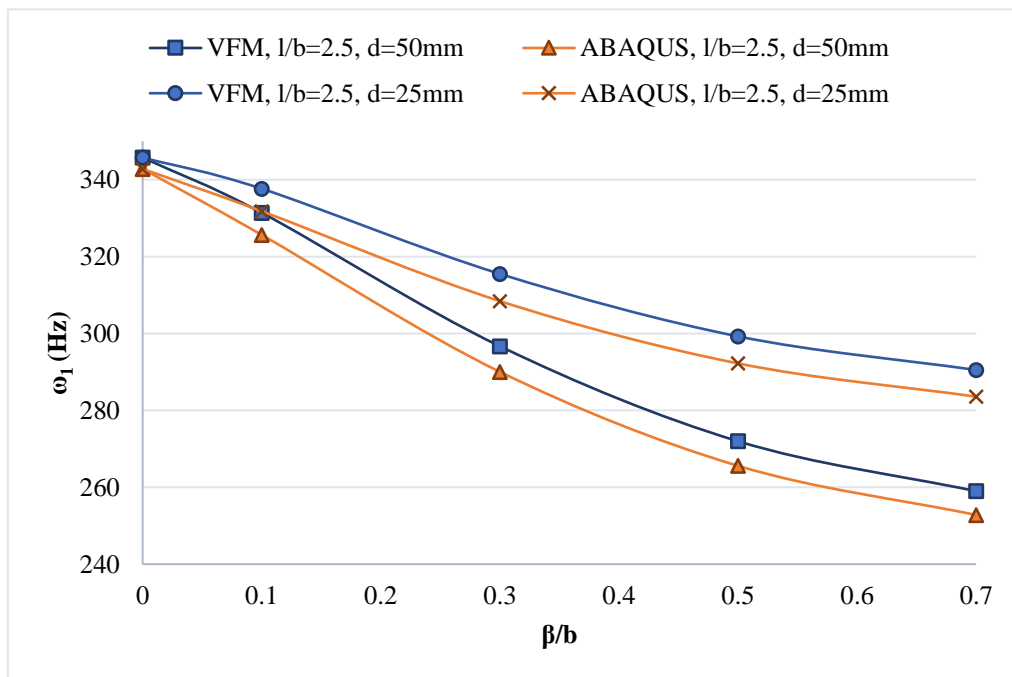
(c)



(d)



(e)



(f)

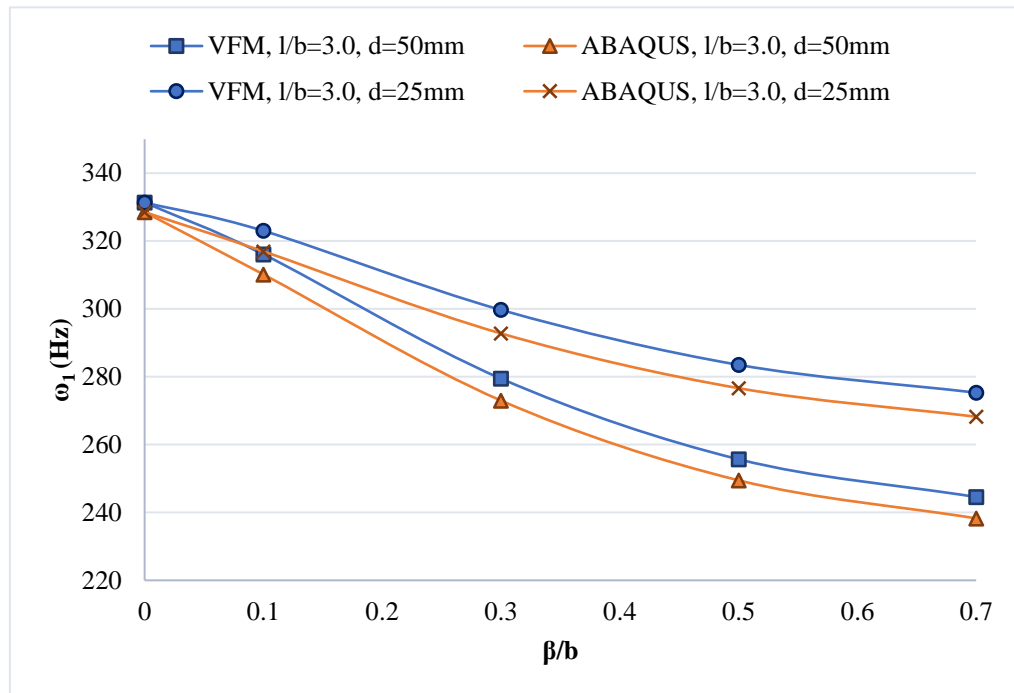


Figure 9-1 Plots of lowest natural frequency against different delamination sizes, $d = 25\text{mm}$ and 50mm , of composite plate with various aspect ratios (b/l).